THESIS

A HIGH-SPEED MASS SPECTROMETER FOR CHARCTERIZING FLASH DESORBED SPECIES IN PULSED POWER APPLICATIONS

Submitted by

Susan J. Ossareh

Department of Mechanical Engineering

In partial fulfillment of the requirements

For the Degree of Master of Science

Colorado State University

Fort Collins, Colorado

Spring 2022

Master's Committee:

Advisor: John D. Williams

Azer P. Yalin
Jacob L. Roberts

ABSTRACT

A HIGH-SPEED MASS SPECTROMETER FOR CHARCTERIZING FLASH DESORBED SPECIES IN PULSED POWER APPLICATIONS

Sandia National Laboratories operates the largest pulsed power facility in the world that hosts the Z machine that is utilized for research in fusion, energy, and national security. It can simulate extreme environments in these research areas in a single "shot" or "pulse of power," where large capacitor banks are rapidly discharged simultaneously, sending power to the center of the machine where a load is compressed into a z-pinch. A shot on the Z machine occurs in 150ns with peak currents on the order of 26 mega-amperes. However, there is a power flow obstacle that limits its ability to reach these extreme conditions. Approximately 1-3 MA of current is lost per shot. This could be partially attributed to chemisorbed contaminants on the cathode and anode stack in the center section of the machine being liberated in a flash desorption process, forming a conductive plasma between the anode and cathode electrodes that causes current to bypass the load and limits the power flow into the load.

This project is focused on the design and development of a high-speed mass spectrometer to make measurements of the gasses evolved from the electrodes that are heated to 1000°C in 100 nanoseconds. The measurements from this diagnostic would allow for more accurate predictive modeling of current loss for Next Generation Pulsed Power Drivers, such as the Z machine. Since a probe does not exist commercially, the project requires the development of new mass spectrometry technology, however a pre-existing probe was used to begin the design process. This

probe is known as the Energy and Velocity Analyzer for Distributions of Electric Rockets (EVADER) probe, which combines an electrostatic analyzer and a Wien velocity filter.

Within this study, two different plasma sources were used separately to simulate the plasma generated in the Z machine, and steady state measurements were made of the ions produced while working towards taking transient measurements. The design and development efforts described in this thesis were guided by: (1) using the EVADER to collect steady state data in its original configuration as a basis of comparison, (2) then replacing an ammeter in the experimental system with a transimpedance amplifier (TIA) circuit to speed up the data sampling rate over that of the ammeter, (3) incorporate a micro-channel plate within the probe to amplify the current feed to the TIA and enable even faster data sampling rates, and (4) design a high speed electric shutter to quickly turn “on” and “off” ion flow to the probe to enable measurement of the temporal response of the probe with the transimpedance amplifier and micro-channel plate elements. The end goal of the project is to improve transient performance of a probe from 10s of seconds to 10s of micro-seconds in a stepwise manner to support pulsed power research.

ACKNOWLEDGEMENTS

First and foremost, I would like to acknowledge and thank my advisor, Dr. John Williams, who encouraged me to foster a growth mindset, aided me in honing my critical thinking skills, and of course provided an endless amount of knowledge and guidance. I would also like to extend my acknowledgments to the rest of my committee, Dr. Azer Yalin and Dr. Jacob Roberts, who assisted with the completion of my thesis.

My colleagues in the Center for Electric Propulsion and Plasma Engineering Lab were incredible. Seth Thompson helped me through any problem and provided detailed expertise and advice. Shawn, Casey, and Cody Farnell were always willing to drop what they were doing to troubleshoot my experiments. I also had the pleasure of working with Theo Grevet, Brookie Hardesty, Sam Reagan, Joseph Clemmer, Matt Collard, Kolbin Dahley, and Tyler Kelly, all of whom created an energetic and positive research environment. COVID-19 made everything feel isolating, so being able to work with these wonderful engineers brought a lot of great conversations and laughs during the hardest of times. And a special thanks to those at Sandia National Laboratories who provided the opportunity for me to pursue this project as my thesis. I am grateful of the funding support to Colorado State University from Sandia.

Finally, a huge thank you to my family and friends. My mother and father, Varteni and Nasser, and my siblings, Parham, Jessica, and Sam, have always encouraged me to meet challenges head on and have shown interest in my work. Finally, my partner, Josh Matheison, as well as all my dear friends, have cheered me on every step of the way. Thank you to you all, you have made this journey possible and wonderful.

TABLE OF CONTENTS

LIST OF TABLES

LIST OF FIGURES

Chapter 1 Introduction

Pulsed power machines store electrical energy in capacitor banks that is delivered to them over a relatively long period of time and then quickly released into a transmission line that compresses the pulse of power, creating high energy density (HED) environments, which simulate extreme conditions. In the Z machine at Sandia National Labs, these pulses deliver 26 MA to an inductive load in the center of the machine that experiences the highest current density in the system. The high current leads to ohmic heating of the electrodes that connect to the load and causes flash desorption of chemisorbed contaminants such as molecular water (H_2O), hydrogen (H_2), carbon dioxide (CO_2), carbon monoxide (CO), and methane (CH_4). The desorbed neutral gas is ionized, creating a dense surface plasma on the electrodes, which could be partially contributing to the non-trivial current loss of 1-3 MA that flows between the two electrodes bypassing the load [1]. A better understanding of the neutral desorption and plasma formation processes through experimentation might enable improvements to be made to the initial boundary conditions used in models of the neutral and plasma flow field formation, which might then enable discovery of methods to improve current delivery to the load. The aim of this research was to begin the design and development of a high-speed mass spectrometer to evaluate multi-species gas desorption in micro-second time scales caused by extreme surface heating rates.

1.1 Pulsed Power Driver

Pulsed power drivers deliver a precise, short pulse of high voltage and current to a load. These machines create extreme conditions that simulate and advance concepts in planetary research, astrophysics, high energy density science, inertial confinement fusion (ICF), weaponry assessment, and material science.

The Z machine at Sandia National Labs is a pulsed power driver that is configured in a cylindrical form. On the circumference of the machine are large capacitor banks, which are slowly charged prior to a "shot." When switches fire, the capacitor charge is released nearly instantaneously to magnetically insulated transmission lines (MITLs), which allows for power to flow to the central vacuum chamber where the load is located. The load (or target) in some tests consists of hundreds of metal wires that dissolve into plasma when the electrical pulse arrives, the large current creates a magnetic field that pinches the particles inward, causing them to compress radially and gather along the z axis.

As the electromagnetic wave propagates toward the load, the current heats the surface of the conductors at a rate of 1000°C/100ns. The geometry of the electrodes leading up to the load is known as the convolute and the innermost MITLs consist of a conical anode-cathode (A-K) stack. The electrodes do not touch, but the gap between them (A-K gap) decreases to 1mm as it approaches the center. Since the Z machine requires MA to be transmitted through the lines, the energy density is at its largest at the load. This region of the machine is where a small, but still significant, amount of the current is shunted across the A-K gap through a dense plasma that forms here, rather than being delivered to the load [2]. The particles enabling the formation of plasma between the A-K gap are likely desorbed contaminant species from the electrodes that are ionized upon being released into the gap. The resulting dense plasma expands across and closes the A-K gap, causing an impedance collapse. The spatial scale that details the regions of interest within the Z machine is depicted in Figure 1.1.

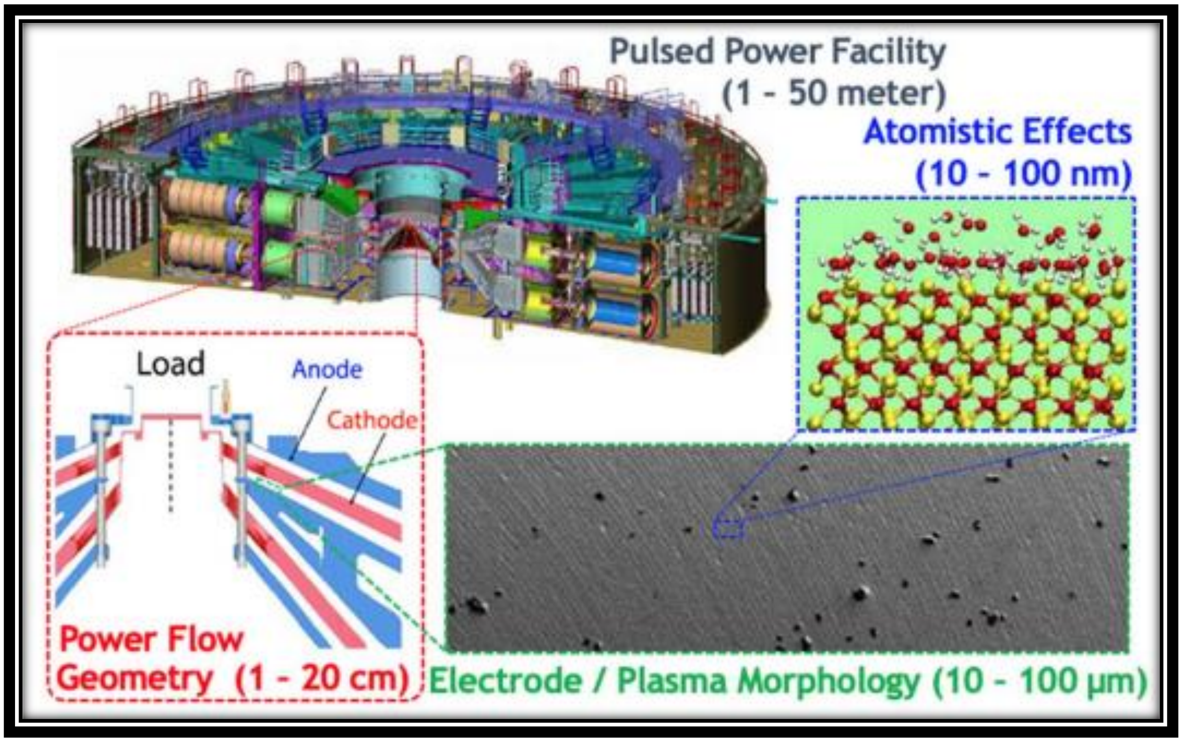

Figure 1.1: A cross-sectional view of the Z Machine with a closer look at the anode-cathode stack (the convolute) and the effects of contaminants on the electrode surfaces. Taken from [2].

MITLs are low-impedance vacuum transmission lines that utilize a self-generating magnetic field for insulation to reduce current loss. The magnetic insulation occurs at about 50ns after the start of the pulse, which confines electrons around to the region near the cathode. Particle-in-Cell simulations conducted at Sandia National Laboratories indicate that current is lost after about 60ns; a complete shot on the Z machine takes 150ns [3]. Surface contamination alters characteristics of the MITLs when desorbed neutrals are ionized via electron bombardment possibly before and while the magnetic insulation process takes effect [4]. This neutral desorption and ionization process yields a dense, expanding surface plasma of ions, which cross magnetic field lines more readily so the magnetic insulation is not as effective as it could be if no plasma formed [5]. Instruments that are implemented in the Z machine to measure the implosion collect data faster than the progression of the shot. This complicated data collection effort and the desire to further improve it and reduce plasma shunting in the MITLs is what drives the mission of this thesis.

1.2 Gas Desorption

Chemisorption is a form of sorption where a chemical reaction occurs between the material surface and the adsorbate, forming a covalent bond. The adsorbates can assemble on a surface as a "head group" and build out away from the surface, forming the "tail group". This assembly of adsorbates act as layers over the material and may diffuse over the gas-solid interface, which indicates that they are not strongly interacting with the substrate itself. The overall process of how surfaces can become contaminated in this self-assembled manner is actively being studied and the layers are referred to as self-assembled monolayers (SAMs) [6]. Figure 1.2 illustrates the layering of contaminants that are believed to form on a metallic substrate where the C, O, and H constituents are carbon, oxygen, and hydrogen, respectively, and the "M" constituent is a generic element from the metal substrate.

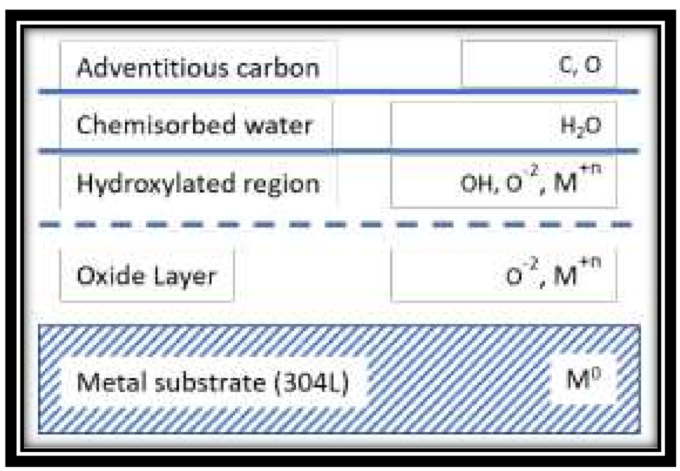

Figure 1.2: Depiction of contaminant species adsorbed to 304L stainless steel. Taken from [1].

Desorption is a process where a substance is released from a surface, or the bulk, of a given material due to a decrease in pressure and/or an increase in temperature. All metals have some degree of contaminant species present on the surface and within the bulk of the material due to fabrication, manufacturing, handling, and environmental exposure.

Chemisorbed contaminants being released in a flash desorption is especially prevalent in the electrodes used in the Z machine. The material used to fabricate the MITLs is 304L stainless steel. The MITLs are cleaned and handled in air, and then are held under vacuum by diffusion pumps. Under these circumstances, the surfaces are likely coated by monolayers comprised of water, hydrogen, oxides, and hydrocarbon adsorbates along with dust particles, which could also be covered in these monolayers.

There are ongoing investigations at Sandia National Labs on how to install the MITLs and then clean their surfaces before taking a shot on the Z machine to avoid or reduce current loss. Achieving ultra-high vacuum (UHV) so that the baseline pressure is much lower was considered as a means to force desorption to occur, delaying the onset of the impedance collapse and reducing current loss, however, the bonding of adsorbates that is electronic in nature is strong enough that improved vacuum pressures ($P \ll 10^{-5}$ Torr) would not effectively clean the electrode surface [7]. Temperature desorption is another method of cleaning materials where the substrate is heated in-situ for an extended period to remove the impurities prior to taking a shot. While this is a common method for cleaning surfaces [8], it is difficult to scale it up to the Z machine and clean the MITLs enough to reduce the current loss significantly. Waiting for the MITLs to cool down after heating and before a shot allows enough time for the surfaces to become contaminated again.

The lack of understanding of how to overcome the issue with desorption is intimately tied to the difficulties of modeling the complex electrode physics and multi-species plasma phenomena that occur in the A-K gap [3]. This thesis will approach the design of the high-speed mass spectrometer with these issues in mind to have a probe that eventually can gather data on the 10s of micro-second time scale and provide better informed boundary conditions in these simulations.

1.3 Time-Resolved Mass Spectrometry

The objective is to begin the stepwise design and development process for creating a high-speed mass spectrometer (mass spec), which could be placed near the center of the Z machine to identify multiple species of neutrals that desorb from the MITLs during a shot. Mass spectrometry instruments ionize neutrals and then manipulate and sort the ions that are created by accelerating and focusing them using electric and magnetic fields. The goal is to use them in pulsed power applications like the Z machine to sample some of the neutrals desorbing from the MITLs during a shot and identify the species, how much of each species is present, and how quickly they desorb. As noted earlier, the formation of the plasma occurs in tens of nanoseconds, therefore this system needs to resolve neutral desorption in the nanosecond time scale, which requires careful timing because a desorbed neutral is only expected to travel ~5 mm off the surface in a nanosecond and the mass spec entrance will likely be tens of centimeters away. The system needs to be able to measure water (18 AMU), hydrogen (2 AMU), carbon dioxide (44 AMU), carbon monoxide (28 AMU), and methane (16 AMU) in a simultaneous manner, however, there is the potential that heavier neutrals from the stainless steel can be desorbed at high temperatures, therefore the spectrometer might need to have the capability of picking up elemental and molecular species of mass between 1-50 AMU or more [9]. There are commercially available mass specs that could be adapted to the project, such as time-of-flight (ToF), quadrupole, and magnetic sector mass specs, which are reviewed and compared next.

1.3.1 Time-of-Flight Mass Spectrometry

A Time-of-Flight Mass Spectrometer (ToF MS) accelerates ions with an electric field from the same position at the same time to a location further into the probe where they are measured. Ions of lighter mass will accelerate to higher velocities, whereas heavier ions with the same charge would have a lower velocity imparted on them. A detector is located some known distance from the acceleration grid, which allows for velocity to be calculated as the drift distance is known and the flight time information is gathered, and the mass can be inferred. The applied electric field in the acceleration stage and drift distance can be used to distinguish mass to charge ratios based on these velocities [10].

There are different configurations of a ToF MS including linear acceleration and reflection systems. The resolution for detecting the species and its charge varies based off the configuration. A linear ToF MS has an acceleration stage where an electric field is applied, which advances the ions through into a straight, electric-field-free drift tube of some defined length, the ions then reach the collector plate at the end of the tube yielding ion current versus time data. Figure 1.3 illustrates the stages of the linear ToF MS. These systems offer poor mass resolution because the initial spatial distributions can differ among the ions causing them to have different kinetic energies as they are accelerated, so they could have varying flight times. There is a way to correct the energy spread, by increasing the drift distance to make the ion flight times much longer [10], which is not easy to implement in the small spaces available in the Z machine.

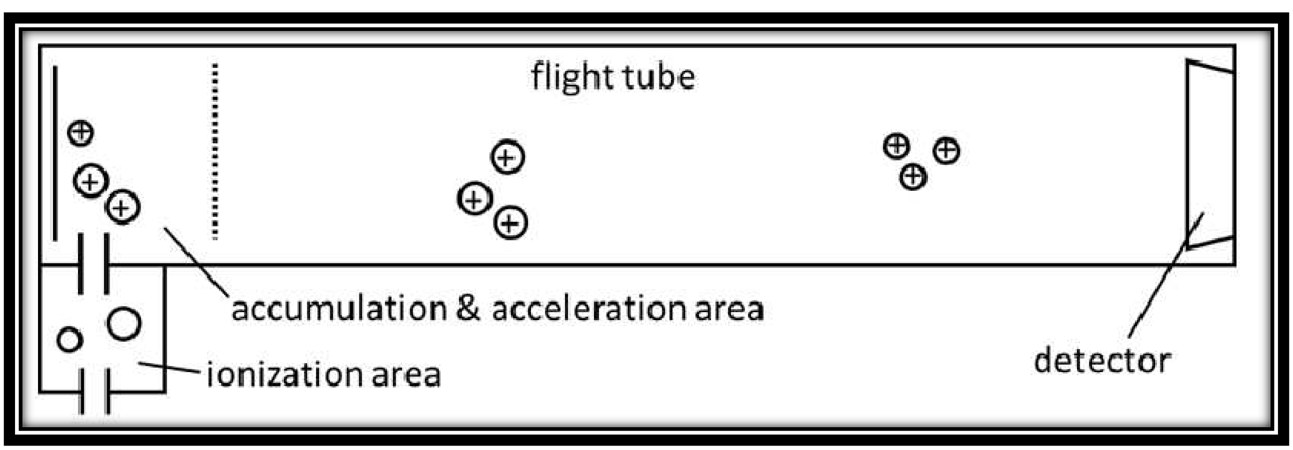

Figure 1.3: Schematic of a linear ToF MS. Particle enter the system on the left and are ionized that increases their charge and then they are accumulated. An electric field is applied to the grid that accelerates the ions through into a field-free drift tube. At

the end of the tube resides the detector that outputs a signal when the ion is collected, yielding the speed of the ion. Figure taken from [9].

Another configuration, as mentioned above, is the reflection system. This mitigates the effect of varying kinetic energies that is noted in linear systems, so its mass resolution is better. Here, ions are accelerated into an ion "mirror" with multiple retarding and accelerating electric fields that causes ions to reflect out into the field-free drift region. Ions with larger kinetic energies penetrate deeper into the fields than the ions with smaller kinetic energies and the same charge, meaning they reside within the reflecting fields for different amounts of time and ultimately leave at the same time [10]. Figure 1.4 portrays the trajectories of two ions with the same mass and charge but differing kinetic energies, and how they leave the reflecting region at the same time. Since this configuration reflects the ions, the probe is more compact than a linear ToF mass spec. The reflection devices have longer drift lengths and therefore longer flight times, which is again, not appropriate for this application because the experiment is already so time dependent.

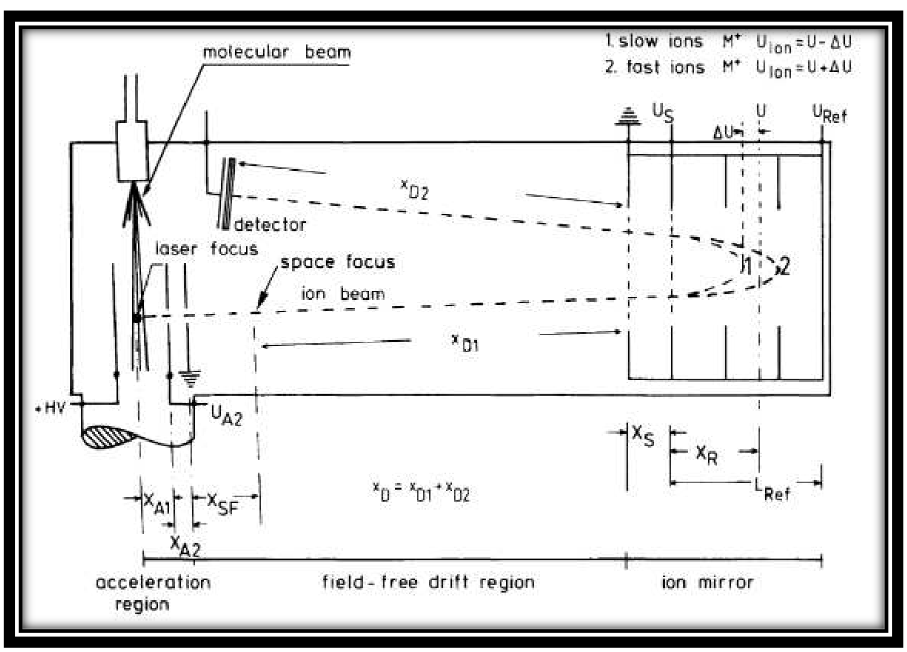

Figure 1.4: Schematic of a reflection TOF MS. The neutrals enter at the left and are ionized, then accelerated down the drift tuber toward electrodes that produce a polarizing electric field that is considered the "ion mirror". The ions are reflected out on a parabolic trajectory at the same time given their masses, where they once again travel through the drift tube and are collected on the detector. Figure take from [10].

A ToF MS was considered as a starting probe for this thesis project, however it was limited by the time spreading of ions and the speed of the detector.

1.3.2 Quadrupole Mass Spectrometry

Quadrupole mass spectrometers (QMS) use four, long, conductive rods arranged in a quadrupole configuration to induce an oscillating electric field along the centerline of the quadrupole as shown in Figure 1.5. A beam of ions is directed along the centerline, and ions of a specified mass to charge ratio will pass through un-deflected depending upon the AC and DC potentials applied. As such, the QMS is a mass filter that only allows one ion mass to be sampled at a time [11] [12].

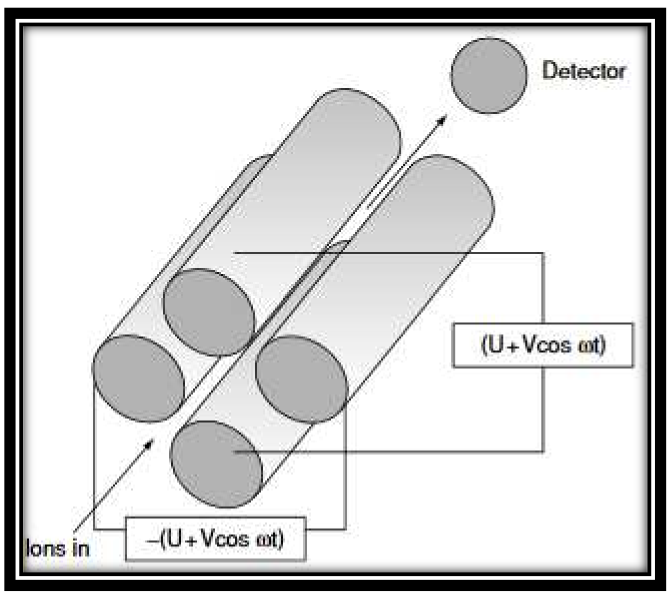

Figure 1.5: Schematic of a QMS depicting the four poles that are connected to DC and AC signals to create an oscillating electric field along the centerline of the poles where a beam of ions is directed. Figure taken from [11].

While quadrupoles are robust and commonly available, they were determined to not be an appropriate candidate for this project due to the lack of multiple mass detection capability in a simultaneous manner since Sandia National Labs is interested in at least 5 different species.

1.3.3 Magnetic Sector Mass Spectrometry

A magnetic sector mass spectrometer utilizes a static magnetic field to deflect ions at different radii based off the ion's mass and charge as shown in Figure 1.6. Lighter weighted particles have a smaller radius in their trajectory than more massive particles (of the same charge state), and hence different species can be spatially resolved simultaneously [13]. Furthermore, the magnetic field can be changed to alter the degree of deflection and enable high mass resolution over a wide range of ion mass.

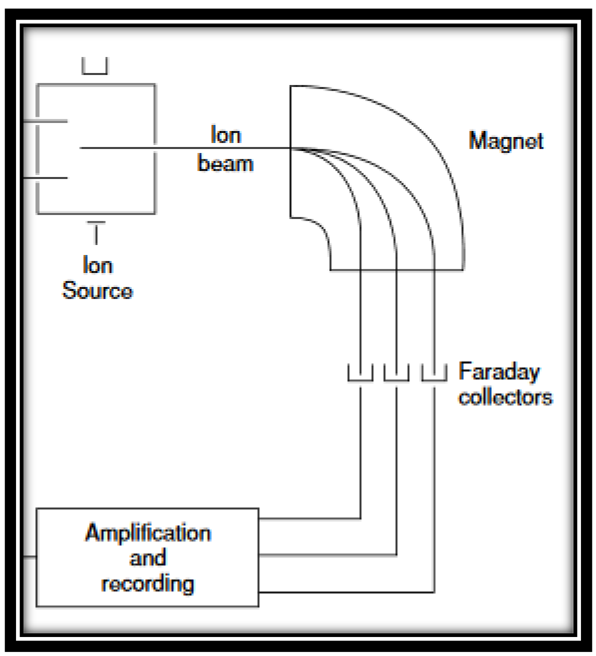

Figure 1.6: Schematic of a magnetic sector where the ions of different masses are deflected perpendicularly by the magnetic field and collected on detectors based off their mass, charge, and spatial distribution. Taken from [13].

The radii that the ions are deflected at are known as the cyclotron radii which can be calculated to determine the placement of the collectors, allowing for multiple species to be detected simultaneously. This option was not chosen as the foundational probe, but it will be implemented in the stepwise changes.

1.4 Energy and Velocity Analyzer for Distributions of Electric Rockets

The Energy and Velocity Analyzer for Distributions of Electric Rockets (EVADER) is a hybrid instrument from Plasma Controls, LLC that combines an electrostatic analyzer (ESA) in-line with a Wien velocity filter (ExB) to obtain ion energy and velocity distributions. This probe was chosen as the foundational instrument, which can be adapted into a high-speed mass spectrometer using a magnetic sector approach. It is modular, compact, and due to its combination of analyzers, can be used to discriminate between species with high accuracy [14].

Figure 1.7 shows the primary components of an ESA and ExB, including the ESA spherical plates for energy per charge differentiation, ion collimators, the collectors, and the use of the ExB electric and magnetic field section for mass, velocity, and charge state differentiation. Note that one component, the ExB collimator/ESA collector, enables the EVADER to act as a standalone ESA or as a filter to the ExB – only allowing selected ions to pass through.

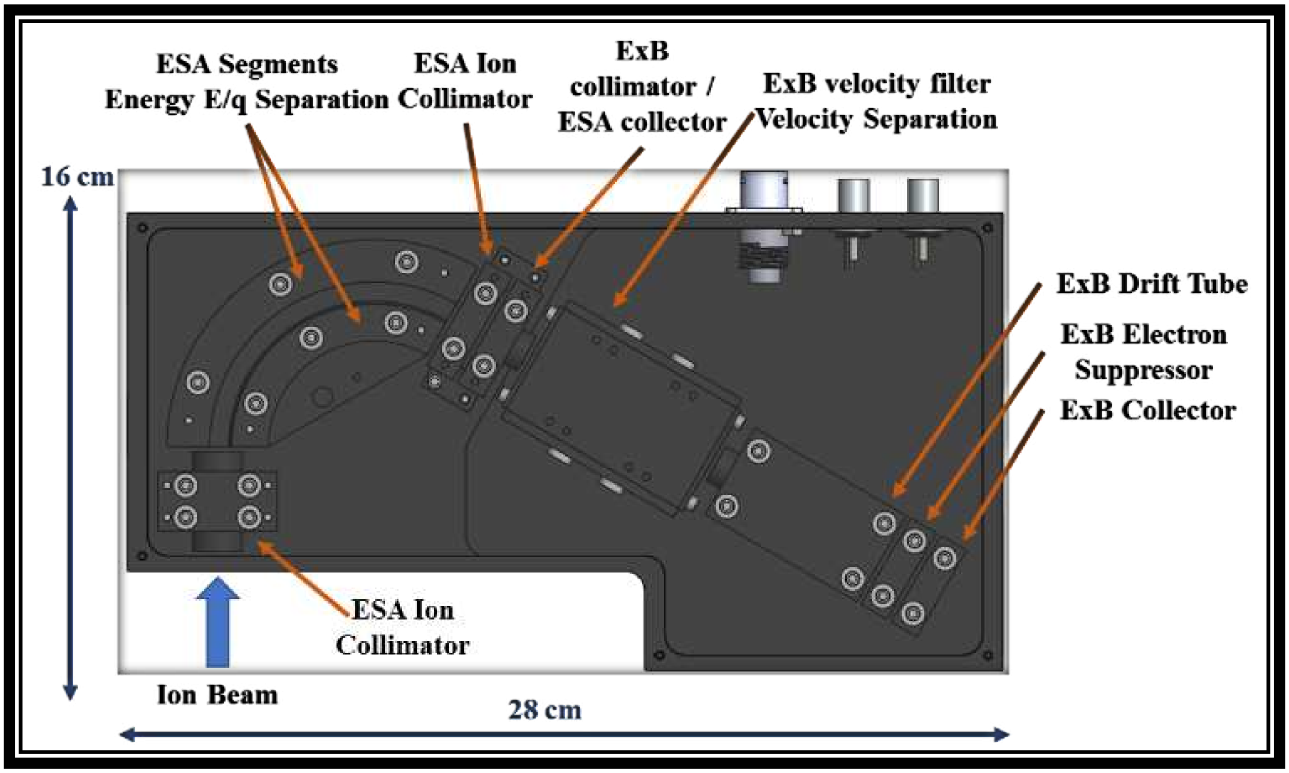

Figure 1.7: A diagram of the EVADER's main internal components that depicts both the ESA and ExB stages. Taken from [14].

An ESA is an analyzer that applies a static electric field to deflect particles, hence obtaining the name electrostatic analyzer. These devices separate ions through deflection-based designs because the configuration matches the curve of the particle trajectory, namely mirror-type analyzers and deflector-type analyzers [15]. The EVADER has a spherical deflector electrostatic analyzer that uses coaxial spherical plates as the deflector plates [15]. A drawing of a spherical deflector plate is shown in Figure 1.8.

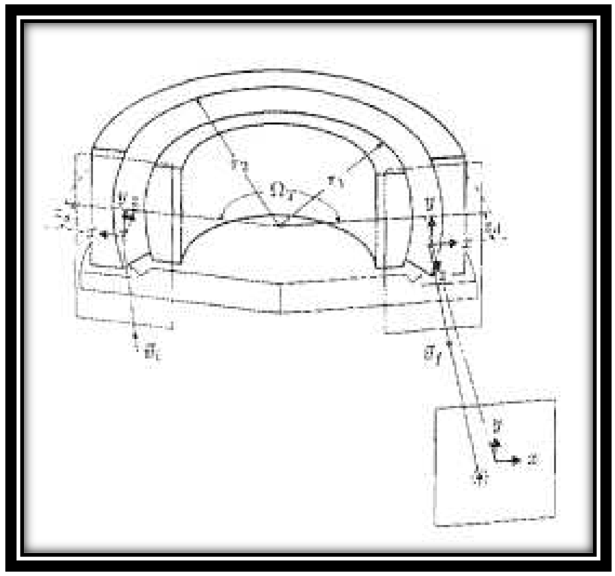

Figure 1.8: A side view of a spherical deflector ESA that has the spherical plates parallel to one another where the electric field is applied. The area between the plates provides a path for the ions to curve through. Taken from [16].

Charged particles of a specific energy (transmission energy) follow a trajectory between the parallel, spherical plates of the ESA. If particles enter at a different energy, they are deflected off the axis and are not able to be passed to the next stage [17]. Ions that are passed are those that match the selected pass energy, E/q, of the analyzer based off the applied accelerating voltage, V_s, and the transmission energy, E_0/q, as shown in Equation (1.1).

$$E/q = -V_s + E_0/q \qquad (1.1)$$

The differing charge states of a particular ion mass will experience the same potentials but have different velocities. This sets a specific energy of ions that can pass through onto the next stage.

Ions then enter the ExB region that consists of parallel electrodes and permanent magnets oriented such that the electric and magnetic fields are oriented at right angles to each other and to the velocity vector of the ions entering this region as shown in Figure 1.9. The trajectory of charged particles are influenced by the net force of the fields they encounter, and specific ions can be made to experience a zero net force and are hence "filtered" by their velocity in the ExB region [18]. A zero net force can be achieved by balancing the magnetic and electric forces as shown in Equation (1.2).

$$F = 0 = q \cdot (E + [u \times B]) \tag{1.2}$$

Where F is the Lorentz force, q is the charge of the particle, E is the electric field, u is the velocity of the particle, and B is the magnetic field. By setting the deflecting force to zero, ions of a particular velocity can pass through, which allows Equation (1.2) to simplify and relate the velocity to the electric and magnetic fields [19].

$$u = \frac{-E}{B} = \sqrt{\frac{2q\Delta V_p}{m}} \tag{1.3}$$

Where q is the charge on the ion, ΔV_p is the potential difference that accelerated the ion into the probe, and m is the ion mass. Particles that pass through the drift tube are recorded as current on the ExB collector.

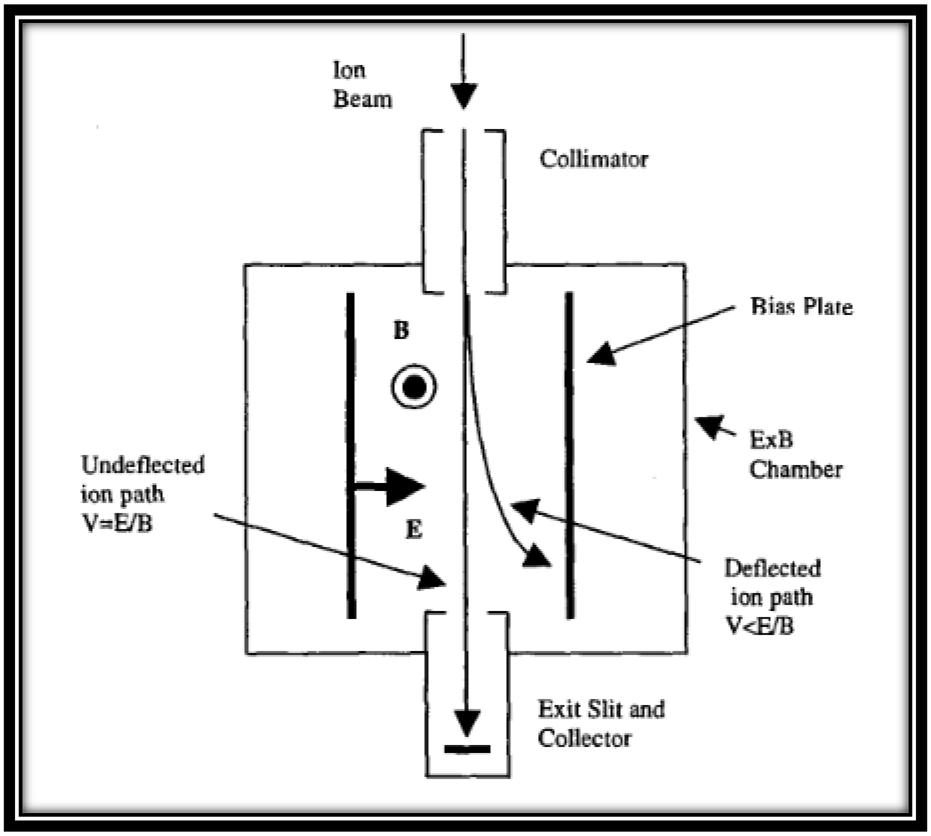

Figure 1.9: Schematic of an ExB probe that illustrates an ion that is deflected due to the Lorentz force and another path of an un-deflected ion. Taken from [19].

The ExB separates the ions according to their charge state [20]. This is done by holding the magnetic field constant with permanent magnets and varying the electric field by applying a varying a voltage difference, $\Delta\varphi$, between the parallel plates. By recording the collector current and voltage difference one can create a plot of current-versus-voltage with distinct peaks corresponding to the ion charge state.

$$\frac{\Delta\varphi}{d} = B\sqrt{\frac{2q\Delta V_p}{m}} \tag{1.4}$$

Where d is the distance between the ExB plates, ΔV_p is the potential difference between the ion creation point and the magnetic sector of the ExB, q is the charge, and m is the mass. Plasma

Controls also developed software to collect data from the EVADER, which yields the ion species peaks associated with each ion charge state.

While the EVADER probe can use the specific energy from the ESA to distinguish between species in the ExB section, it is difficult to account for molecular ionization and dissociation [21]. It is desirable to ionize the molecule without breaking it down to know which molecular species is present. While that is difficult to avoid, the EVADER has a molecular detection range of 1-200 AMU that can encompass most of the common molecules and metallic molecules that the MITLs are more likely to desorb. Analyzing the mass signatures from the EVADER scans can allow inference of whether some molecules dissociated significantly or not.

Chapter 2 Experimental Setup

Each step in the design and development process of a high-speed mass spec needs to be tested to troubleshoot and decide if it is a viable decision. This chapter describes the plasma sources, plasma diagnostic equipment, and laboratory facilities used in the stepwise process.

2.1 Plasma Sources

The EVADER probe is the baseline design mass spec for the project, and it can only measure ionized particles, therefore, plasma needs to be generated from neutral atoms to test the probe. Two different plasma generating sources were used for testing: the first was an 8-cm gridded ion source that allowed for the properties of the ions entering the probe to be set such as the energy and current density. Knowing a lot about the plasma makes it easier to verify that the data from the EVADER is correct. The other plasma source used is called the "Flamethrower," which is a novel electric propulsion device that is under development at CSU. The Flamethrower produces an intense plasma nearby its exit aperture that is comprised of energetic electrons, multi-charged ions, and neutrals. The plasma produced nearby the Flamethrower freely expands into the regions downstream creating an energetic plasma plume comprised of energetic ions that form a relatively divergent beam. The Flamethrower ion beam cannot be customized like the gridded ion source. Rather the ions from the Flamethrower have a wide distribution of energies and their current density at the probe entrance is typically higher than the current density produced by the gridded ion source. The Flamethrower plasma source was chosen because it is believed to be more representative of the plasma formed on the MITLs in pulsed power machines.

2.1.1 Gridded Ion Source

An ion source is a device that creates a broad beam of ions by accelerating them, using a set of biased grids, from plasma created in a discharge chamber via electron bombardment of a neutral gas. A visual is provided in Figure 2.1 for ease of understanding the workings of the source.

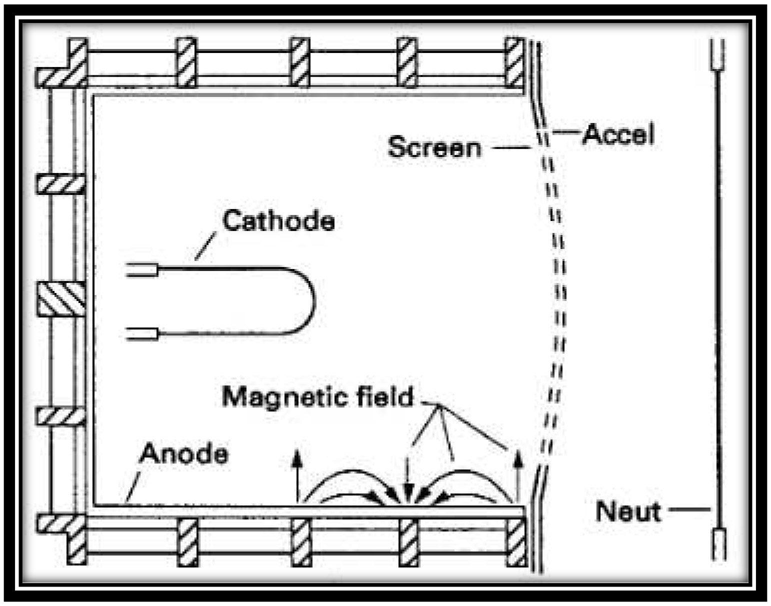

Figure 2.1: Side view, cross-sectional illustration of a gridded broad-beam ion source. Consists of five main components: the cathode, discharge chamber, magnetic rings, grids, and neutralizer. Taken from [22].

The ion source operates by introducing a controlled flow of an inert gas – usually Argon, Krypton, or Xenon – into the body of the source known as the discharge chamber. Simultaneously, the cathode that sits within the discharge chamber is used to emit electrons that are accelerated from its surface through a thin sheath. These energetic electrons collide with the atoms of the gas sometimes stripping them of an electron, resulting in the formation of ions. Within the discharge chamber are magnets that produce magnetic fields near the wall, confining the electrons via within the discharge chamber such that they have a higher probability of colliding with atoms. Some of the ions produced within the discharge chamber drift toward the downstream end where an ion-optics assembly formed from a set of grids is located [22]. There are typically two grids, the screen and the accelerator (accel) that are oppositely biased to create an electric field that electrostatically accelerates the ions to high velocities. Just beyond the grids, immersed within the beam, is a neutralizer that emits electrons into the ion stream to current and space-charge neutralize it [22].

As mentioned earlier, the purpose of employing a gridded ion source for the testing of the EVADER is to control the properties of the ions introduced to the probe. Figure 2.2 includes the descriptions and connections of the power supplies that are typically used to operate the ion source. The use of an ion source makes it possible to verify the data gathered with the EVADER because the energy and current density of the ions are known.

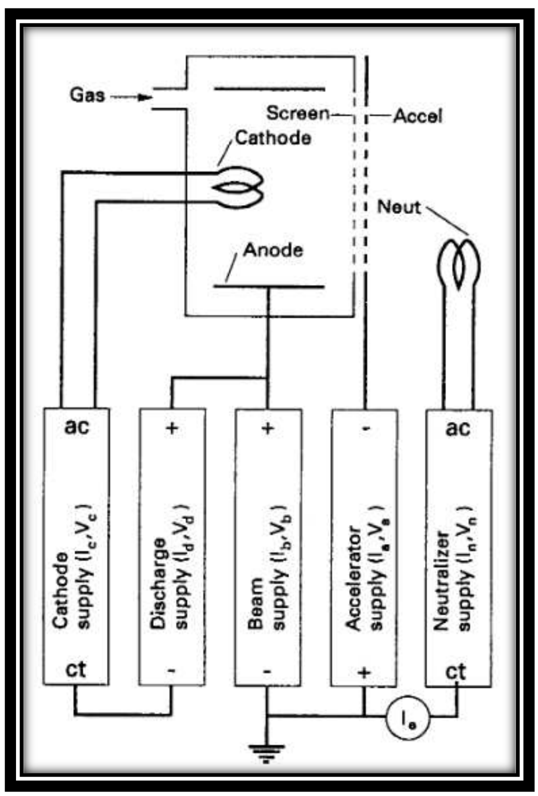

Figure 2.2: Schematic diagram of the power supplies connected to a gridded ion source depicting all the aspects of the source that can be set. Taken from [22].

The CSU 8-cm gridded ion source is a source that utilizes grids with small holes that are placed in a hexagonal pattern over a circular area that is 8-cm in diameter. The ion source is mounted on the ceiling of a ~1 m diameter, ~cylindrical vacuum chamber called "Hydra" within the Center of Electric Propulsion and Plasma Engineering (CEPPE) lab. It can be used to produce a broad beam of ions with energies of 50-1500 eV and beam currents of 25-250 mA. The beam is directed downward toward a graphite target. To analyze the ion species in the beam plasma, the EVADER rests on the "floor" of the vacuum chamber above the graphite beam target, and the entrance aperture of the probe is aligned with the centerline of the ion source as shown in Figure 2.3.

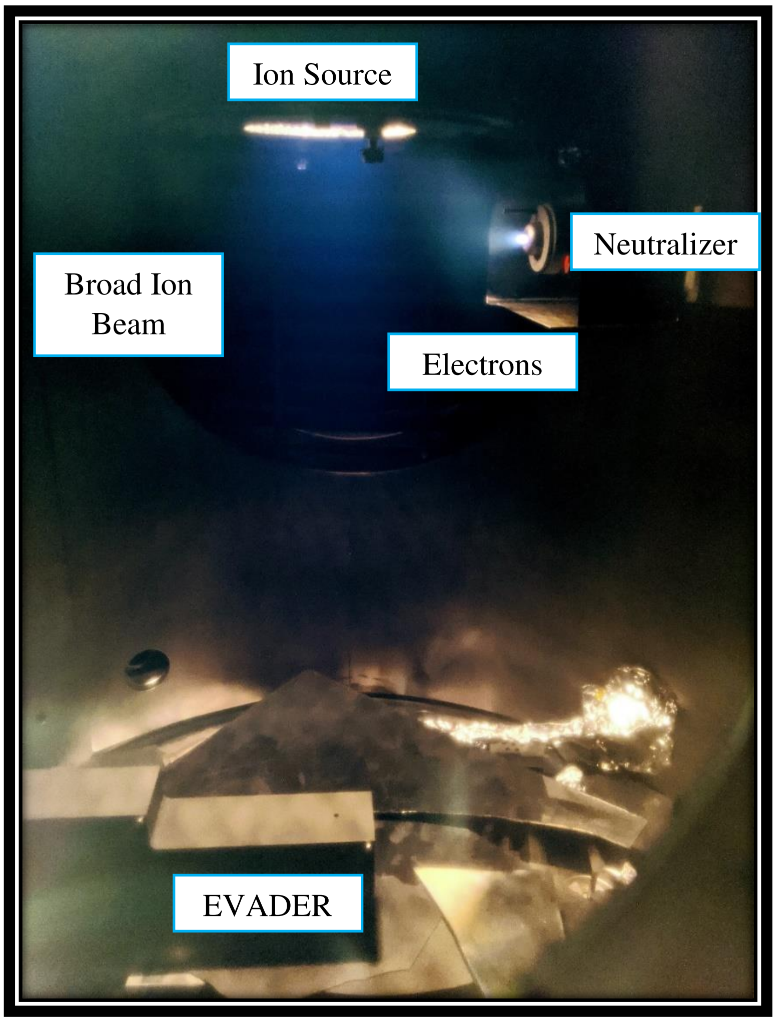

Figure 2.3: The laboratory gridded ion source generating a beam that is projected toward the EVADER probe within the Hydra vacuum chamber.

The ion source is controlled with a power supply system that consists of several power supply modules: the neutralizer, discharge chamber, cathode (electron source), screen (beam) grid, and accelerator grid. The separate modules allow for customization of the beam. A photograph of the front panel is shown in Figure 2.4.

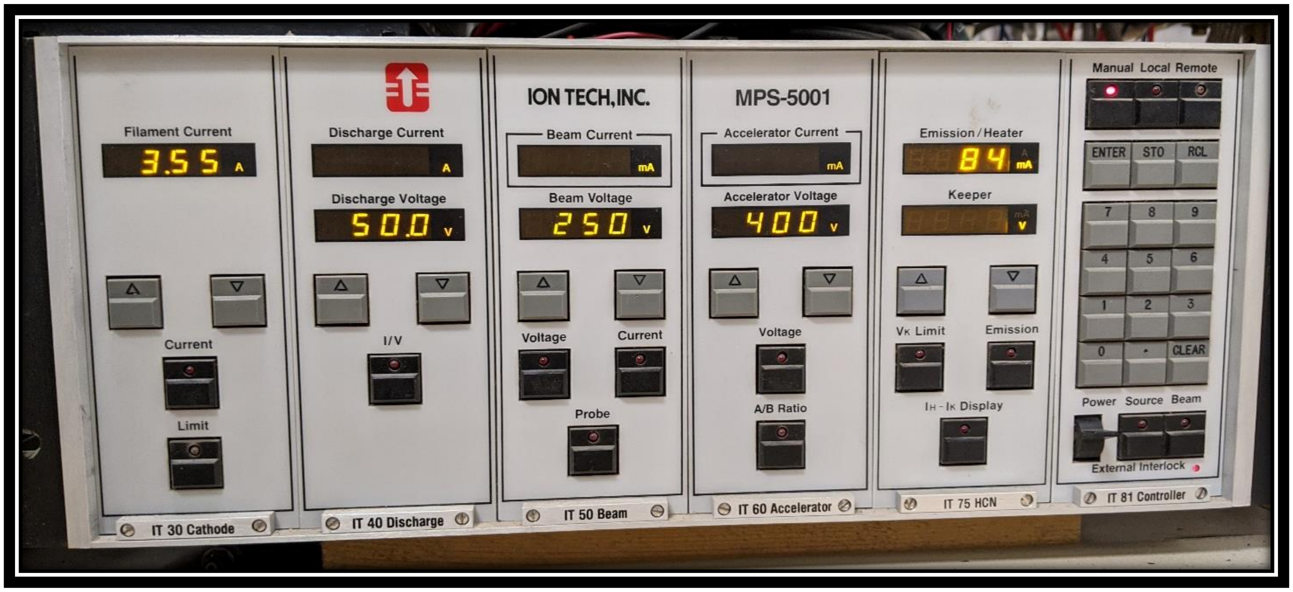

Figure 2.4: Ion source power supply at the CEPPE lab. From left the right the modules are Cathode, Discharge, Beam, Accelerator, and Hollow Cathode Neutralizer (HCN) supplies.

For the lab set up, Argon gas was used as the working gas in the Hydra vacuum chamber. It is flowed to the ion source, ionized, and accelerated to produce an Ar ion beam. Argon is also sent to the hollow cathode neutralizer to operate the neutralizer and release electrons into the beam. Therefore, there are two gas flows to control. They need to be at a high enough flow rate to run the ion source but low enough to maintain high vacuum conditions. For the data presented in this thesis, both the flows were set to 3 standard cubic centimeters per minute (sccm), which resulted in a chamber pressure of ~5x10^{-5} Torr—low enough to propagate the beam from the ion source to the probe with minimal attenuation.

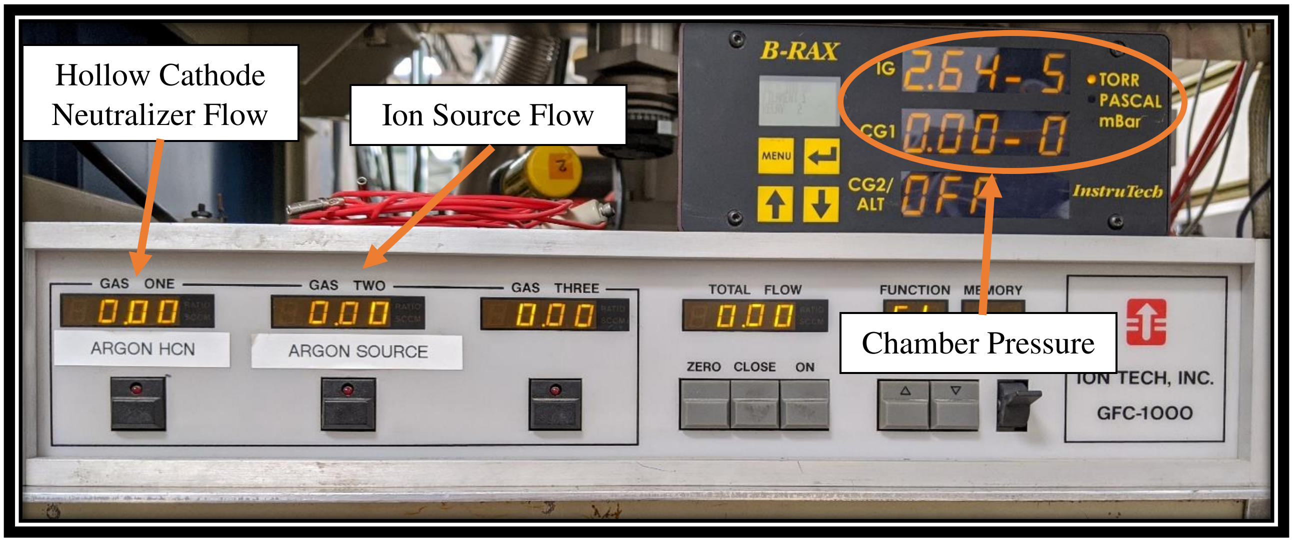

Figure 2.5: The laboratory mass flow gas controllers and chamber pressure gauges.

2.1.2 Flamethrower

The Flamethrower is a novel, compact plasma source capable of generating measurable thrust and hence worthy of evaluation as an electric propulsion device first proposed and patented by Gorokhovsky [23]. It employs a non-local configuration [23] to produce plasma and accelerate ions from their creation point with an electric field embedded in the plasma through an energetic expansion process. This geometry differs from a gridded ion source in a multitude of ways. The concept is based on a plasma discharge maintained between two nearly identical, adjacent bodies, where one is biased positively (the anode or hidden anode using the non-local naming convention), and the other is biased negatively (the cathode). Figure 2.8 contains a photograph taken of the Flamethrower thruster mounted on a thrust stand.

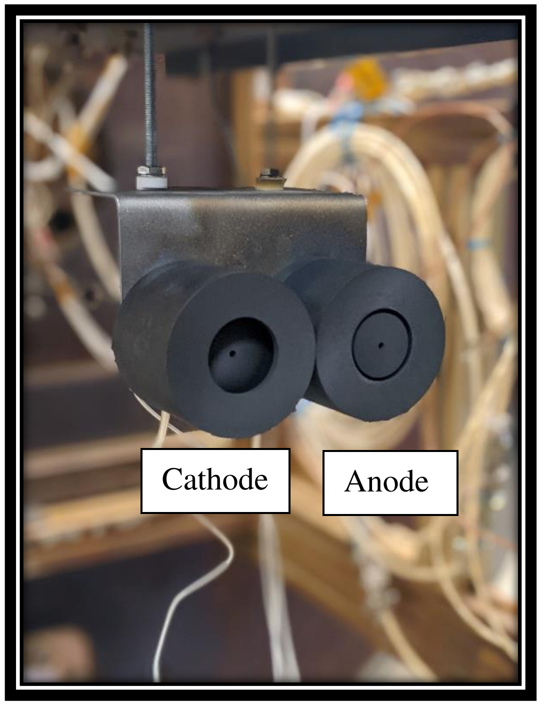

Figure 2.6: The Flamethrower thruster, consisting of two nearly identical bodies where one is biased negatively, and the other is biased positively. The "hidden" anode has an elevated orifice plate component to allow all the ions produced downstream of the orifice plate to expand freely from this region and form a beam.

Inert gas is flowed into both bodies, the negatively biased part acts as a cathode, which provides electrons via a neutralized plasma bridge process that are accelerated along their path toward the hidden anode and ionizes the gas supplied to the hidden anode through electron bombardment. The graphite body surrounding the cathode is called the keeper, which is positively biased to the cathode, drawing out the electrons via a dense plasma formed in this region. These electrons then flow through the plasma bridge to the positively charged anode that is hidden behind the graphite orifice in the other body, causing the cathode and anode bodies to couple. Very strong plasma ion generation rates are caused to occur just downstream and within the orifice region of the hidden anode where the coupling process is choked. A strong potential gradient develops in this region that is effective at accelerating the ions produced in this region out and away from the hidden anode body [23] [24]. Figure 2.7 shows a photograph of the Flamethrower in operation and the plasma being produced through the coupling of the cathode to the hidden anode.

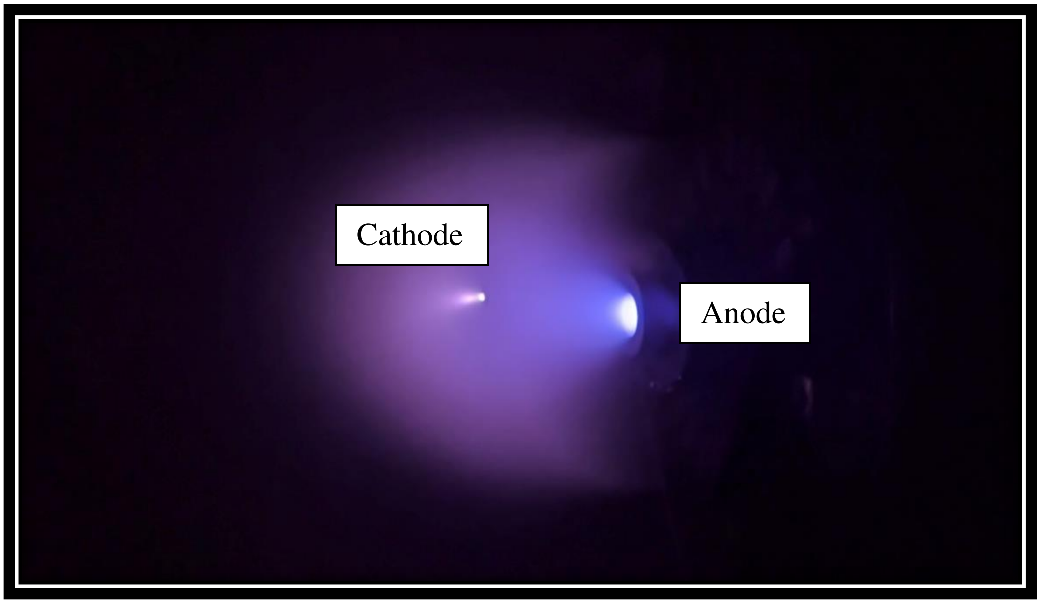

Figure 2.7: Photograph of the Flamethrower cathode coupled with the anode to produce a dense, energetically expanding plasma.

The hidden anode concept is what makes this source unique. As shown in the solid models in Figure 2.8, the inside of the Flamethrower shows a stack of alumina silicate discs with a graphite nozzle and body encasing the discs and the anode. The anode is placed in the center of the alumina silicate just behind the orifice to isolate the anode from collecting electrons except those flowing through the nozzle.

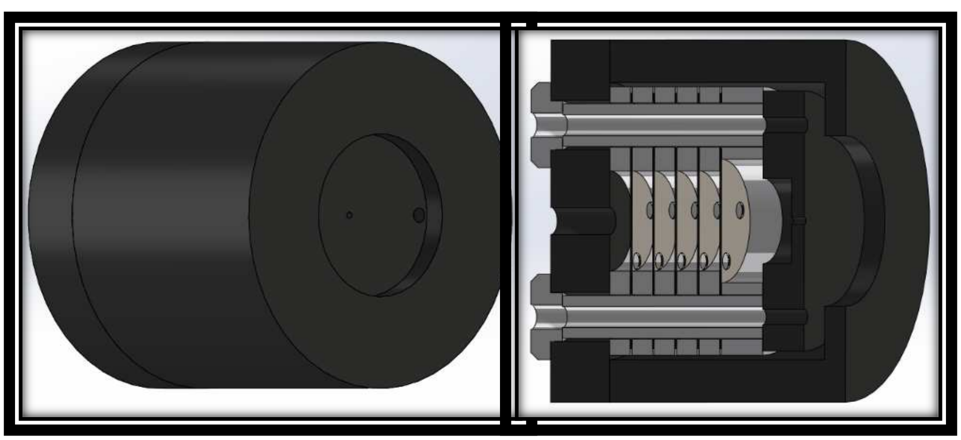

Figure 2.8: The left image shows a solid model of the hidden anode component of the Flamethrower. To the right is a cross-sectional view of the hidden anode component.

The Flamethrower set up consists of mounting the cathode and anode adjacent to one another on a thrust stand with their axes oriented horizontally. Krypton gas was used as the propellant. The EVADER is situated on a motion stage that can shift the position of the probe to be at an arbitrary axial distance away from the Flamethrower. The probe aperture is aligned with the axis of the hidden anode orifice. Figure 2.9 shows a photo of the set up within the vacuum chamber. This ion source was used in a cylindrical, 1.6 m diameter vacuum chamber.

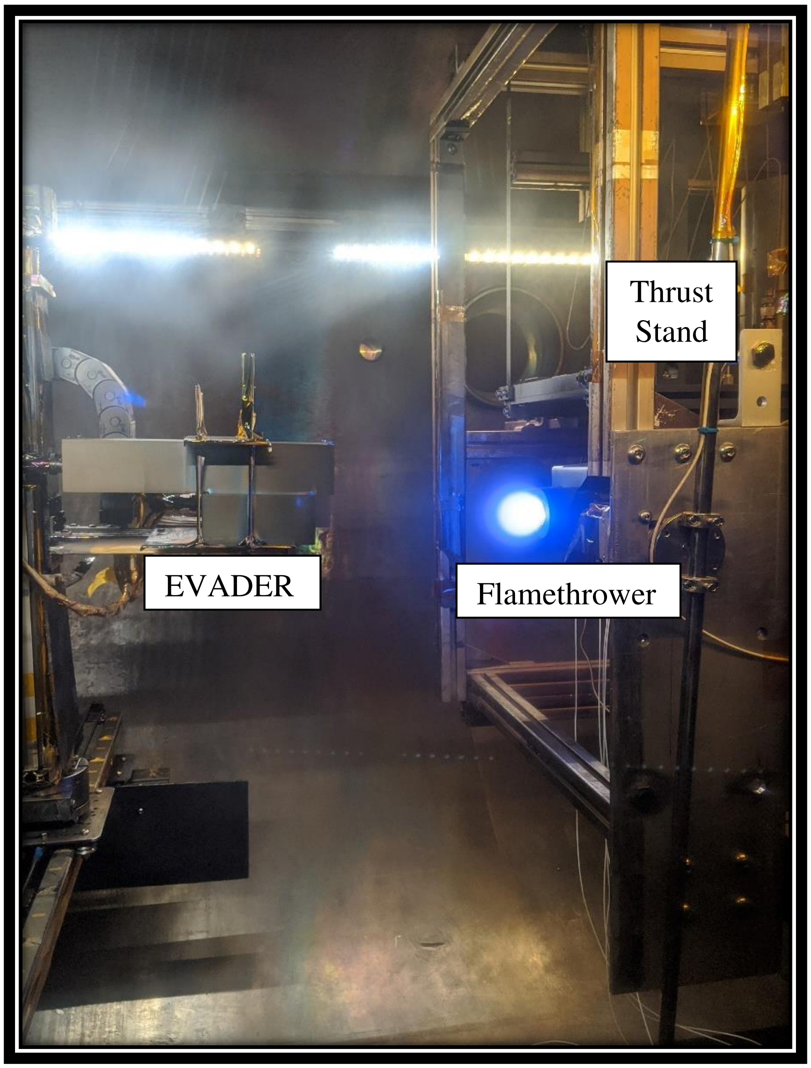

Figure 2.9: The Flamethrower mounted to a thrust stand and producing a plasma at a 100 W power level setting, the EVADER is shown at an axial position 30 cm downstream of the plasma source.

On the airside of the setup, there are two flow meters to control the flow rate of Krypton through the cathode and the anode. Then there are two power supplies, where the positive lead of one connects to the keeper and the positive lead of the other connects to the anode. The negative leads of both power supplies are connected to the cathode. This causes the cathode to be biased negatively and the anode and keeper to be biased positively.

2.2 Plasma Diagnostics

As mentioned above, the EVADER probe was chosen as the foundational equipment to begin the development effort of a new probe that could characterize the neutral species temporally being evolved from a surface in the tens of nanosecond time frame. The experimental set up of the probe was changed as the probe was modified in steps to begin the effort of effectualizing the final design. The experimental probe set ups that were evaluated in this thesis are presented below.

2.2.1 EVADER | Traditional Configuration

In the traditional configuration, the EVADER is hooked up to three power supplies and a low-current electrometer. The connections are shown in Figure 2.10.

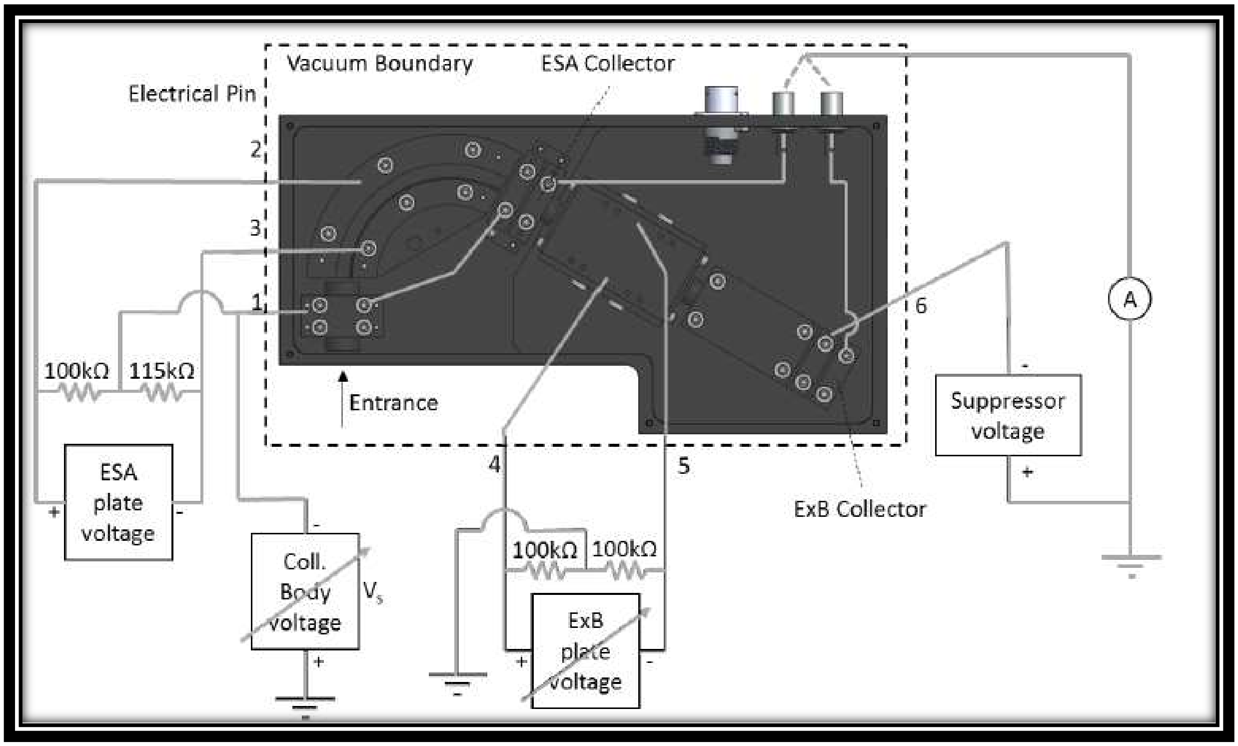

Figure 2.10: Wiring diagram for the EVADER to operate in its original configuration that is intended to be used to characterize ions directed into its entrance aperture in a steady-state manner.

The probe works by taking two traces, the first is where it is operated as an ESA, and then the second is where the ExB is used (incorporating the ESA and ExB stages). The three power supplies are illustrated in the wiring diagram as the ESA plate voltage, the collimator body voltage, and the suppressor voltage. A programmable electrometer, a Keithley 6517b, not shown in the diagram serves as both a variable voltage source capable of either sourcing or sinking current and an ammeter. The Keithley power supply component was used to sweep a range of voltages across elements in the EVADER depending on the mode of operation chosen (ESA or ESA-ExB), and its connections are denoted by the arrow that crosses through the power supplies in Figure 2.10.

To operate just the ESA, only two of the power supplies are active: the ESA plate power supply and the collimator body power supply. In Figure 2.10, the collimator body power supply has an arrow through it that indicates that it is swept through a range of voltages via capabilities built into the Keithley electrometer. The ESA plate power supply biases the plates relative to each other, and the resultant electric field strongly influences the trajectory of the ions that enter the ESA region. This bias specifies the energy per charge that an arbitrarily charged ion must have to "curve or pass" through the ESA stage to its exit. Once the pass energy is set (determined by multiplying the voltage difference by a geometrical factor of 3.55), the collimator body power supply is swept over a range of voltages that correspond to an ion energy range (measured relative to the vacuum chamber wall) from 0 to ~300 eV. The current flowing to the ESA collector plotted as a function of the ion energy corresponds directly to the ion energy distribution function.

Another option for the EVADER probe is to set the voltage across the ESA plates and the voltage of the entrance collimator with fixed voltage power supplies such that a specific ion energy per charge is passed to the exit of the ESA. Then the Keithley power supply is connected across the ExB plates to create a variable E field within the ExB stage. The magnetic field, B, was steady due to the implementation of permanent magnets. The ExB stage is encased in mu metal to shield the stage from external magnetic and electric fields which occur within the Z machine. This ExB stages allows one to characterize the mass and charge state of the incoming ions. The suppressor power supply is also active in this second mode of operation, which acts to retard any secondary electrons that are emitted from the collector, so this current does not perturb the measurement of the ion current.

2.2.2 EVADER | Transimpedance Amplifier Modification

The traditional configuration collects data that corresponds to the steady state characteristics of the ions entering the probe because the rate that the Keithley can be made to sweep voltages and read the corresponding current is relatively slow at about 0.1 settings and readings per second. An ESA or ESA-ExB measurement can take up to several minutes depending upon the size of the voltage steps. Also, running the EVADER in the traditional configuration revealed that the currents from the electric propulsion devices were quite small, on the order of pico-amperes. Therefore, the first iterative change of the EVADER was to replace the ammeter part of the Keithley with a transimpedance amplifier. This was the initial step in phasing out the Keithley entirely, so the system is not restricted by the speed of controlling the electrometer.

The current that was measured with the EVADER in the traditional configuration from the gridded ion source was on the order of pico-amperes. Such low levels of current are difficult to measure and require integration or averaging to reduce noise and specialty elements to mitigate leakage of current. It was decided that the development of a two-stage operational amplifier (op amp) circuit, would provide a significant signal for high-speed measurements of low current. The type of op amp circuit chosen was a transimpedance amplifier (TIA), where the first stage amplifies the current and the second converts the low-level signal of the first stage to an output voltage easily read by a high-speed data acquisition system [25].

A TIA significantly increases the frequency bandwidth over which measurements can be made while decreasing the noise; therefore, it was implemented into the experimental setup for ease of collecting data and making changes to the probe down the road. However, the path to understanding and implementing a circuit that could handle signals at the pico-ampere range was quite difficult. It began with just setting up a simple 741 op amp with a feedback resistor, where the collector lead was connected to the non-inverting input terminal on the op amp and the feedback resistor. This creates a virtual short which forces all the current to be driven through the feedback resistor and converts the current to a voltage [26]. The 741 op amp was tested but could not yield a signal below 100 mA without experiencing excessive noise. Another op amp, the OP27A-JG advertised to be able to handle low currents at high speeds, was tested in a circuit that was enclosed in an aluminum electronics box to help reduce noise. This one was successful up until 500 μA, still very far from the pico-amp range. The final iteration was an evaluation board from Texas Instruments, the LMP7721, which was affordable and can collect low-measurement data at high speeds. It is manufactured in a non-inverting form, but with the option to be modified into an inverting or transimpedance amplifier configuration. Figure 2.11 was the TIA configuration for the evaluation board. Some notable elements were the high impedance resistor of $100\ M\Omega$, the LMP7721 op amp that could only handle a voltage difference of 6 V, the triax input jack that helps send the low-level current into the evaluation board without losses or noise, and the guard buffer that prevents the signal from being affected by other external currents or voltages.

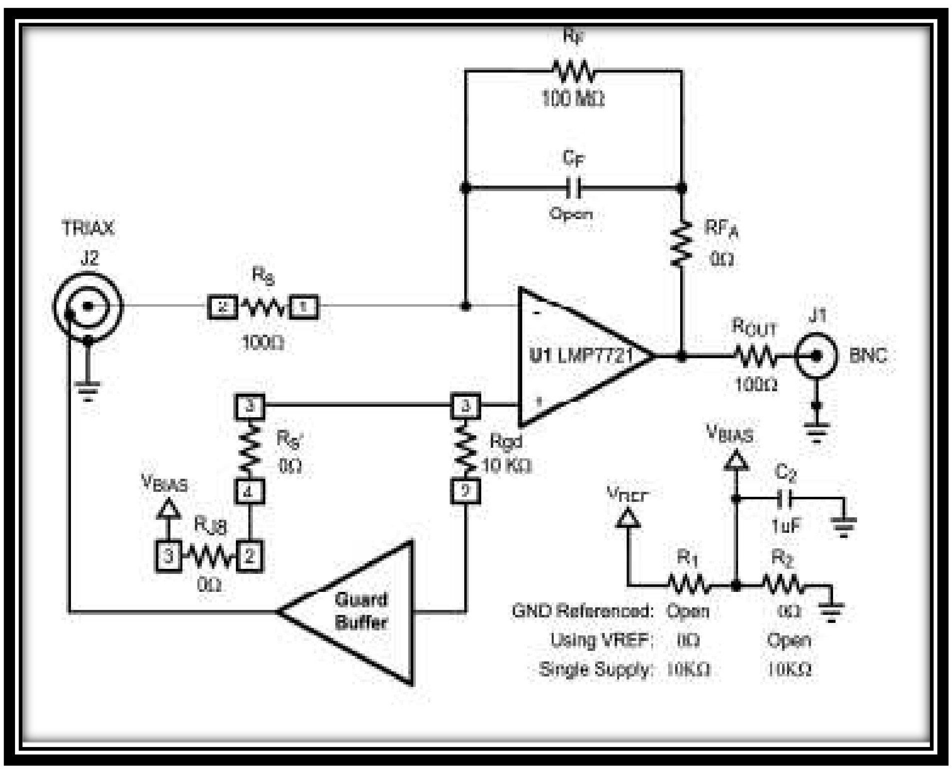

Figure 2.11: The Texas Instrument TIA schematic for the LMP evaluation board [27].

The TIA circuit was bench tested at 100 Hz and successfully measured currents in the 10s of pico-amps. It was then fixed in an electronics box for noise mitigation and connected to the output of the EVADER from the vacuum chamber to the Keithley 6517b. The Keithley was utilized to sweep the voltages in the probe, and the TIA circuit was connected to an Agilent 34401A digital multimeter that was used to read the signal from the TIA.

2.2.3 Faraday Probe

Another plasma diagnostic tool called a Faraday probe was set up in the Orion chamber that was used to measure the current density in the plasma plume expanding from the Flamethrower. While this probe is not a part of the EVADER, it can help provide information on the beam created by the Flamethrower and allow one to characterize the performance of the Flamethrower as an electric propulsion device.

Faraday probes work by biasing the probe negative to collect ions from the plasma it is immersed within and repel electrons. The probe is swept radially through the beam using a motion stage so that a measurement of current density as a function of position can be obtained. The motion stage in Orion can position the Faraday probe over a range of angles from ~55° below the centerline of the Flamethrower to 80° above the centerline at a fixed radial distance of 73.66cm. The measured current density profile (a data set of probe angle and current density) was integrated to calculate the total ion current leaving the Flamethrower, which is termed the beam current. It was noted that actually reaching the ion saturation regime is difficult because as the probe becomes more negatively biased to repel all the electrons, it begins to arc to the chamber. This experiment only biased the probe to -20V, not enough to completely repel all the electrons, which caused an underestimate of the beam current. This integrated value is also inaccurate because some of the ions flowing from the Flamethrower experience charge exchange collisions with the background gas that prevent the original streaming beam ions from reaching the Faraday probe. That being said, the preliminary ion flux measurements can be used to determine the detection limit of the

EVADER. This was done by decreasing the beam current and testing if the EVADER collector would collect a measurable ion current.

$$I_b = 2\pi r^2 \int_0^{\frac{\pi}{2}} j(\theta) sin\theta d\theta \qquad (2.1)$$

As mentioned above, the Faraday probe is mounted on a motion system consisting of an arm that is rotated using a stepper motor. The motor is controlled by a LabVIEW program that sets the angular motion range of the arm. The LabVIEW program also records the current flowing to the Faraday probe and converts this current to a current density by dividing by the probe area.

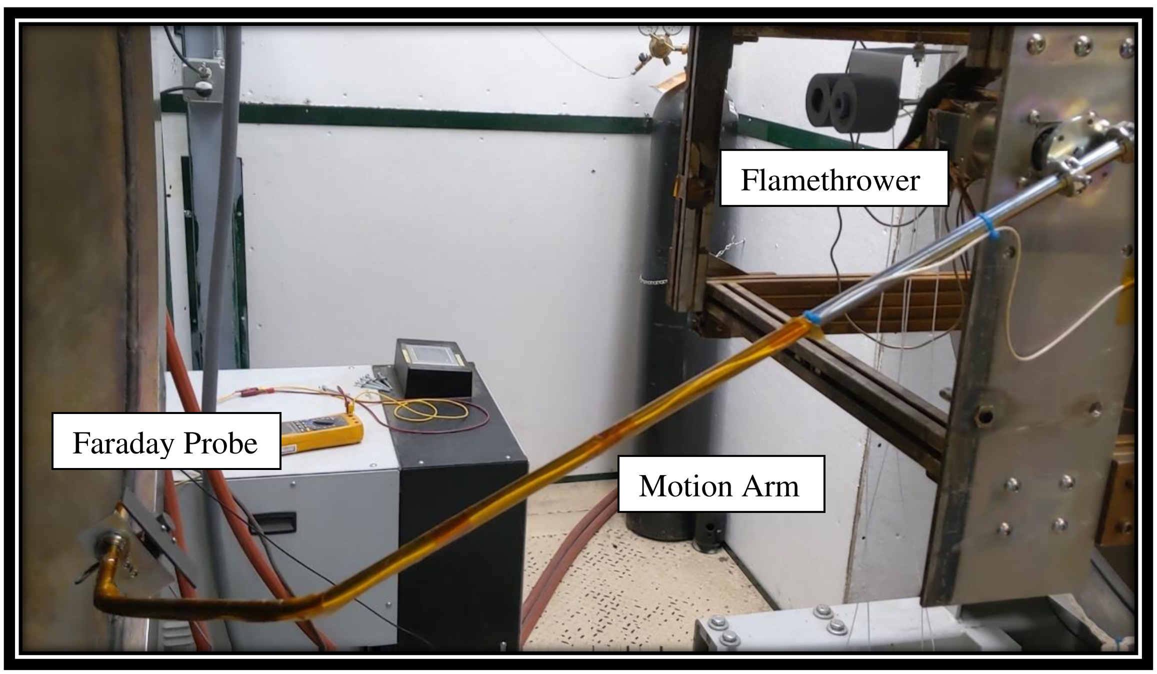

Figure 2.12: Photograph captured in the CEPPE lab of the Faraday probe moving in an arc in front of the Flamethrower.

2.3 Vacuum Facilities

There were two vacuum chambers utilized for the tests in this project. The first was the Hydra vacuum chamber that is roughly three feet tall and two feet in diameter. It is equipped with a cryopump to reach hi-vac and hosts the gridded ion source. Then there is the Orion chamber that is five feet in diameter and fifteen feet long. Orion reaches hi-vac with the use of two diffusion pumps.

2.3.1 Hydra Vacuum Chamber

The Hydra chamber was a smaller chamber that reaches low pressures using one cryopump. The inside was rather simple, it hosts the gridded ion source on the ceiling, pointing down toward the EVADER probe. All the cables were wrapped in aluminum foil to protect them from degrading rapidly. Ultra-pure Argon was used as the main gas propellant in the chamber for the ion source.

Figure 2.13: Front view of the Hydra chamber.

2.3.2 Orion Vacuum Chamber

The Orion chamber is much larger than Hydra, it reaches low pressures by using two diffusion pumps. The chamber can achieve baseline pressures of 1.0×10^{-6}Torr.

Orion is also equipped with a thrust stand based on a hanging; double pendulum that was used to measure the thrust produced by the Flamethrower. This measurement along with flow rate and power enable one to calculate the specific impulse and thruster efficiency—parameters important to judge if an electric propulsion device is competitive with other devices. The gas lines and electrical leads are routed through the thrust stand in a manner to avoid interference with thrust measurements. Figure 2.14 shows a photograph of the plasma source mounted to the thrust stand. The thrust generated by the Flamethrower is conveyed through the mount to the bottom thrust stand plate. This force displaces the bottom plate relative to the fixed plate located above it where a linear variable differential transformer (LVDT) is used to measure the displacement. An in-vacuum calibration system is used to convert the LVDT displacement measurement to a thrust value.

Figure 2.14: Photograph of the Flamethrower mounted to the bottom plate of the thrust stand, facing the EVADER.

A motion stage is also shown in Figure 2.14 that was used to position the EVADER probe in the region downstream of the Flamethrower. The stage allows for precise alignment of the EVADER relative to the source and provides the option to position the probe over an axial range from ~10 cm to 150 cm. A closeup photograph of the motion stage is shown in Figure 2.15.

Figure 2.15: The EVADER is secured to a motion stage that can position the probe throughout the chamber to a desired location.

Chapter 3 Results and Data Analysis

This chapter contains a description of how data was collected and analyzed. After this, results are presented for EVADER measurements on the gridded ion source and Flamethrower with and without the TIA circuit.

3.1 Data Collection Procedures

A procedure was implemented to collect consistent data. Since the experiment was operated in two different vacuum chambers and the plasma source in each differs, there are two different procedures. In the Hydra chamber, the ion source was controlled with the IonTech power supply. Argon gas was flowed into the ion source at 3 sccm through the cathode and the neutralizer. Then the emission current on the neutralizer module was set to 200 mA, and on the discharge module, the voltage was set to 60 V and the cathode filament to 3 A. The cathode filament needed to have a large amount of current applied to thermionically emit electrons. The grids were set so that the accelerator grid was at -200 V and the beam grid was at 800 V. The values for the grids are variable and are picked to avoid the beamlets from reaching the perveance or crossover limit as shown in Figure 3.1 [28].

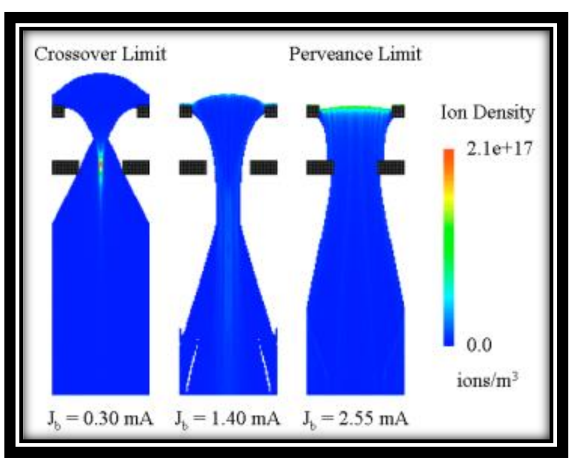

Figure 3.1: The ion beamlet profiles from an ffx simulation, where the beamlets are going through the screen and accelerator grids. The left beamlet is in the cross over limit (too low beamlet current) and the right beamlet is in perveance limit. The center beamlet has no direct impingement, which is ideal [28].

Once the beam is on and set, the ion energy was adjusted so the screen voltage was 300 V and the accelerator voltage was -250 V. The next step was to run the EVADER probe in its traditional configuration to act as the basis of comparison.

Both ESA and ExB data were collected, and these data are referred to below as traces. A trace is where the EVADER signal is plotted against the energy or plate voltage corresponding to the details explained in Chap. 2.

The EVADER has three cables that connect from the probe itself to the power supplies outside of the vacuum chamber. One cable has 6 wires that corresponds to the pinouts in Figure 2.10 that all connect in an electronics box shown in Figure 3.2. The other cables are triax cables that connect to feedthroughs, one is connected to the ESA collector and the other is connected to the ExB collector. Figure 3.3 shows a photograph of the electronic box, power supplies, and electrometer.

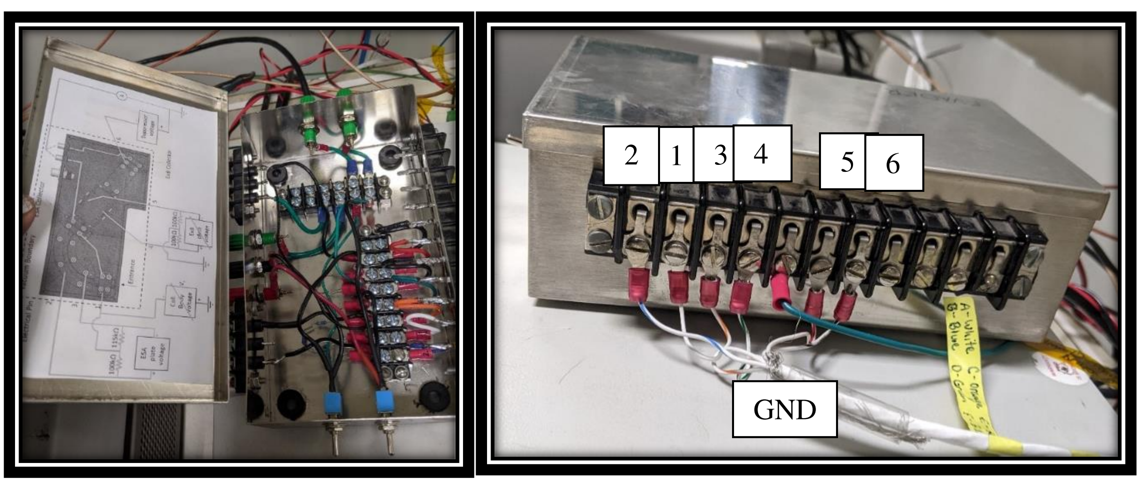

Figure 3.2: The EVADER electronics box that connects the EVADER electrical leads to the corresponding connections on the power supplies and electrometer.

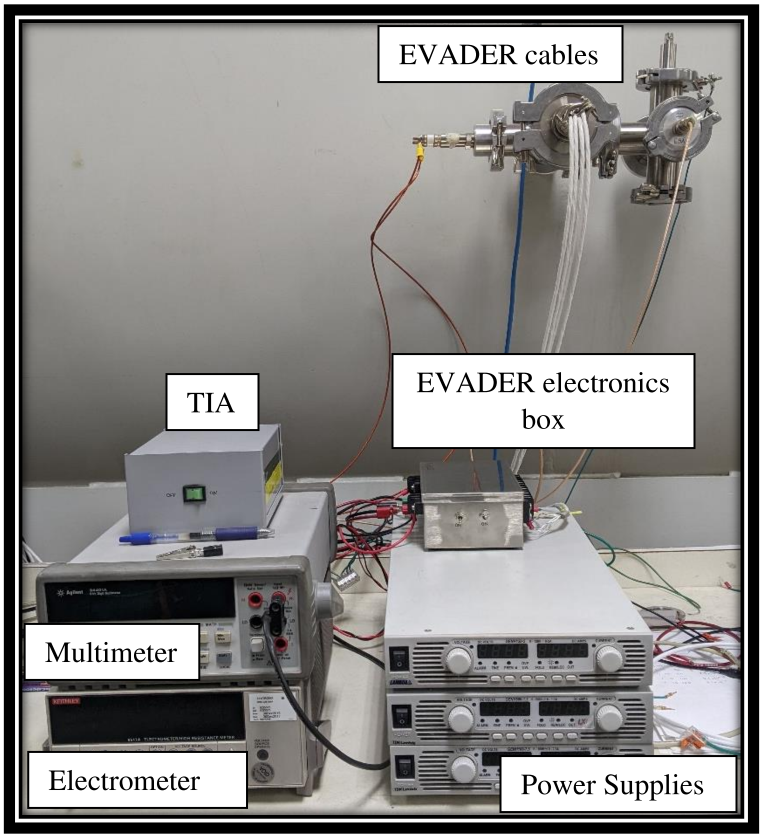

Figure 3.3: Transimpedance amplifier circuit configuration that includes the TIA in an electronics box on top of the multimeter, Agilent 34401A, and electrometer, Keithley 6517b. Photo taken in the CEPPE lab.

At this point, traces were taken with the EVADER in the traditional configuration with just the Keithley and in the TIA configuration with the ion source. Then the experimental apparatus was moved to the Orion vacuum chamber to take traces with the Flamethrower plasma source.

It is worth mentioning that an 8-cm ion source from the CEPPE lab was taken to Sandia National Laboratories to work on the development of the high-speed mass spectrometer from the EVADER. However, the Keithley 6517b was unavailable, so a Sorenson power supply capable of voltages 0-600 V was used to sweep the voltages, and a Keysight B2981A was used in conjunction to measure the current. Otherwise, the rest of the set up was the same. The experiment was set up at Sandia to expand the testing resources by simulating the desorption process occurring in the MITLs through temperature programmable desorption (TPD). The TPD chamber was set up to heat a sample of 316 stainless steel while under vacuum and desorb any contaminants off the metal. The ion source would ionize the contaminant neutrals and the EVADER would then detect all the species within the chamber. Unfortunately, the TPD study could not be conducted, however the Keysight set up was tested with just the ion source and EVADER.

Within Orion, the Flamethrower was hooked up to the thrust stand and operated by sending 60 sccm of Krypton to the anode and 30 sccm of Krypton to the cathode. The gas flow rates needed to be high to start the plasma discharges. The flow rates were adjusted to lower values after the device was started. The keeper power supply was set to 600 V and 1.5 A and the anode was set to 400 V and 2 A. These values are also arbitrary, they just needed to be high enough for the Flamethrower plasma discharge to be initiated. Once the Flamethrower discharge was started, the flow rates were changed to 10 sccm for the anode and 5 sccm for the cathode. When the flowrate was decreased, the voltage to the hidden anode increased into a range between 50 and 200 V depending upon the discharge current that was chosen. Initial operation was performed at a hidden anode current of 0.5 A. Figure 3.4 shows a photograph of the two power supplies during initial operation.

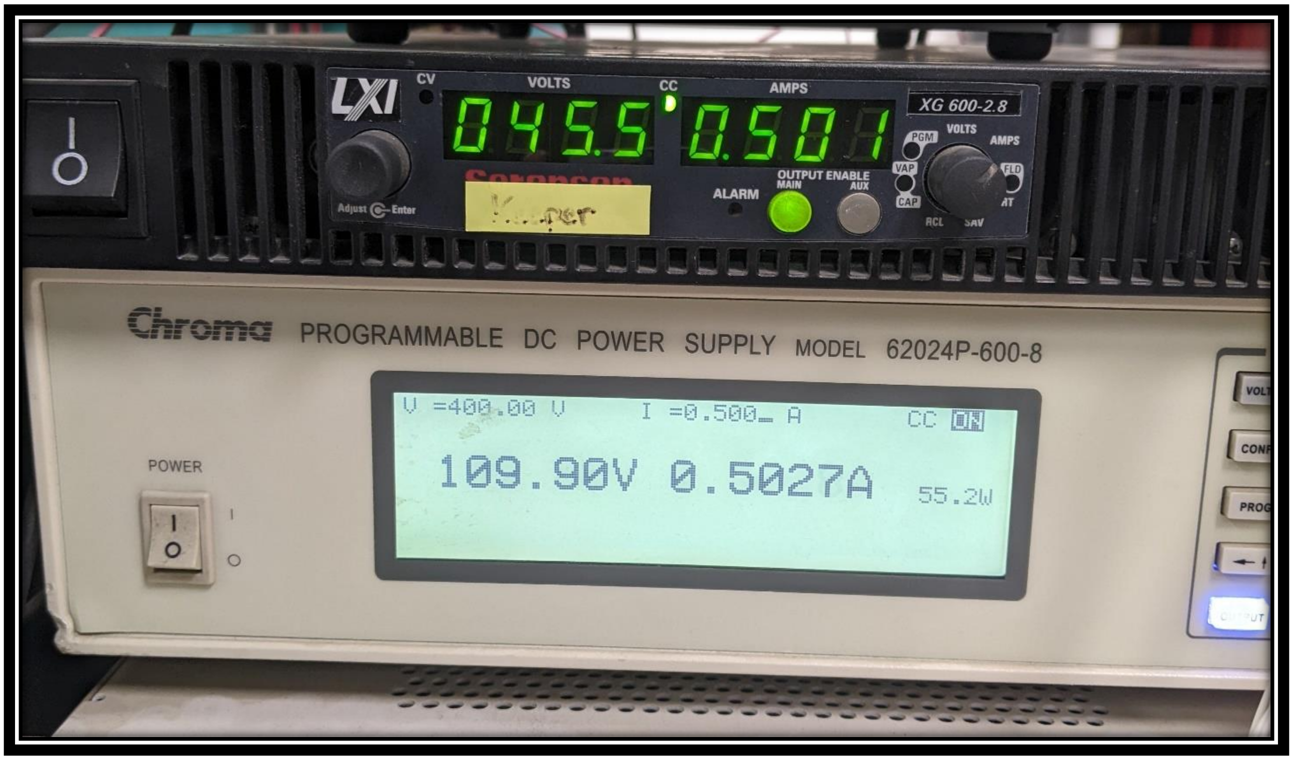

Figure 3.4: The power supplies on Orion to operate the Flamethrower. The top power supply's positive lead is connected to the keeper, and the bottom power supply's positive lead is for the anode. The negative leads on both power supplies are connected to the cathode. A ballast resistor is installed in the electrical lead going to the keeper, and this causes the keeper power supply voltage to be higher than it would be without the ballast.

Once the Flamethrower is on, the EVADER was used to take traces in the traditional and TIA configurations, however, in Orion, there is a diagnostic suite that allows the EVADER to take traces at a variety of distances from the Flamethrower.

Figure 3.5: Probe suite in Orion vacuum chamber that allows 4 degrees of freedom. Here the EVADER is 150 cm away from the Flamethrower.

Once the traces are taken by the EVADER probe, the EVADER was sent towards the back of the vacuum chamber and the Faraday probe was used to measure the current density of the beam, which was used to calculate the ion current flowing from the Flamethrower. Finally, the thrust stand was used to measure the thrust and calculate thruster efficiency and specific impulse.

3.2 Results

This section presents results from the various experiments that were performed with the instruments and plasmas described above.

3.2.1 Evader Measurements with the Gridded Ion Source

The ion source was operated at the conditions listed in Table 3.1.

Table 3.1: Ion Source Beam Parameters

Test	Pressure	$\dot{m}_A$	$\dot{m}_C$	V_B	I_B	V_A	I_A
Type	*Torr*	*sccm*	*sccm*	*V*	*mA*	*V*	*mA*
ESA	9.10E-5	3	3	300	17	-250	1
ExB	9.07E-5	3	3	300	17	-250	1
ESA	9.74E-5	3	3	300	17	-250	1
ExB	9.68E-5	3	3	300	17	-250	1
ESA	9.66E-5	3	3	300	17	-250	1
ExB	9.66E-5	3	3	300	17	-250	1

An ESA trace from the EVADER yielded the uncorrected ion energy distribution that is shown in Figure 3.6.

Figure 3.6a represented the raw data of current to voltage when the ESA pass energy was set to 375 eV, where the current is the signal produced by the ions and the voltage is the range of voltages applied to the ESA ion collimator. The trace is corrected in Figure 3.6b by adding the energy of the beam as seen in Equation (1.1) so the ion energy distribution function is properly portrayed as the actual energy of the beam. This is more desired than the raw data because it gives a distribution of the plume ions by their energy per charge to characterize the plasma

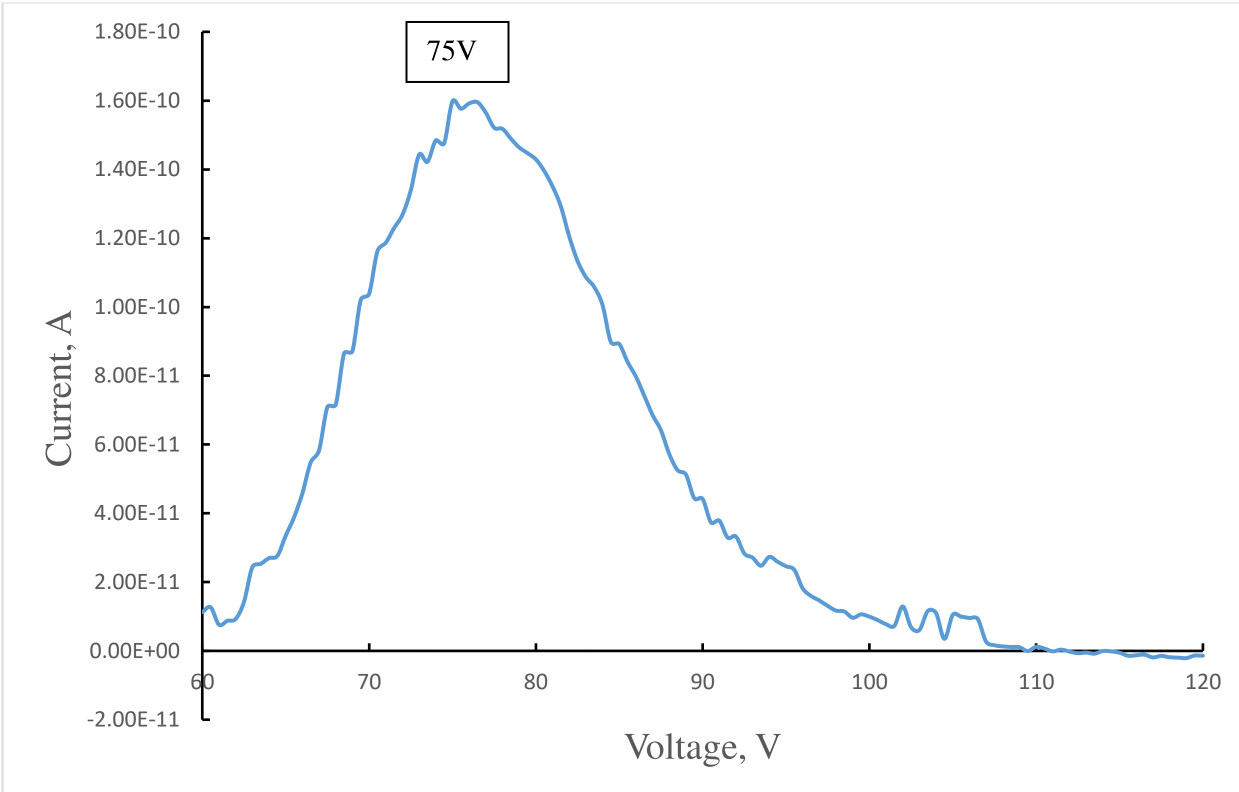

a) Raw, uncorrected ESA data plotted against the voltage applied to the ESA collimator.

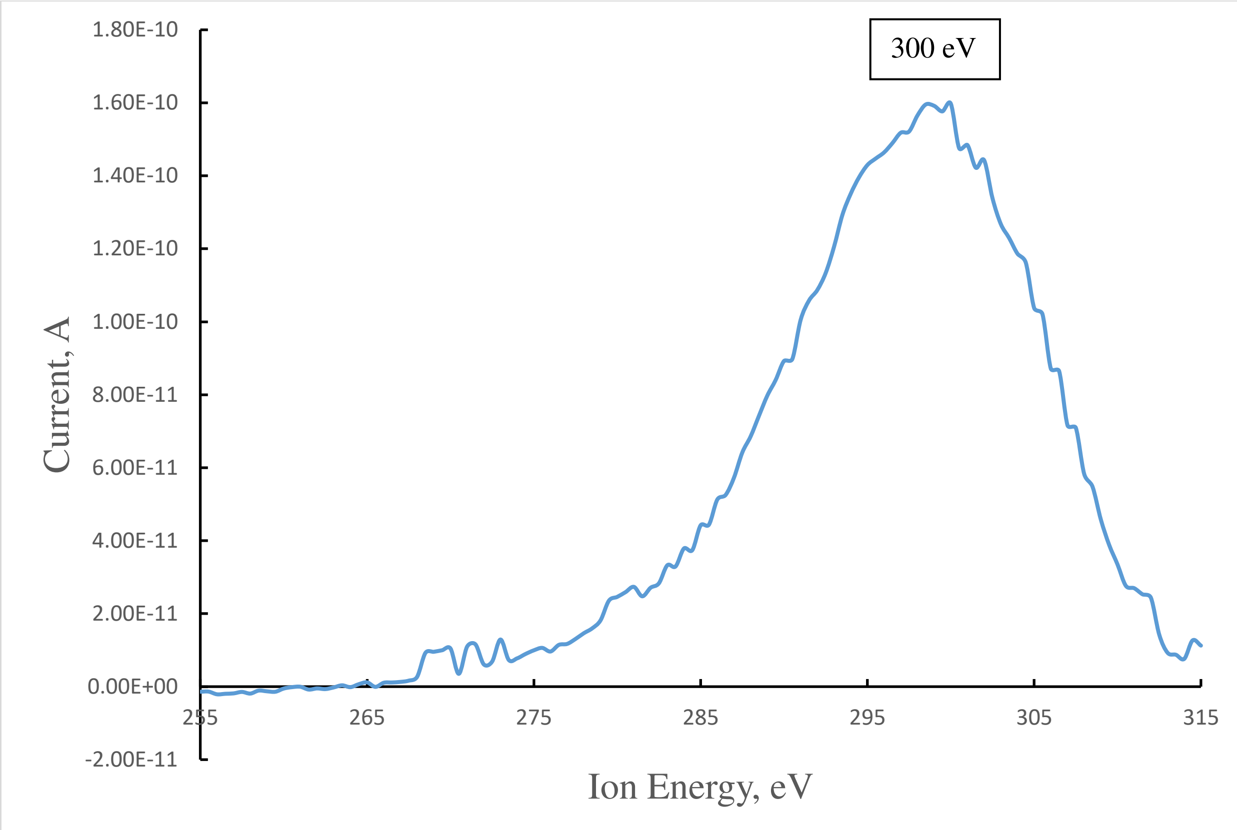

b) Corrected ESA data plot for an Ion Energy Distribution Function (IEDF) with ion energy referenced to ground potential.

Figure 3.6: a) An uncorrected ion energy distribution trace recorded using the electrostatic analyzer stage in the EVADER in the traditional configuration with the Keithley ammeter. The magnitude of the voltage applied to the ESA collimator was swept from 60-120 V, and the fixed voltage applied between the spherical plates corresponded to a pass energy of 375 eV. b) The actual swept voltage applied to the plates is negative of ground, which accelerates ions entering the probe, and hence the ions detected under these conditions correspond to ion energies of 315 eV to 255 eV. Plotting the ExB collector current versus ion energy (measured relative to ground) results in an ion energy distribution function plot where the most probably energy is observed to occur at the expected 300 eV location.

In Figure 3.6a, the most probable location for ions to be detected occurred at 75V. As mentioned in the caption of Figure 3.6a, the magnitude of the voltage is plotted on the trace, but this voltage is actually negative of ground and the ions entering the ESA are accelerated by this amount. A 300 eV ion was expected, and, when it is accelerated from its initial energy of 300 eV by an additional 75 V, it would have the needed 375 eV to pass through the spherically curved, nested plates and be recorded as current to the collector—so the peak occurring at 75 V was expected. The full width, half maximum energy range was ~18 eV, which corresponds to a convolution of the actual energy spread of the ion beam and the energy resolution of the ESA stage. For making measurements of the ion species in a plasma, the ExB stage used. An ExB trace corresponds to a plot of the current to the ExB collector versus the voltage difference applied to the plates within the ExB state. A typical ExB probe trace is shown in Figure 3.7. where a single pronounced peak is shown at 44 V that corresponds to singly charged Ar ions at ~300 eV.

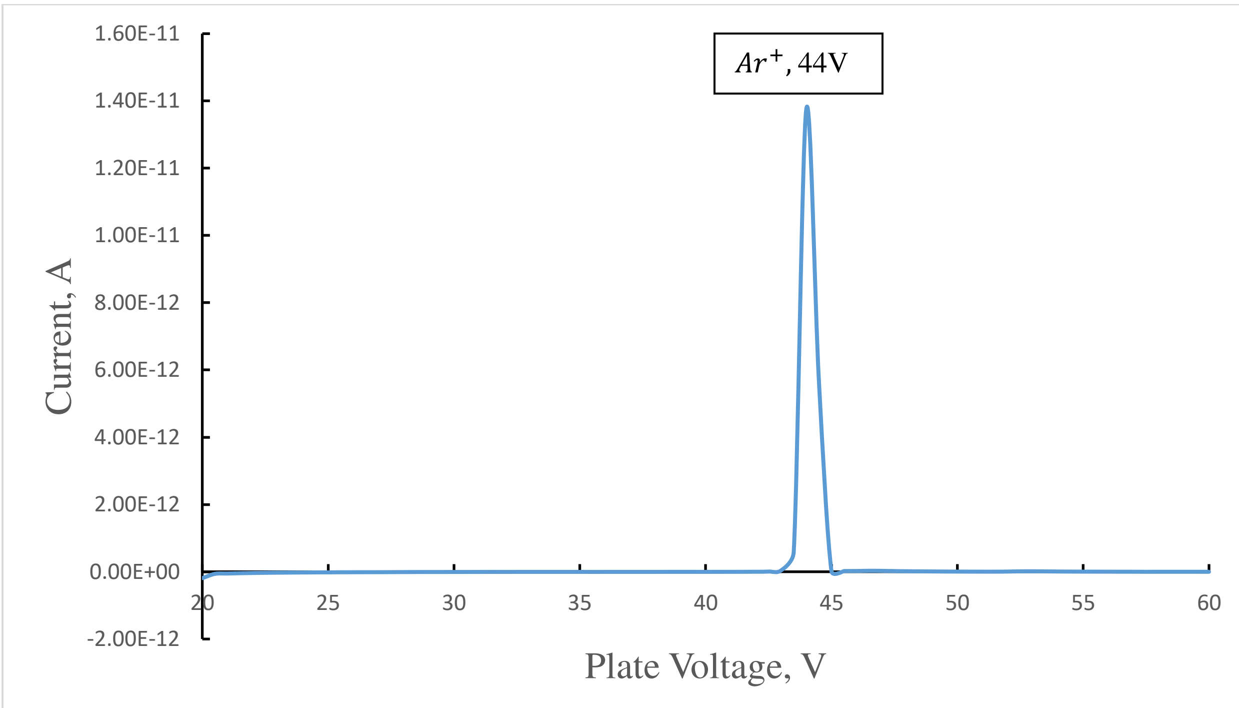

Figure 3.7: Typical ExB trace obtained using the ESA and ExB stages within the EVADER probe in the traditional configuration that uses a Keithley ammeter. The ion source was operated under conditions where mostly singly charged Ar ions at 300 eV were passed to the probe.

Since the ion source was operated on Argon gas, the well pronounced peak indicates singly charged Argon. However, there are other species present in the vacuum chamber due to the finite ability of the vacuum systems to pump all particles out, including those that are outgassing and desorbing from the chamber walls. An EVADER ExB trace can be used to identify those other species by looking for other peaks that can sometimes be brought out by using a logarithmic scale to plot the collector current. The additional species can be ascertained by noting the voltage where a peak occurs and then using a modification of the Lorentz force balance equation, which is given in Equation (3.1).

$$V = V_0 \cdot \sqrt{q} \cdot \sqrt{\frac{m_0}{m}} \tag{3.1}$$

Where V is the voltage that the unknown species would show a signature, V_0 is the known voltage that a singly charged Argon species appears, q is the charge of the unknown species, m_0 is the mass of Argon, and finally m is the mass of the unknown species.

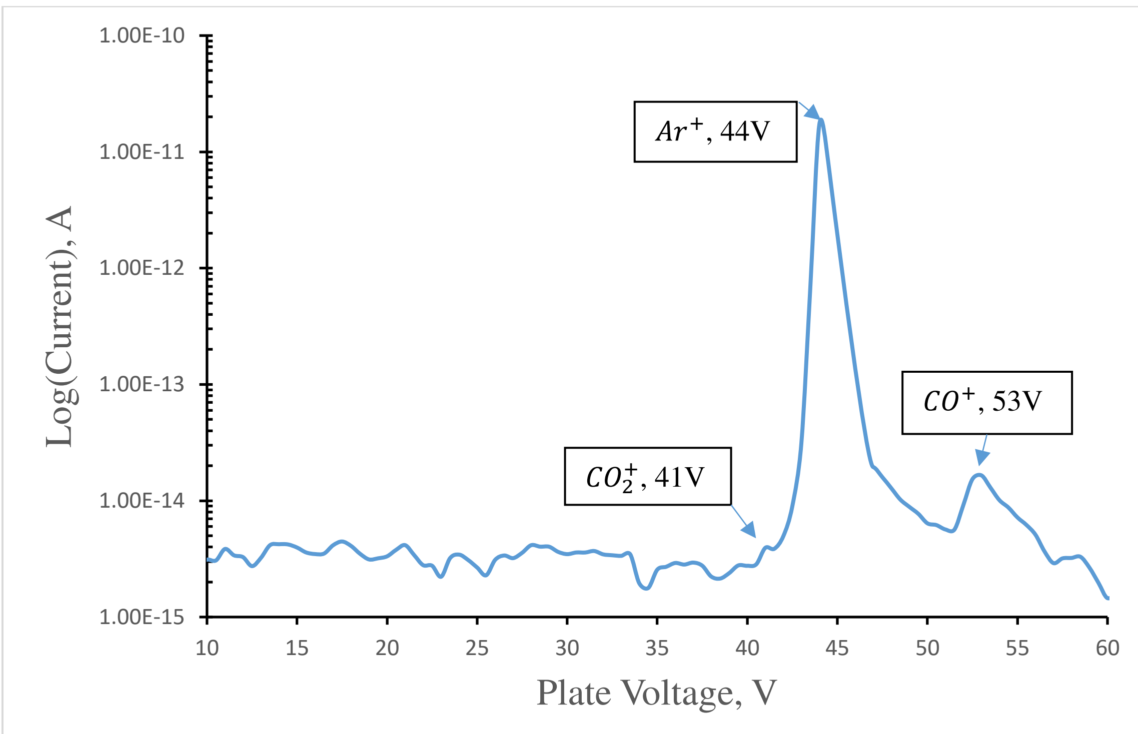

Figure 3.8: Setting the current signal on a logarithmic scale, other species in the ion beam become apparent. Most notably for the Figure 3.7 data, there is a significant peak occurring at 53V. This could be a singly charged carbon monoxide signature as the calculated mass is roughly 27.6 AMU which is close to 28 AMU.

In Figure 3.7, the data in Figure 3.8 is re-plotted, and the second largest peak detected appears to be nitrogen, which has a mass of 28 AMU. The reference species, Argon, has a mass of 40 AMU and the singly charged ions occurred at 44V. This information indicates that the signature for carbon monoxide, CO^+, should occur at 52.5 V based off Equation (3.1), which is rewritten as Equation (3.2) below with values substituted in.

$$V = V_O \cdot \sqrt{q} \cdot \sqrt{\frac{m_O}{m}} = (44V) \cdot \sqrt{1} \cdot \sqrt{\frac{40}{28}} = 52.5\ V \tag{3.2}$$

These results are then reflected in Figure 3.8 that yields a carbon monoxide signature at about 53 V. Given the species of interest listed earlier, they can be searched for within Figure 3.8, and as noted, there is a small signature of carbon dioxide where the mass is 44 AMU and occurs at 41 V. The carbon monoxide ions are presumed to be created when carbon monoxide gas is ingested by the ion source, ionized, and then extracted through the ion optics assembly with the Ar ions. Other species, even isotopes, can be detected with this method. It is worth mentioning that swapping out the Keithley with the Keysight ammeter and a Sorenson power supply yielded results that were identical to those obtained with the Keithley. It is noted that there were peaks detected for both singly and doubly charged Ar when larger ranges of plate voltages were used as shown in Figure 3.9 a and b. The location of singly ionized water molecules is listed in Figure 3.9b, about where a minor peak is observed.

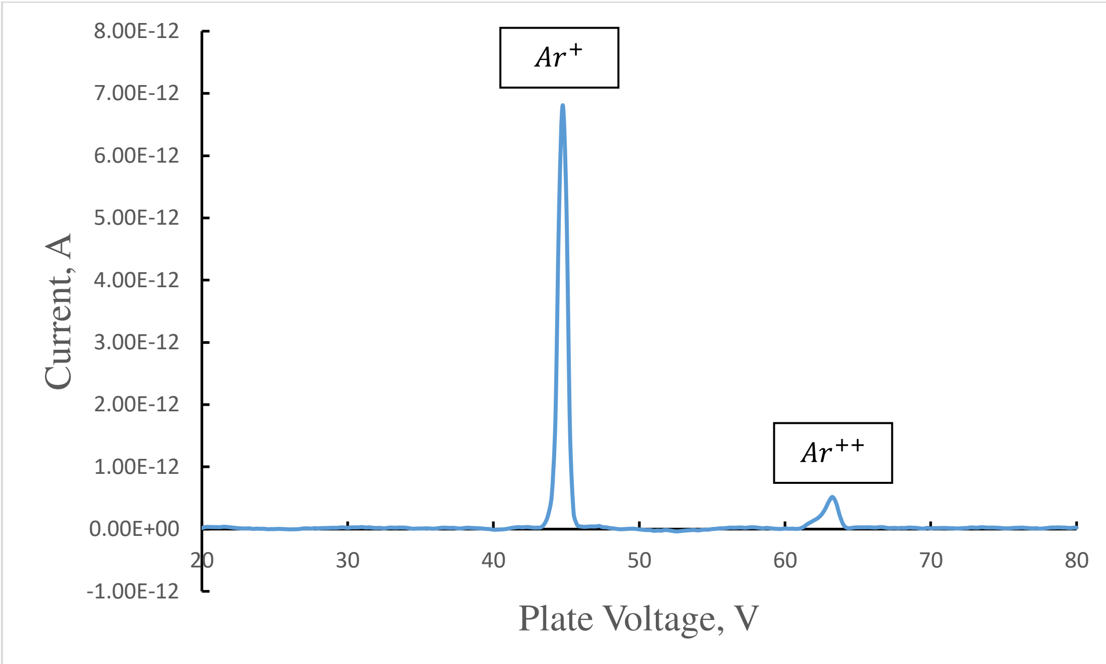

a) ExB trace

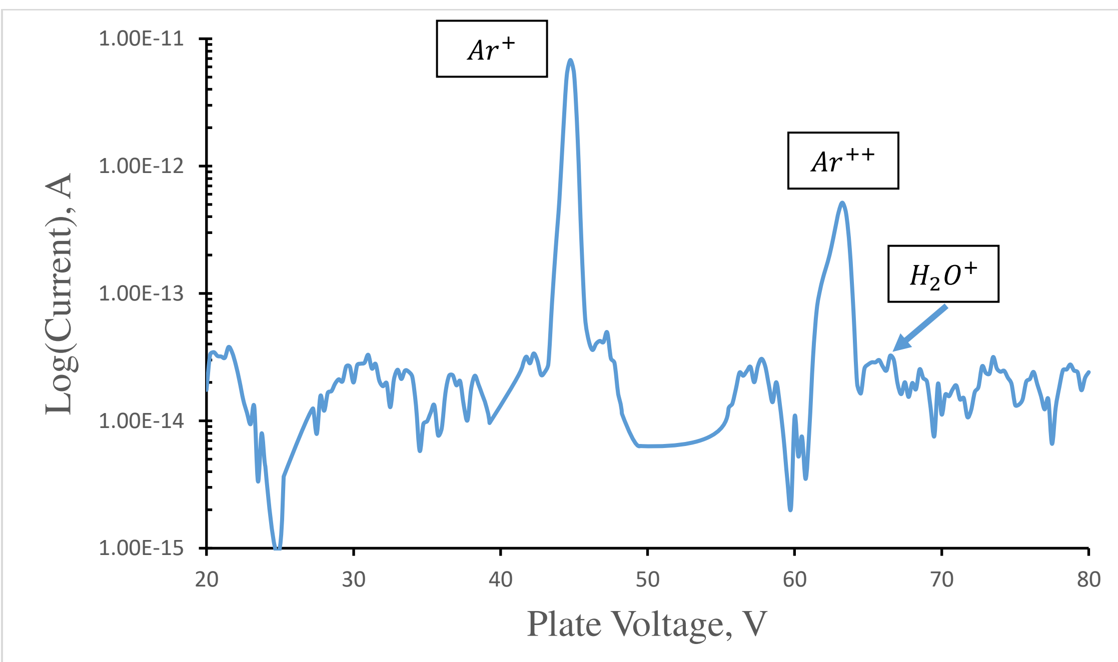

b) Logarithmic signal for a better visual of other species in the beam

Figure 3.9: A) The Keysight and Sorenson configuration produced a ExB trace that shows singly and doubly charged Argon ions are present in the beam. B) Taking the log of the current signal shows other species might be present, and, as an example, current corresponding to singly ionized water molecules (18 AMU) would be expected to occur at 65.6V.

3.2.2 EVADER Configuration with Transimpedance Amplifier

Replacing the low-current measurement ammeter with a transimpedance amplifier was the next step to developing a high-speed mass spectrometer. A high-fidelity ammeter such as the Keithley or the Keysight are great for accurate, low-current measurement, however, their sampling rate is restricted typically to no more than 10 samples per second. Using a transimpedance amplifier, current-to-voltage op amp circuit allows for a much faster sampling rate.

Figure 3.10: The LMP7721 Evaluation Board from Texas Instruments that was re-soldered with surface components and a triax jack to measure low current.

The TIA configuration involved the EVADER cable from either the ESA or ExB stage to first enter the TIA circuit and then the Keithley, which was set in voltage measurement mode. Meanwhile, a separate power supply was used to sweep the ESA collimator or the ExB plate voltages depending upon the stage being used. Note that using a separate power supply to sweep voltages was similar to the test configuration used at Sandia, which utilized a Keysight ammeter that did not have built in power supply like the Keithley does. To successfully take traces, the TIA evaluation board had to be cleaned prior to operation and could only be handled with gloves. In addition, the board was housed in an electronics box, and it was stored in a vacuum sealed, non-static bag with desiccant between uses. This new system was considered successful because even though the signal was converted to a voltage, there was not a loss in detectable current.

Since all the parameters listed in Table 3.1 on the ion source were kept consistent, the peak energy was expected to occur at |-75V| in the raw, uncorrected ESA trace to match the expected 300 eV ions to the 375 eV pass energy. The results of the trace are shown in Figure 3.11a and b, these are fairly similar to Figure 3.6 a and b as expected.

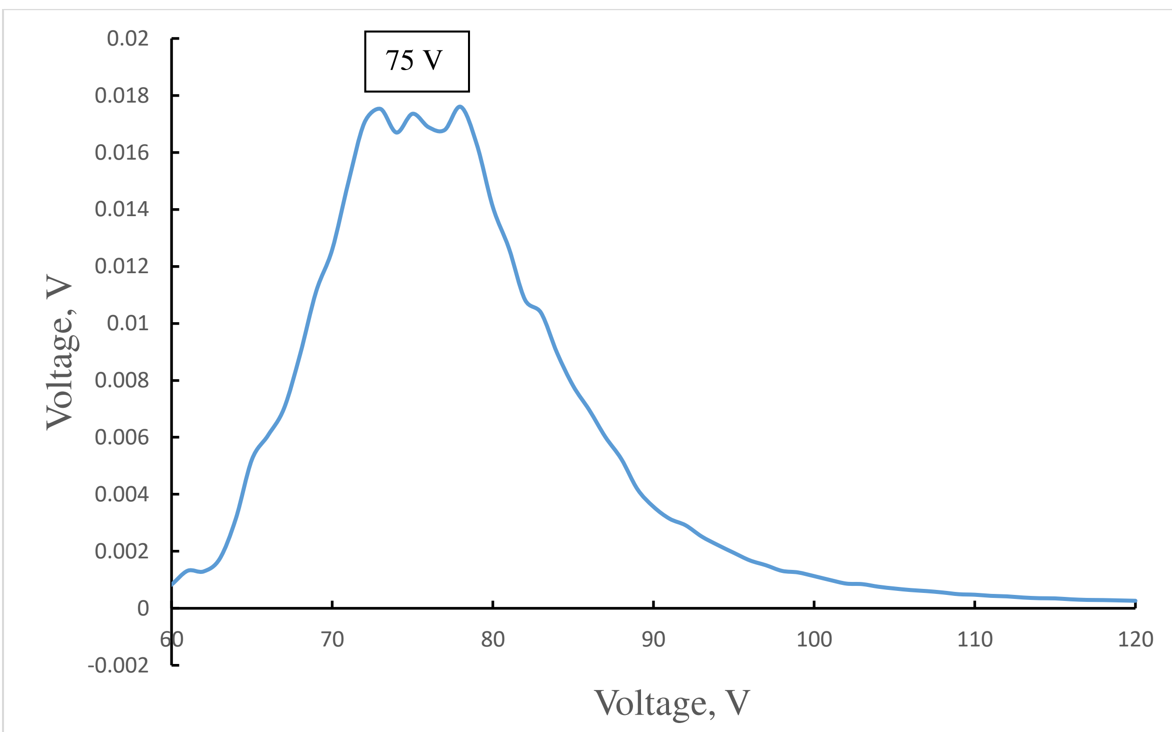

a) Raw, uncorrected ESA trace

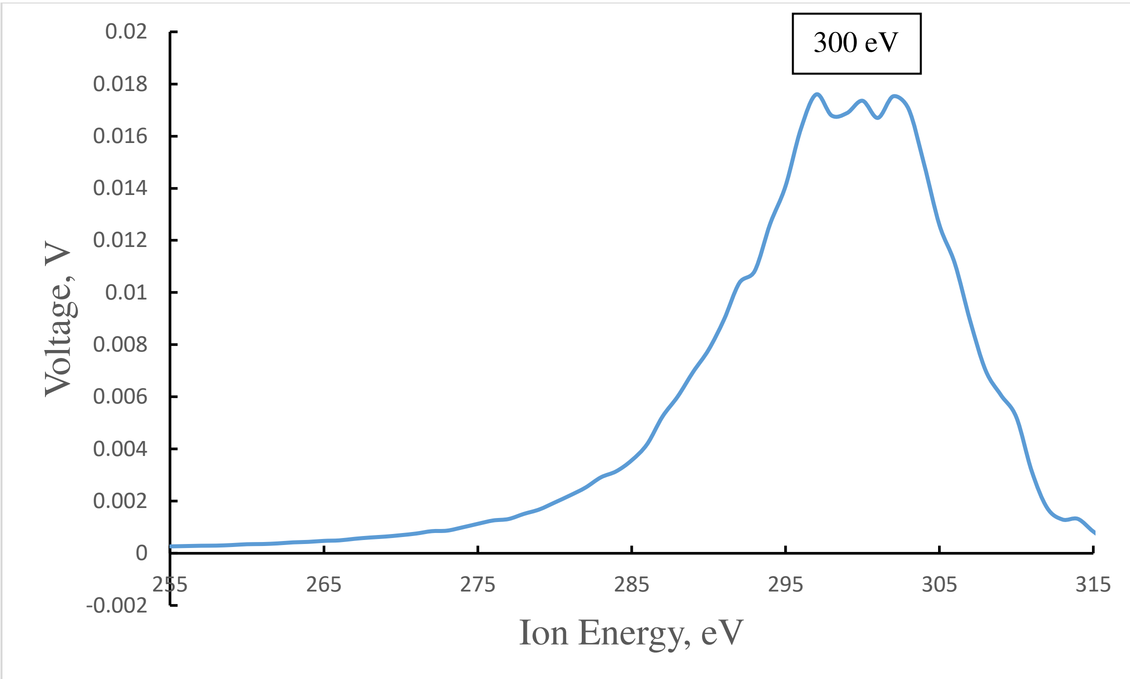

b) ESA trace corrected with pass energy

Figure 3.11: The EVADER signal is sent through the transimpedance amplifier circuit into an electrometer. The peak energy given by the ESA portion of the probe is still 75V. And the signal was amplified and converted to the mV range.

Following suit, the ExB stage of EVADER instrument was connected to the TIA board and singly charged Ar ion were detected at a plate voltage of 44 V as shown in Figure 3.12.

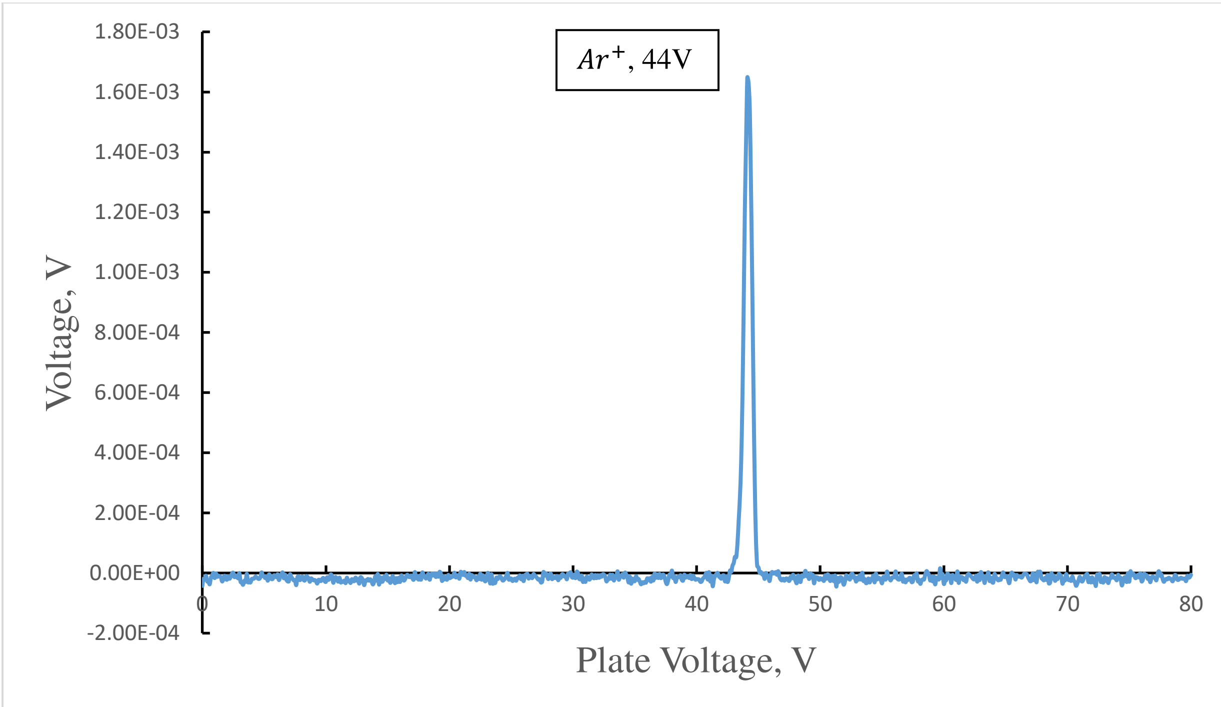

Figure 3.12: ExB trace recorded with the transimpedance amplifier circuit. As expected for Argon, the singly charged peak is registered at 44V. The signal was converted to voltages with the peak being in the low mV range.

The results between the two configurations are compared in the following sub-section to ensure the iterative step was successful and could be used to replace the ammeter within the Keithley. Both configurations were tested on the ion source because the source allows fine control of the incoming ion energy.

3.2.3 Traditional Configuration of the EVADER Probe for Characterization of the Flamethrower Plasma Source

As mentioned earlier, the Flamethrower was operated in the Orion chamber on krypton (Kr) gas at an anode voltage of ~110 V and a current of 0.5 A for a total power of ~55 W. The pass energy of the ESA stage of the EVADER was set at 375 eV. The actual operating parameters of the Flamethrower are shown in Table 3.2 along with the axial location of the EVADER relative to the probe.

Table 3.2: Operating Conditions of the Flamethrower using the Traditional Configuration of the EVADER.

Test	**Pressure**	$\dot{m}_A$	$\dot{m}_C$	V_A	I_A	V_K	I_K	**Distance**
Type	*Torr*	*sccm*	*sccm*	*V*	*A*	*V*	*A*	*cm*
ESA	4.3E-5	5.9	5.0	111.2	0.5	50.2	0.5	30
ExB	4.3E-5	5.9	5.0	111.3	0.5	50.0	0.5	30
ESA	4.1E-5	5.9	5.0	112.0	0.5	49.8	0.5	73.66
ExB	4.1E-5	5.9	5.0	112.2	0.5	49.7	0.5	73.66
ESA	3.8E-5	5.9	5.0	113.2	0.5	49.5	0.5	133.66
ExB	3.8E-5	5.9	5.0	113.3	0.5	49.5	0.5	133.66

Figure 3.13 contains ESA traces of current as a function of voltage that was swept from 150 to 450 V at three different axial distances. The swept voltages of 150 to 450 V correspond to ion energies relative to ground of 225 eV and -75 eV, respectively. Although no ions were expected to be in the range from 0 to -75 eV, the large 450 V sweeping voltage limit was used to ensure that the IEDF characteristics near 0 eV were captured because this is where charge exchange ions would be expected to show up.

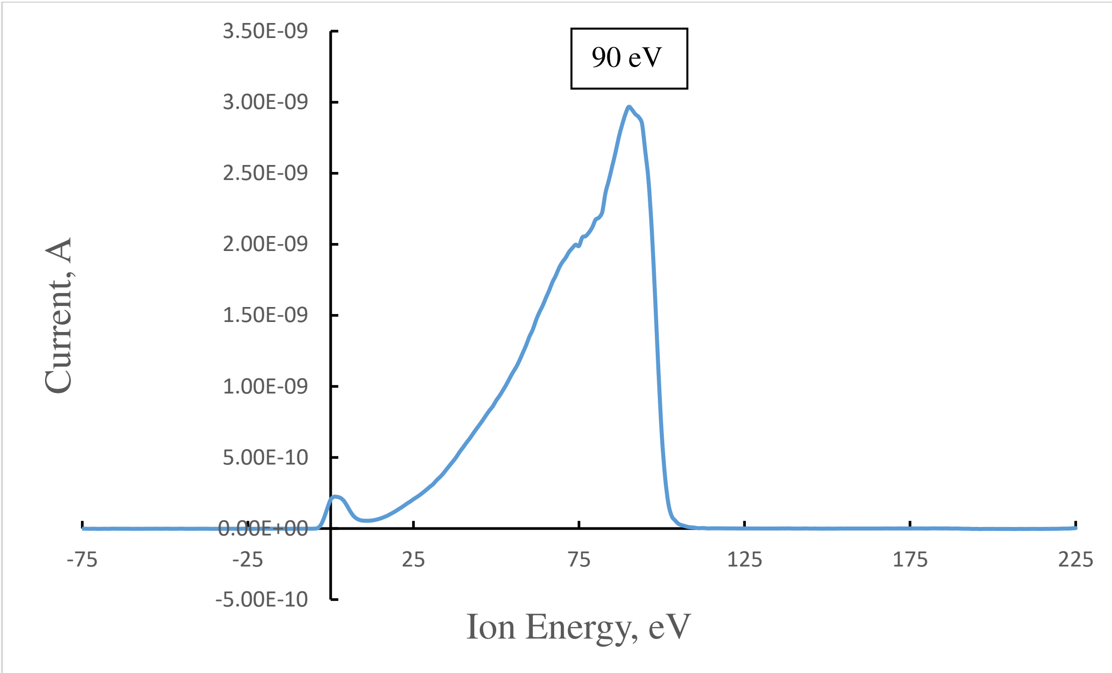

a) 30 cm

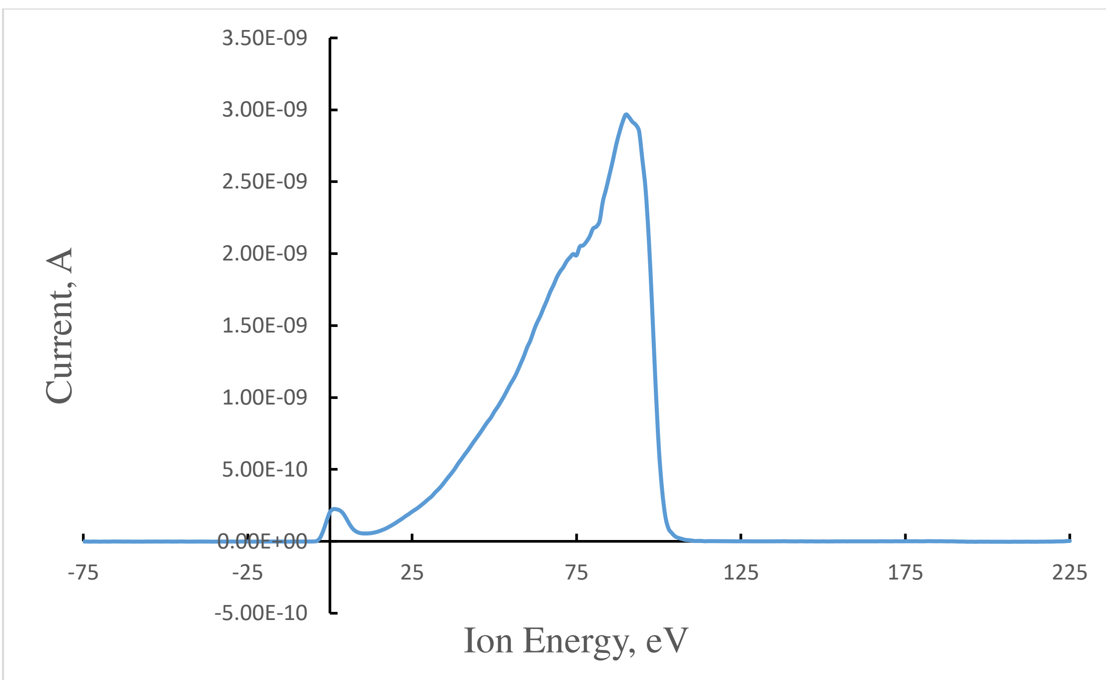

b) 73.66 cm

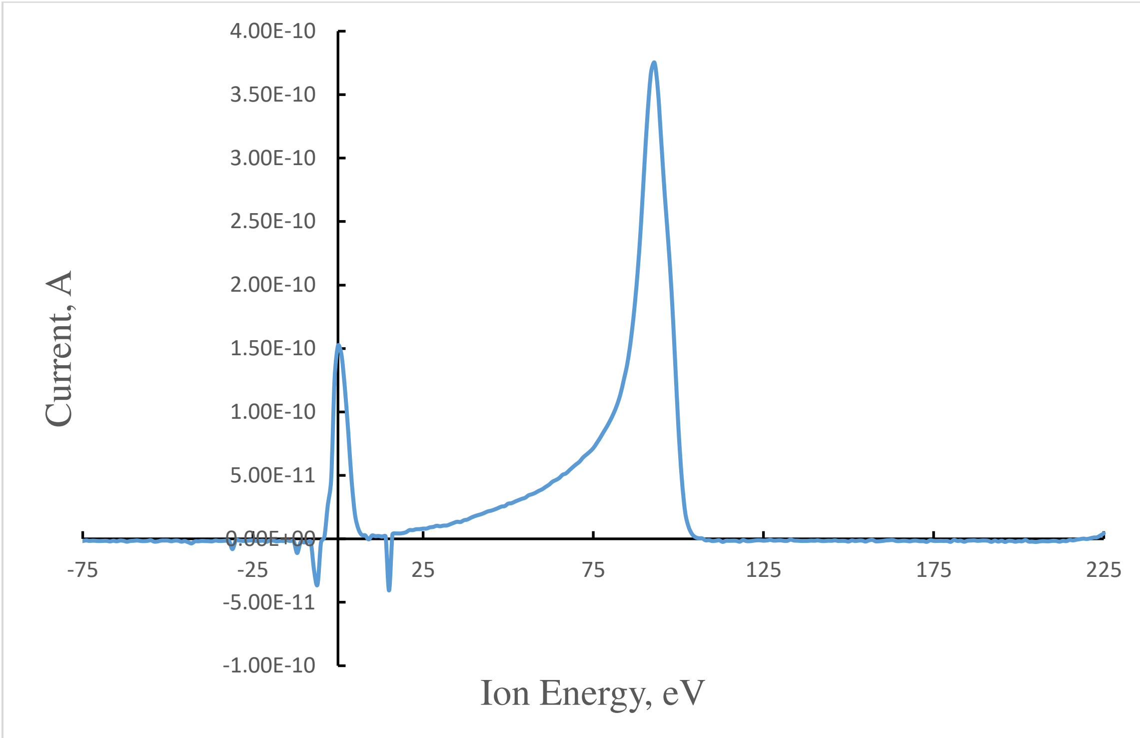

c) 133.66 cm

Figure 3.13: A) A trace using just the EVADER in its traditional configuration on the Flamethrower. The EVADER's aperture was 30 cm away from the orifice of the Flamethrower. B) An ESA trace using the EVADER in its traditional configuration however the EVADER was located 73.66 cm away from the orifice because that is the same distance as the arc radius of the Faraday probe. C) The ESA trace when the EVADER was located 133.66 cm away from the flamethrower that was just an arbitrary distance.

The most probable ion energy was consistently occurring at a swept voltage of around 285 V (ion energy of 90 eV measured with respect to ground) for each distance, the only change was the magnitude of the signal, which decreased as the probe moved further downstream away from the orifice of the thruster due to the expansion of the plume and attenuation by charge exchange collisions. The most probable ion energy was expected to be near the discharge voltage minus the magnitude of the cathode coupling voltage—the voltage that the cathode floated relative to the vacuum chamber walls, which was typically about 20 V—or about 112 V – 20 V = 92 V (92 eV). This energy was expected because it is believed that the largest numbers of ions are produced near the hidden anode potential (measured relative to ground) and these ions fall from that potential to the plasma potential in the vicinity of the probe, which was expected to be near ground potential.

This ion energy would correspond to a swept voltage of about 285 V. It is possible to operate the Flamethrower at higher power levels, and Figure 3.14 contains photographs of the Flamethrower operated at higher power (and right after being switched off) where excessive heat was being deposited into the hidden anode orifice plate causing it to glow red. Higher power levels of operation were not characterized with the EVADER in this thesis.

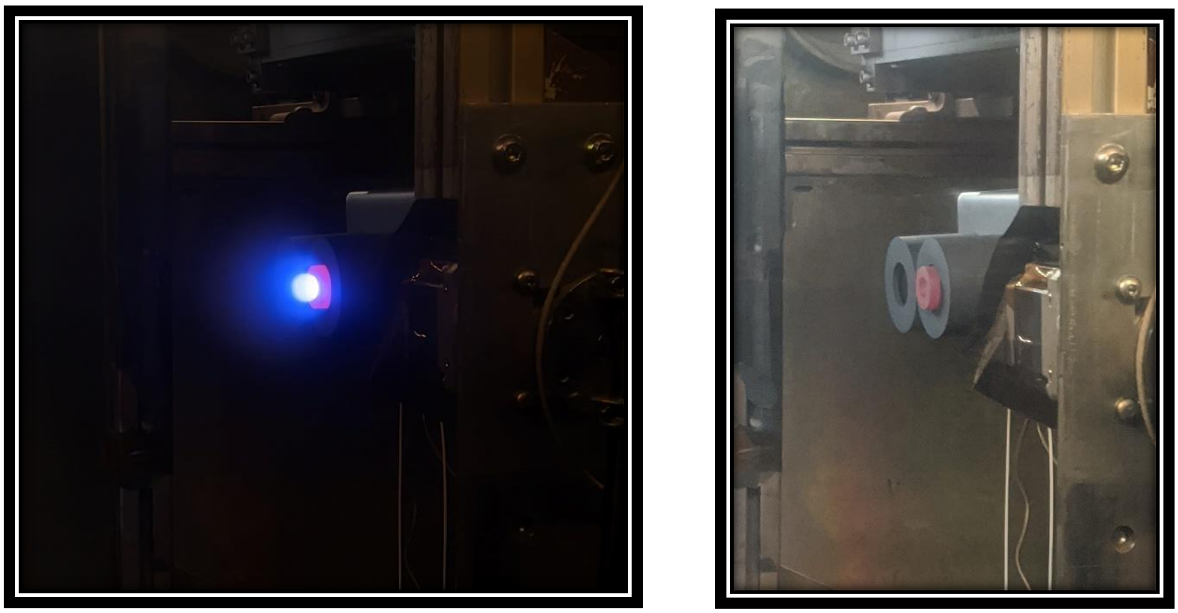

Figure 3.14: The Flamethrower anode orifice was glowing red hot during operation at 300 V (left) and continues to glow red afterwards (right). The electrons and ions were collecting on the orifice instead of being accelerated into the beam, therefore the data collected by the EVADER would not accurately reflect the expected results. Photos taken in the CEPPE lab.

The ESA traces for the Flamethrower are observed to have two peaks instead of one, where the second peak is much smaller but still significant. This smaller second peak occurs near where the plasma potential is expected to be at the probe location and is due to charge exchange collisions that result in low energy ions being produced at the local plasma potential. Charge exchange is when a fast ion passes a slow moving neutral and exchanges as electron with the neutral. After the charge exchange process occurs, one has a fast moving neutral and a slow-moving ion. Charge exchange collision cross sections are much larger than momentum collision cross sections, and so these collisions dominate the collisional processes affecting ions in a plasma that expands through a gas of background neutrals. More charge exchange ions are expected to be produced from the expanding energetic ion stream as the Flamethrower plasma plume expands further downstream. In Figure 3.13 a, b, and c, the charge exchange ions show up at a swept voltage of ~372-374 V, which corresponds to an ion energy of 3 eV to 1 eV measured relative to ground. This also suggests that the plasma potential in the vicinity of the probe was in the 1-3 V range above vacuum chamber ground, which was expected.

Figure 3.15 shows ExB traces taken at the three separate distances from the thruster with the ESA pass energy set to 285 eV where the largest number of streaming ions were observed to occur. These ExB traces were recorded over a plate voltage range from 10 to 40 V. Singly, doubly, and triply charged Krypton ions are observed at 17 V, 24 V, and 37 V respectively.

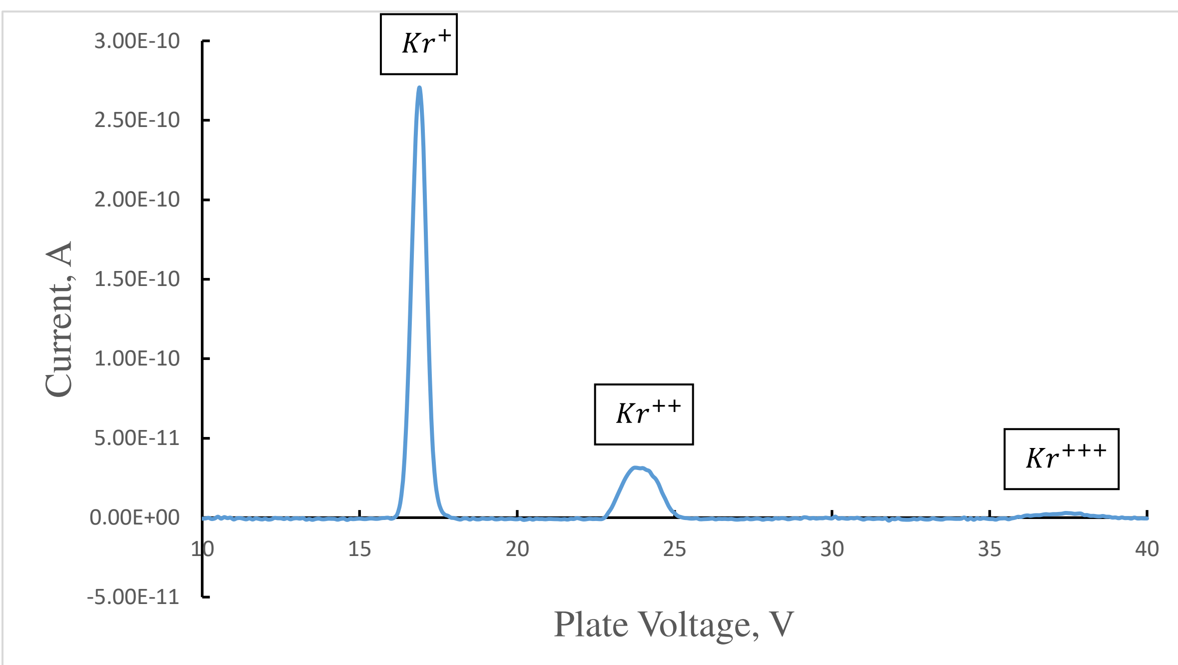

a) 30 cm

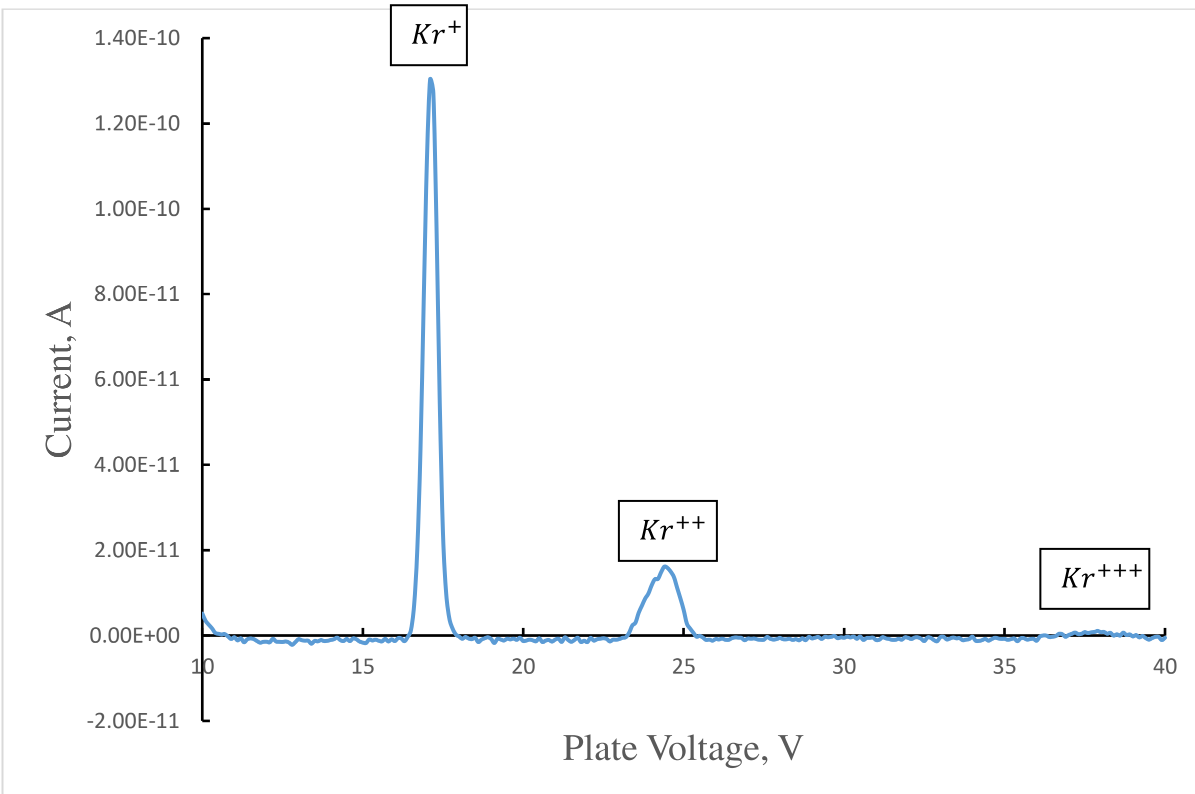

b) 73.66 cm

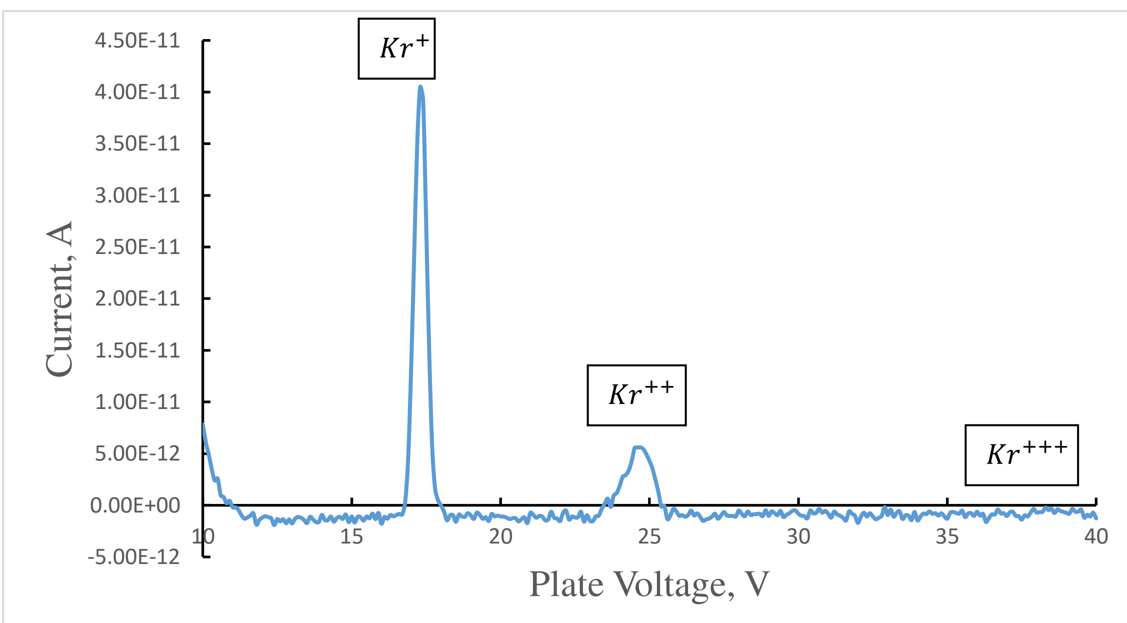

c) 133.66 cm

Figure 3.15: A) ExB trace taken 30 cm away from the Flamethrower. B) ExB trace taken 73.66 cm away from the Flamethrower. C) ExB trace taken 133.66 cm away from the Flamethrower.

From Figure 3.15, plot A was taken 30 cm away from the thruster orifice that shows a large signal of the singly charged current at about 2.75E-11 A and doubly charged of about 4E-11 A. In the following plots, the magnitude of the signal decreases for all the peaks as the probe moves farther away because the density of particles is less as they expand from the Flamethrower and charge exchange with the background neutrals. The signal also becomes noisier due to lower signal strength relative to the noise floor.

3.2.4 TIA Configuration of the EVADER Probe for Characterization of the Flamethrower

The Flamethrower was set to all the same parameters as it was in the traditional configuration of the EVADER probe to keep the results consistent. Then the EVADER was used to record ESA and ExB traces at the three different distances from the thruster.

Table 3.3: *Transimpedance Amplifier Configuration of the EVADER while Operating the Flamethrower.*

Test	**Pressure**	$\dot{m}_A$	$\dot{m}_C$	V_A	I_A	V_K	I_K	**Distance**
Type	*Torr*	*sccm*	*sccm*	*V*	*A*	*V*	*A*	*cm*
ESA	4.0E-5	7.2	5.4	106.8	0.5	48.2	0.5	30
ExB	4.0E-5	7.2	5.4	106.5	0.5	48.2	0.5	30
ESA	3.8E-5	7.2	5.4	106.7	0.5	48.2	0.5	73.66
ExB	3.8E-5	7.2	5.4	106.8	0.5	48.2	0.5	73.66
ESA	3.7E-5	7.2	5.4	106.9	0.5	48.1	0.5	133.66
ExB	3.7E-5	7.2	5.4	107.0	0.5	48.1	0.5	133.66

Figure 3.16 shows the ESA traces taken at 30 cm, 73.66 cm, and 133.66 cm away from the Flamethrower while in the TIA configuration.

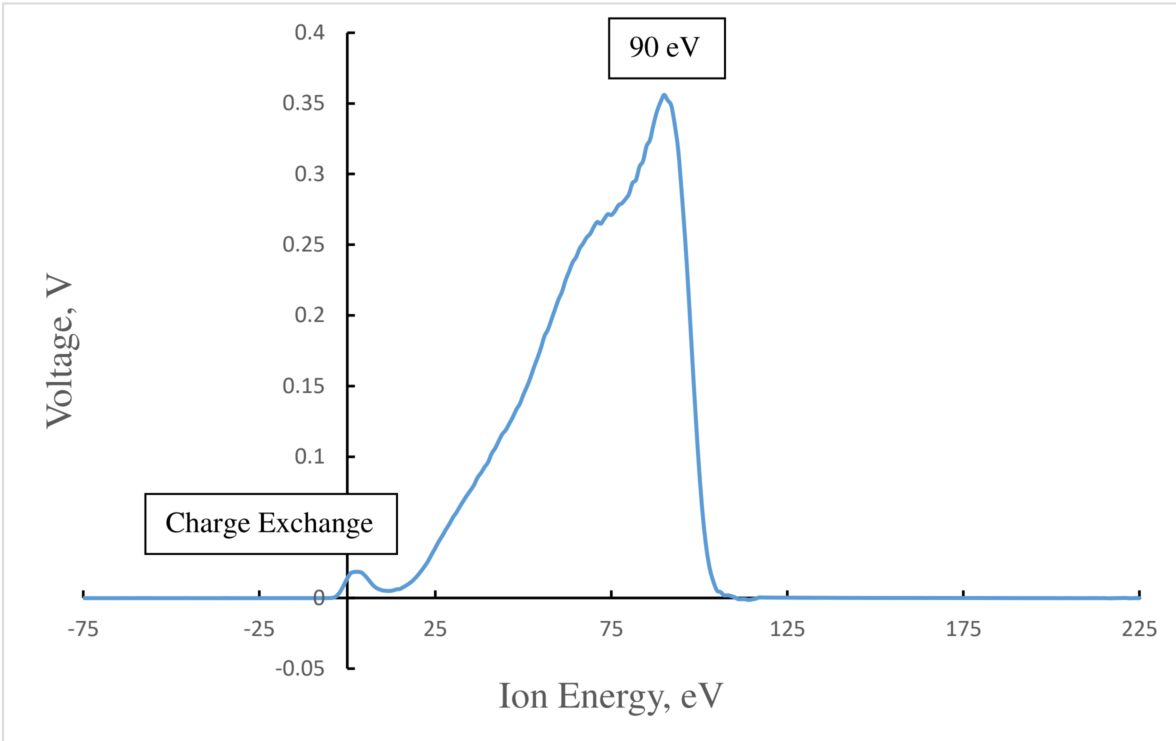

a) 30 cm

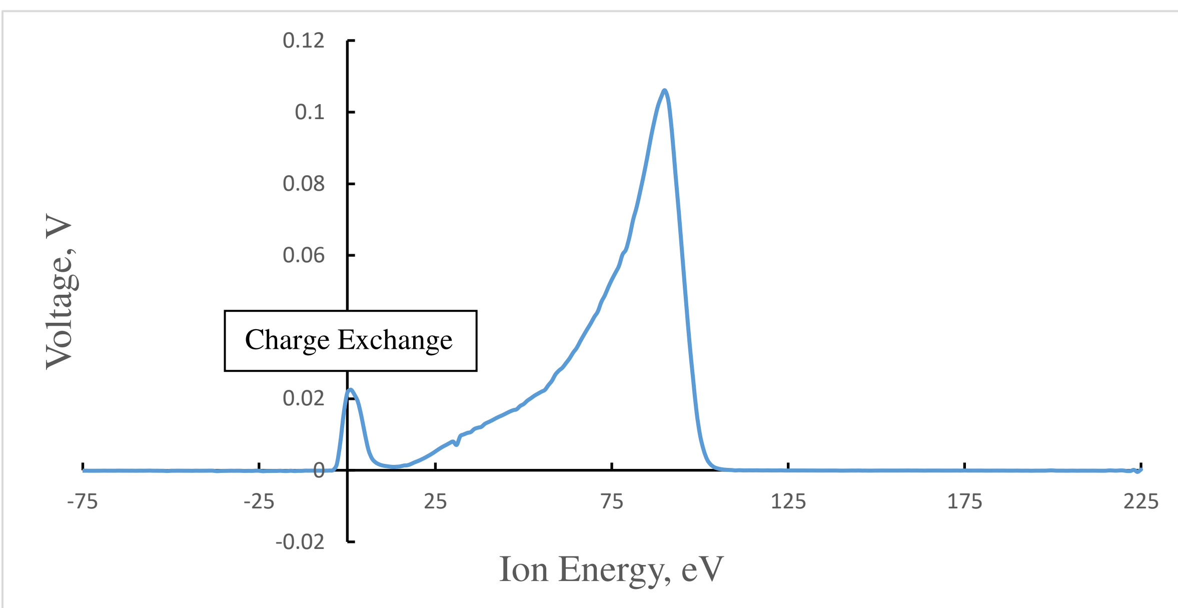

b) 73.66 cm

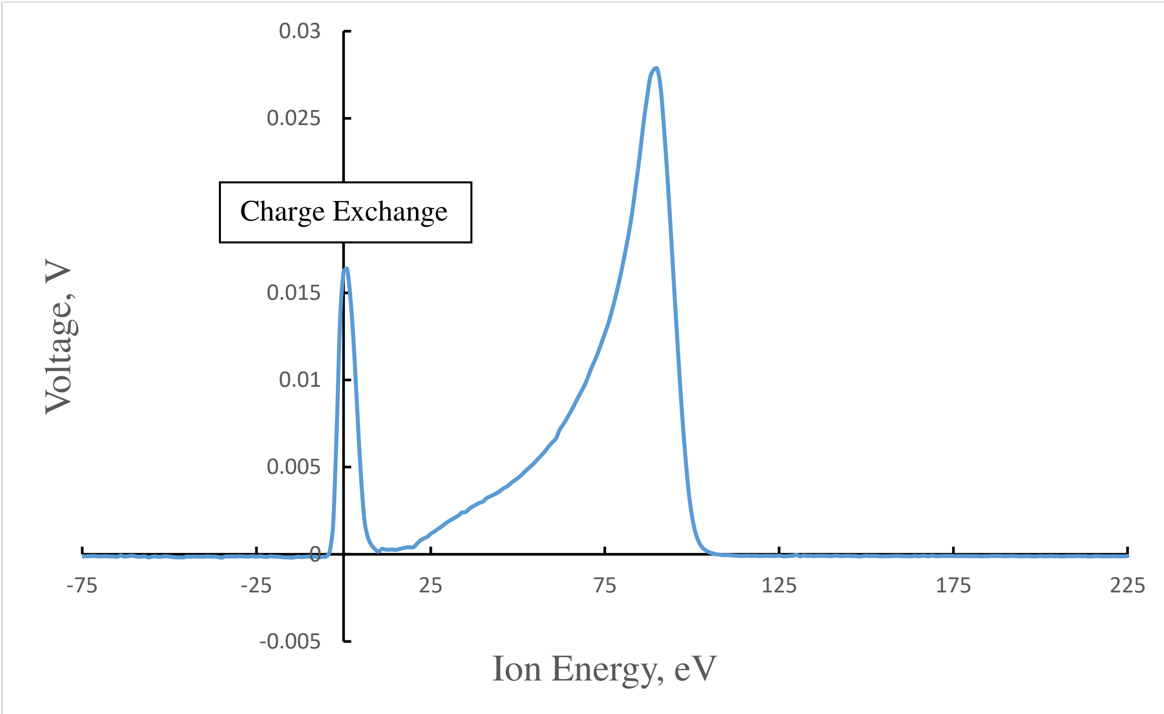

c) 133.66 cm

Figure 3.16: A) The ESA trace from the EVADER taken 30 cm away from the Flamethrower in the TIA configuration. B) The ESA trace from the EVADER taken 73.66 cm away from the Flamethrower. C) The ESA trace from the EVADER taken 133.66 cm away from the Flamethrower.

The traces shown in Figure 3.16 are considered to be identical to the ones shown in Figure 3.13.

The ExB traces recorded with the TIA board are shown in Figure 3.17 at the three separate distances, and they are also identical to the ExB traces obtained with the Keithley other than the triply charged ion signal, which appears to drop below the noise floor of the TIA circuit with the feedback resistor that was chosen.

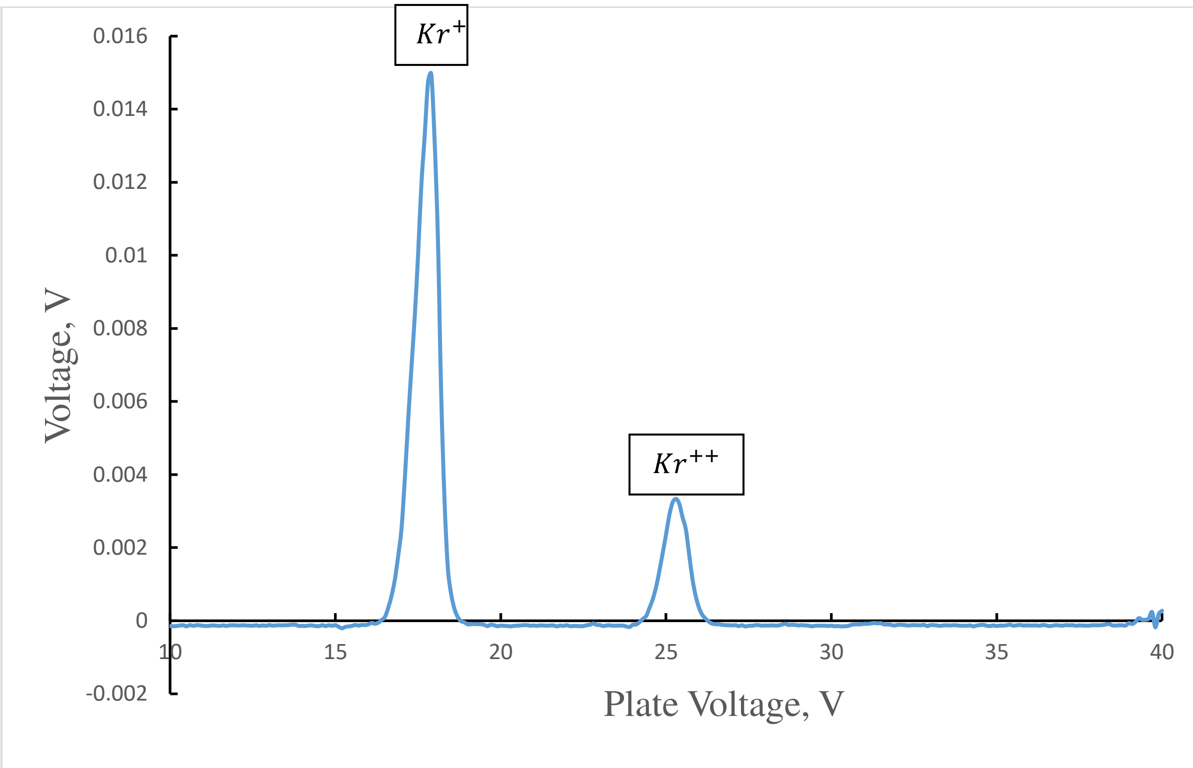

a) 30 cm

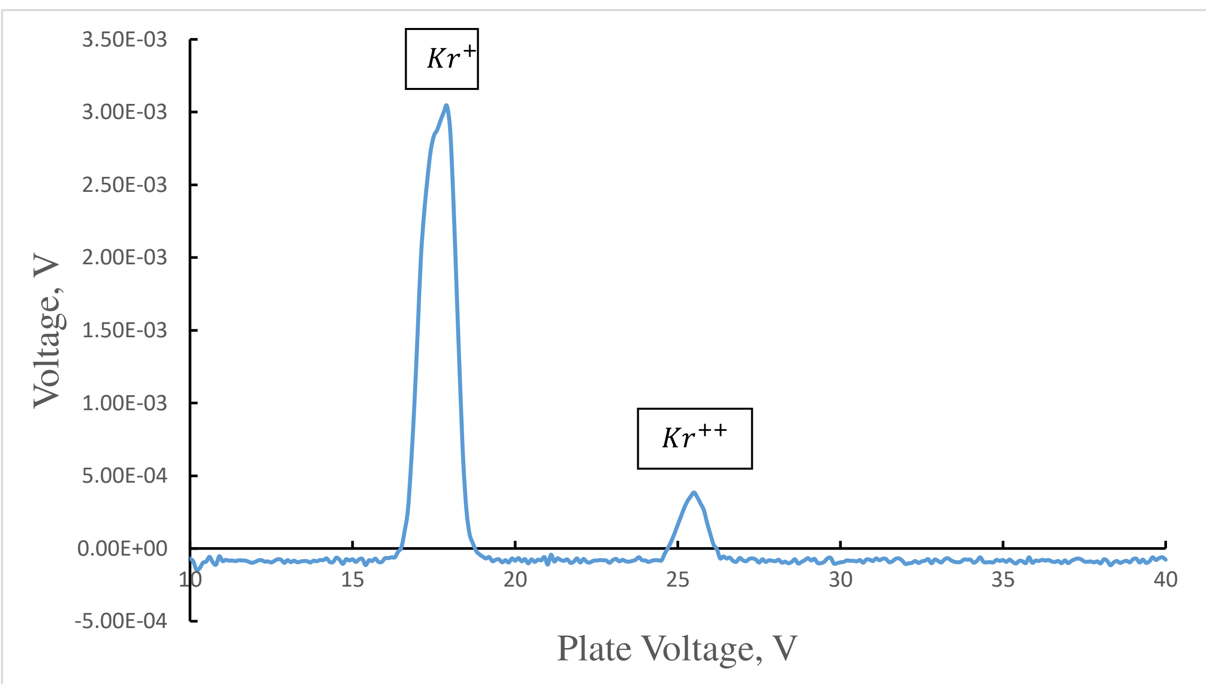

b) 73.66 cm

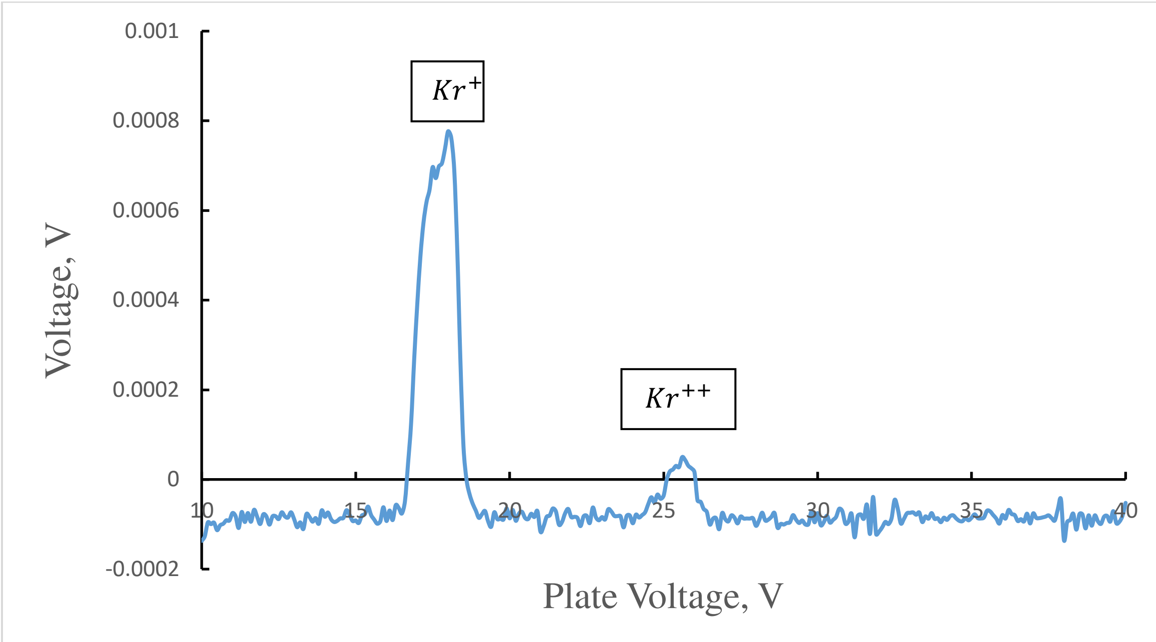

c) 133.66 cm

Figure 3.17: A) The ExB trace with the EVADER in the TIA configuration, located 30 cm from the Flamethrower. B) The ExB trace with the EVADER in the TIA configuration, located 73.66 cm from the Flamethrower. C) The ExB trace with the EVADER in the TIA configuration, located 133.66 cm from the Flamethrower.

Similar to Figure 3.15, it can be seen that as the probe moves further away from the thruster, the results are noisier, and the signal magnitude decreases. This is again likely since the plume expands and charge exchanges with the background neutrals.

3.2.5 Faraday Probe and Thrust Stand Test Results

The Flamethrower plasma plume profile was evaluated using a Faraday probe and the performance of the Flamethrower as an EP device was evaluated using thrust stand measurements.

A Faraday probe measures current density, and if these measurements are made over a region downstream of a plasma source, they can be used to calculate the beam current. The beam current was calculated by spherically integrating current density measurements made over a circular arc of 27” radius that was centered on the hidden anode component of the Flamethrower. As mentioned previously, this was determined to be inaccurate because it does not distinguish between the streaming ions, charge exchanged ions, energetic plume electrons, or secondary electron emission. Further research is taking place to take more accurate measurements of the beam current, but for now, the method of calculating the beam current was utilized.

Figure 3.18: Photograph of the Faraday probe.

A current density profile is shown in Figure 3.19.

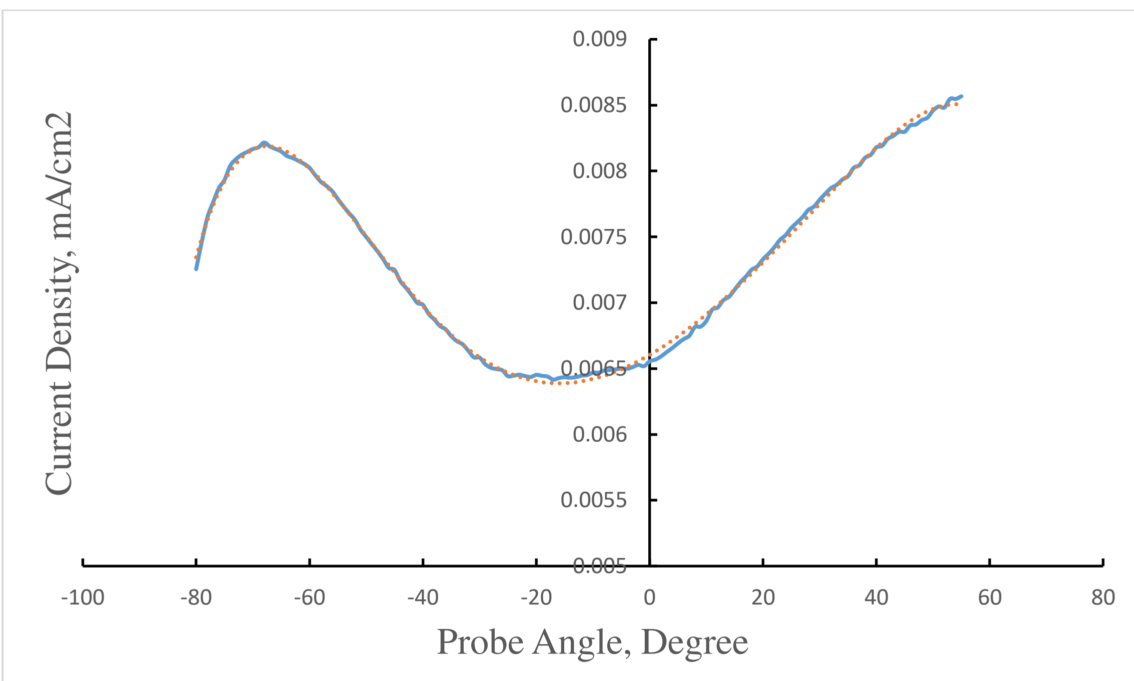

Figure 3.19: The current density profile through the beam on an arc. The trace shows that the current density is fairly equal through the plume, so the Flamethrower creates a torodial beam versus a Hall Effect Thruster would have a large current density directly in line with the orifice.

The trendline of one side of the trace is then fit with a polynomial to the 6^{th} power. The equation of the trendline is utilized to solve for the kernel and then summed, that produces a curve that increases and saturates, thus revealing the beam current of the Flamethrower.

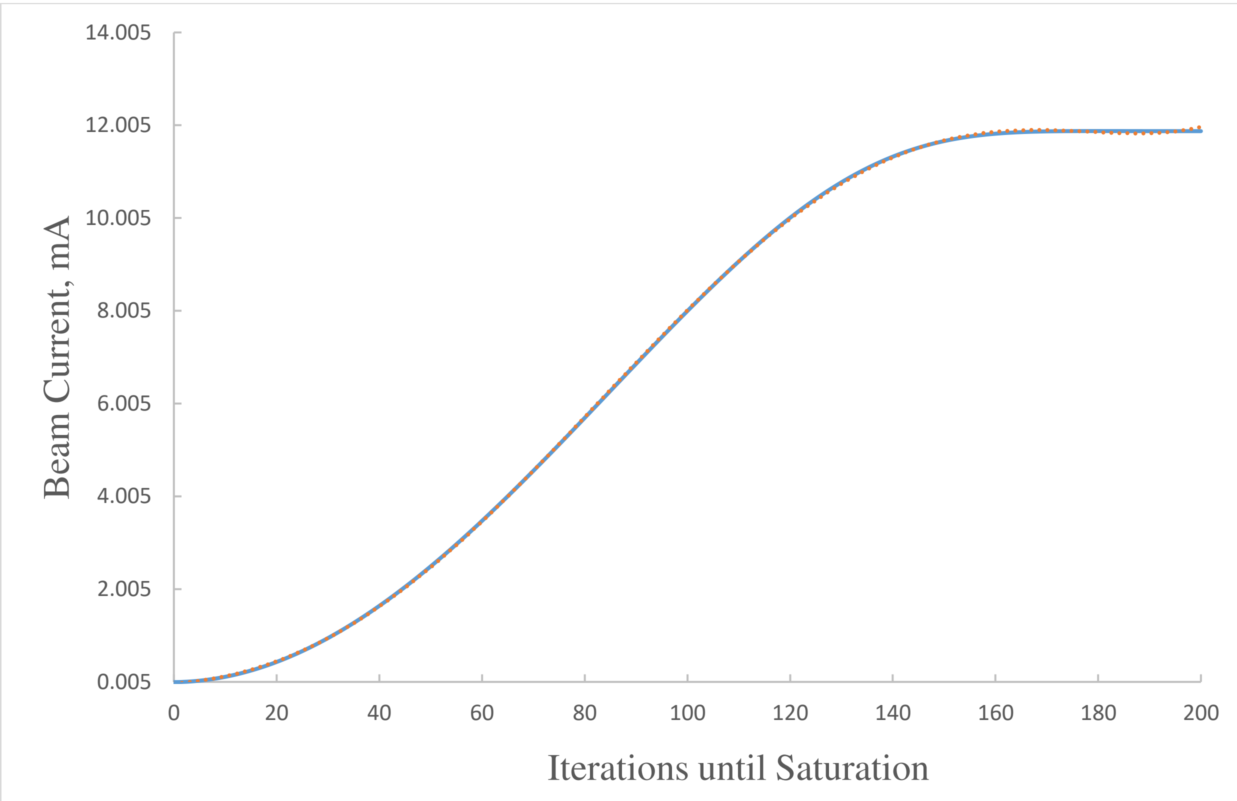

Figure 3.20: The current saturates around 11.88 mA that indicates that is the beam current.

Figure 3.20 shows the beam current when the Flamethrower was operated at roughly 100 V and 1A. While this is not the lowest operating point of the Flamethrower, it is the lowest that was scanned by the Faraday probe. Unfortunately, the motor for the probe arm burnt out before other traces could be taken.

The thrust stand used an LVDT to measure the thrust produced by the Flamethrower while it operates. It was calibrated using known weights on a line that yields an error of about 0.1mN includes the data set from the thrust stand that can then be used to calculate the specific impulse and efficiency.

Table 3.4: *Measurements and Calculations of the Flamethrower taken from the Thrust Stand.*

$P_{chamber}$	V_A	I_A	V_K	I_K	$\dot{m}_A$	$\dot{m}_C$	T	$I_{sp,anode}$	η_{anode}
Torr	*V*	*A*	*V*	*A*	*sccm*	*sccm*	*mN*	*s*	*%*
2.16E-5	104.6	1	42.1	0.5	8.88	5.55	0.46	84.18	0.18
2.11E-5	104.7	1	41.2	0.5	8.99	5.55	0.90	163.80	0.69
1.80E-5	193.3	1	41.2	0.5	6.33	5.55	1.24	321.58	1.01
1.75E-5	205.1	1	40.7	0.5	6.33	5.66	1.05	271.90	0.68
1.75E-5	213.7	1	40.6	0.5	6.33	5.55	1.63	422.65	1.58

Some of the items from Table 3.4 have been adjusted, such as the pressure to correct for Kr since the ionization gauge was calibrated on N_2. Overall, the Flamethrower does not perform as efficiently as a more common electric propulsion device such as a Hall effect thruster or an ion thruster. The specific impulse of some electric propulsion devices is an order of magnitude greater than what was measured with the Flamethrower. Although this configuration of the Flamethrower does not result in terrific thruster performance, it is still a useful plasma source to use for evaluation of the EVADER probe.

3.3 Data Analysis

This section involves normalization of the data collected so that the various equipment configurations used could be compared.

3.3.1 Comparison of Traditional to TIA EVADER Configurations

The TIA converts current to voltage, so the traces collected with the TIA cannot be directly compared to the Keithley and Keysight ammeters unless the voltage from the TIA is divided by the large feedback resistor that was used. There is some uncertainty of the actual value of the feedback resistor as installed due to board cleanliness and effects of humidity for some examples, but other unknown factors may also affect its "in circuit" value. Therefore, the TIA data was divided by the feedback resistor of $100\ M\Omega$ to convert the data back to a current.

The measurements made with the Keysight ammeter are being included on the ion source evaluations. Sandia National Labs did not have a Keithley 6517b available, so a Keysight B2981A ammeter was used in junction with a Sorenson power supply, and there was a need to determine if this change in equipment affected ESA or ExB data. New software was developed in Python to accompany the change in equipment. Data collected from all three equipment configurations were compared to see if there was a substantive change in the signal. In other words, data collected with the three set ups – Keithley, Keysight, and TIA – were normalized with respect to their standard deviation and compared on an arbitrary collector signal scale. Figure 3.21 contains a comparison plot of ESA data obtained with the gridded ion source operated at a beam voltage of 300 V.

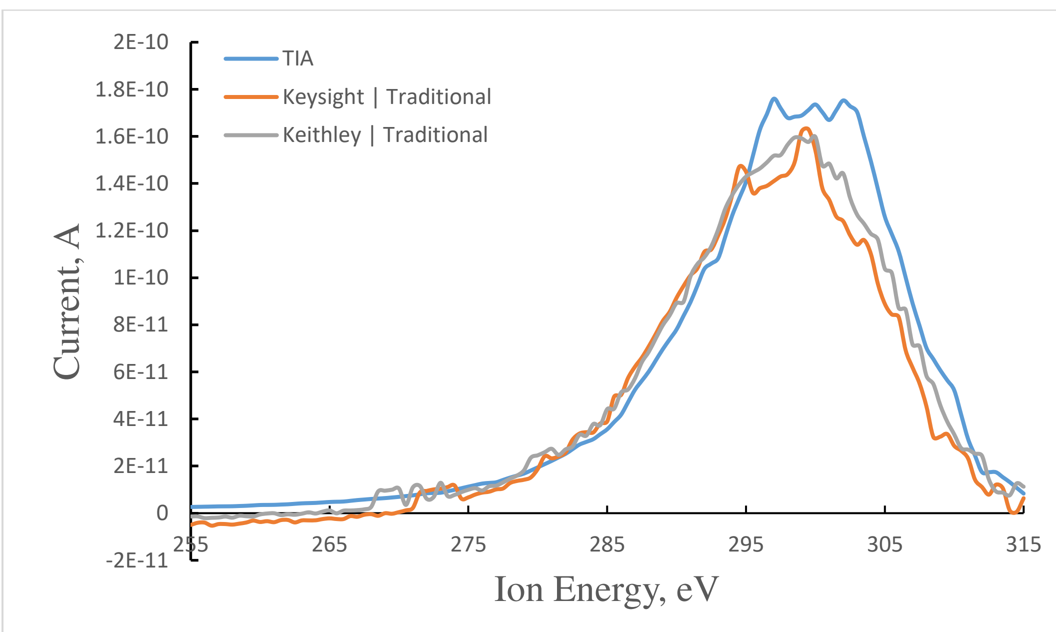

Figure 3.21: The ESA stage of the EVADER immersed in the ion source beam for each configuration.

The ESA results from the ion source of the different configurations are all similar. It appears that the TIA is successfully amplifying the signal above the magnitude of the traditional configuration plots. ExB traces are also compared in Figure 3.22. They successfully all occur at the same voltage, indicating that the different configurations all recognize the ion species, however the magnitudes do differ. Multiple trials at the same testing parameters do not indicate a trend so it could potentially be inconsistencies within the beam itself, but it is unknown. Overall, the TIA signal is still at a higher magnitude than the other traditional configurations.

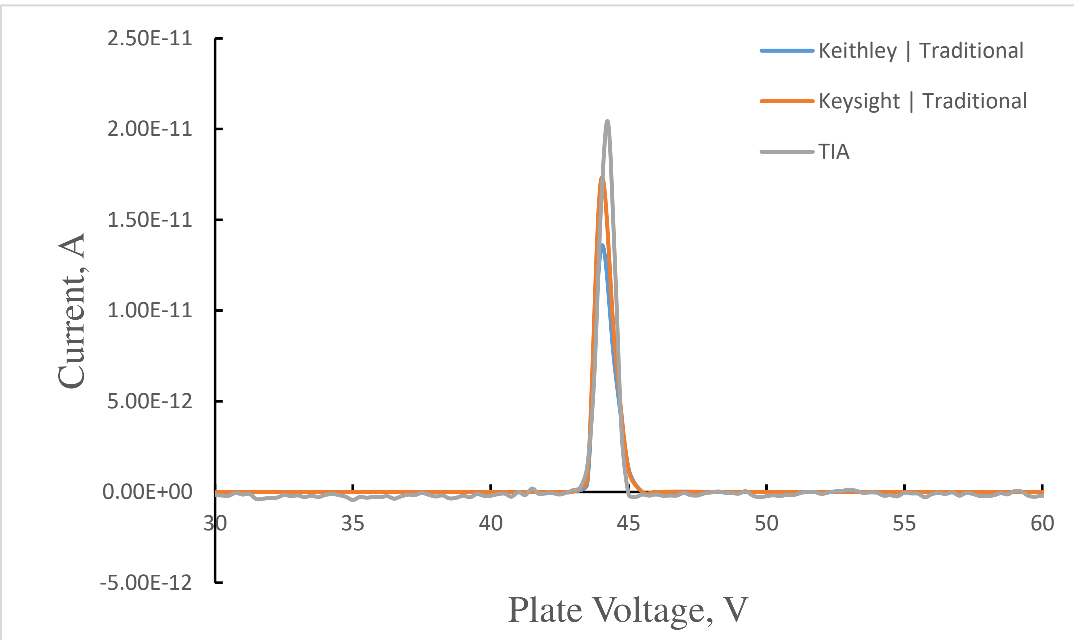

Figure 3.22: One of the trials that compares testing the different configurations of the EVADER while immersed in the ion source beam.

Similarly on the Flamethrower, the traces for both sectors of the EVADER probe in both configurations can be compared with the signal as a current. The trend suggests that the TIA was amplifying the current before converting it to a voltage.

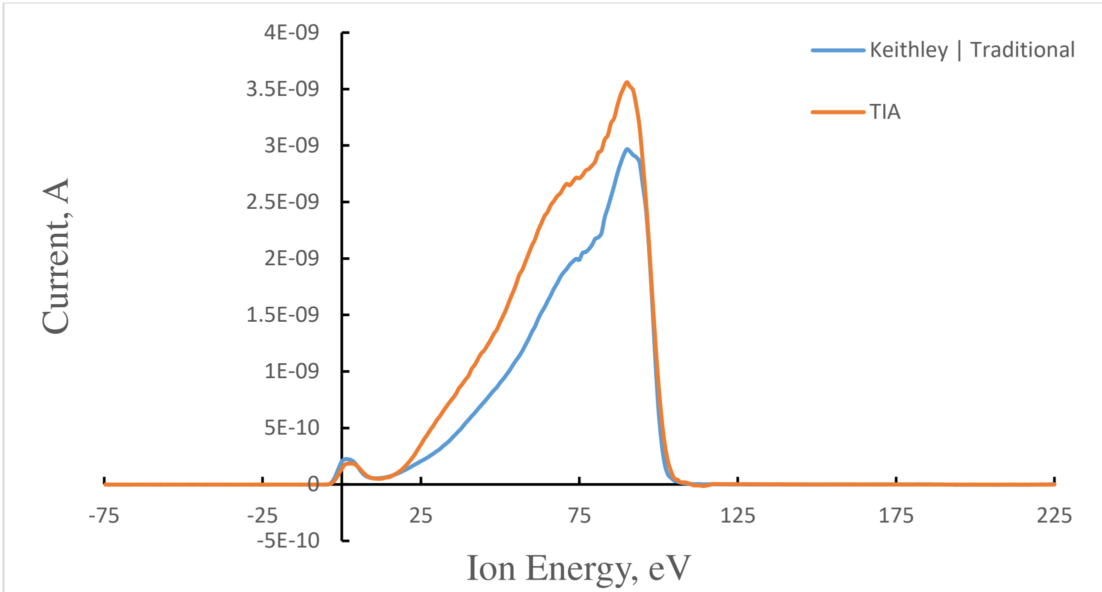

a) Trial 1

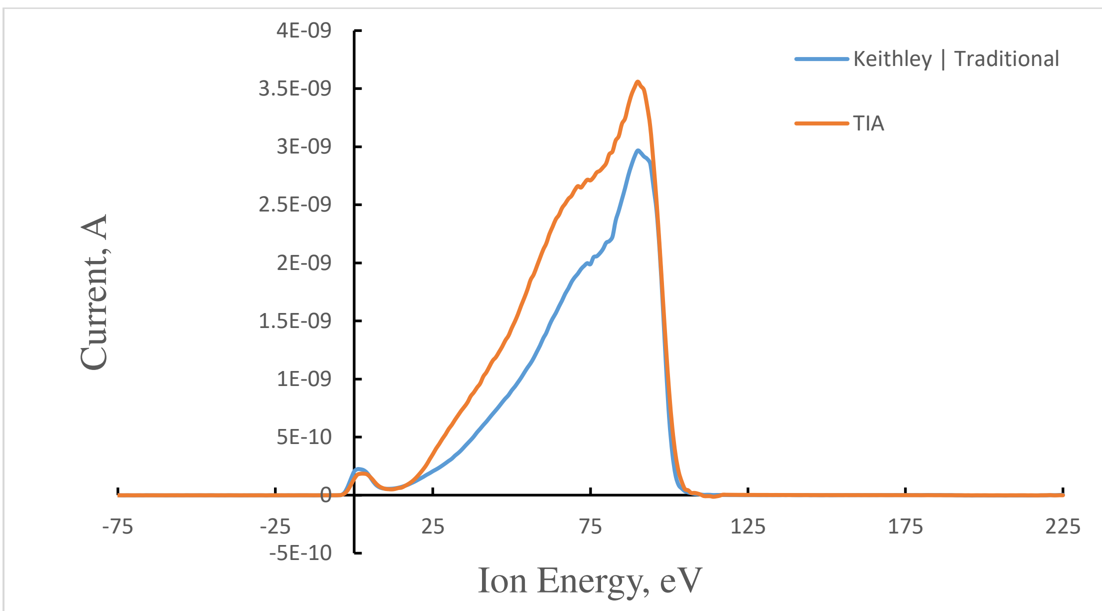

b) Trial 2

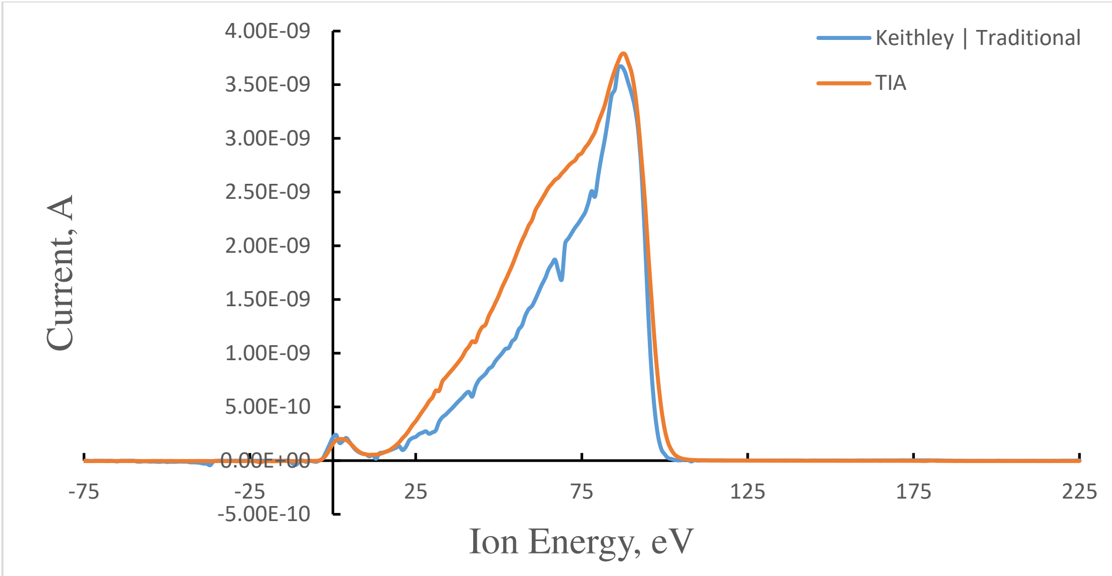

c) Trial 3

Figure 3.23: Three trials of the comparison of ESA traces from the EVADER to determine if the magnitudes and peak energies are similar.

When the traces for the ExB stage were directly compared, it was difficult to distinguish a trend. At times, the TIA configuration reported a higher current than the Keithley and other times it was lower. This could be due to the sensitivity of the evaluation board for the TIA as it needed to be cleaned and properly stored, and this data was collected over the course of two days. Further data collection would be needed at 30cm to confirm the TIA's success on the ExB stage against the Flamethrower.

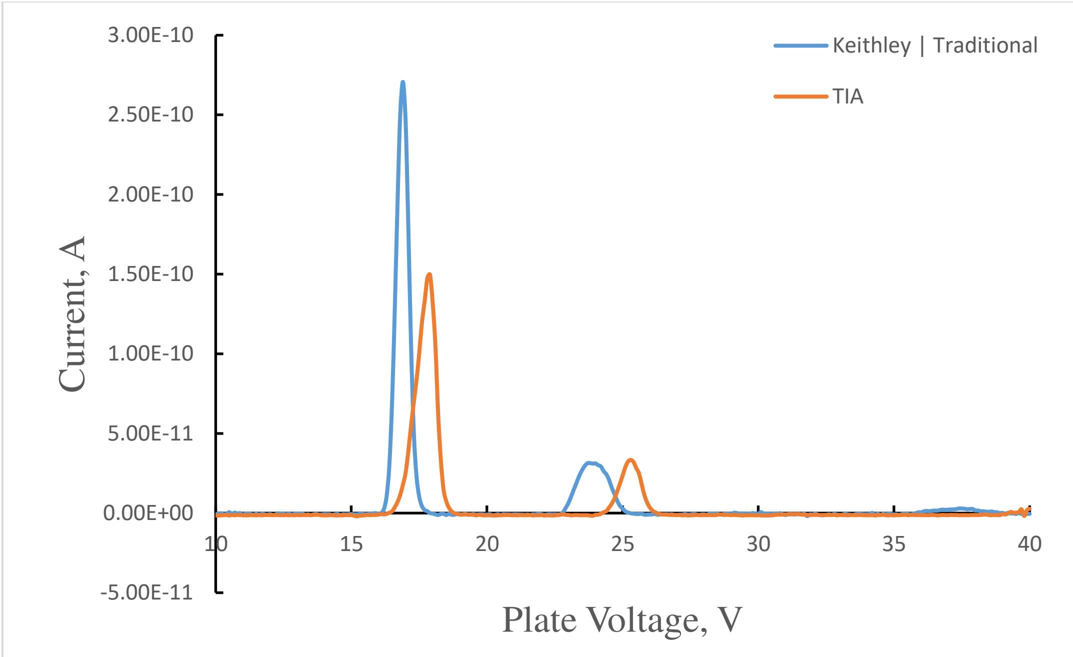

a) Trial 1

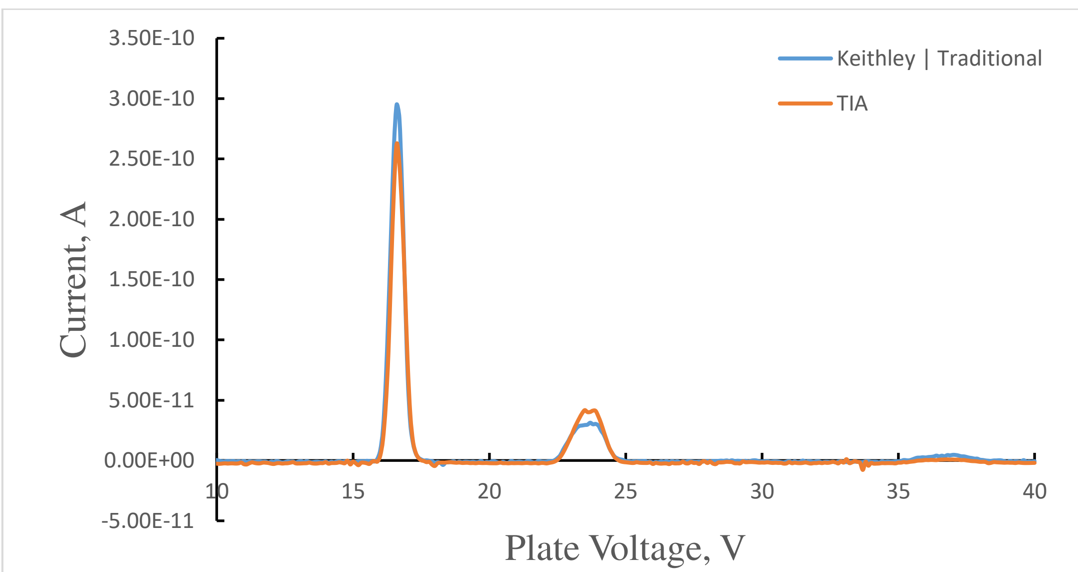

b) Trial 2

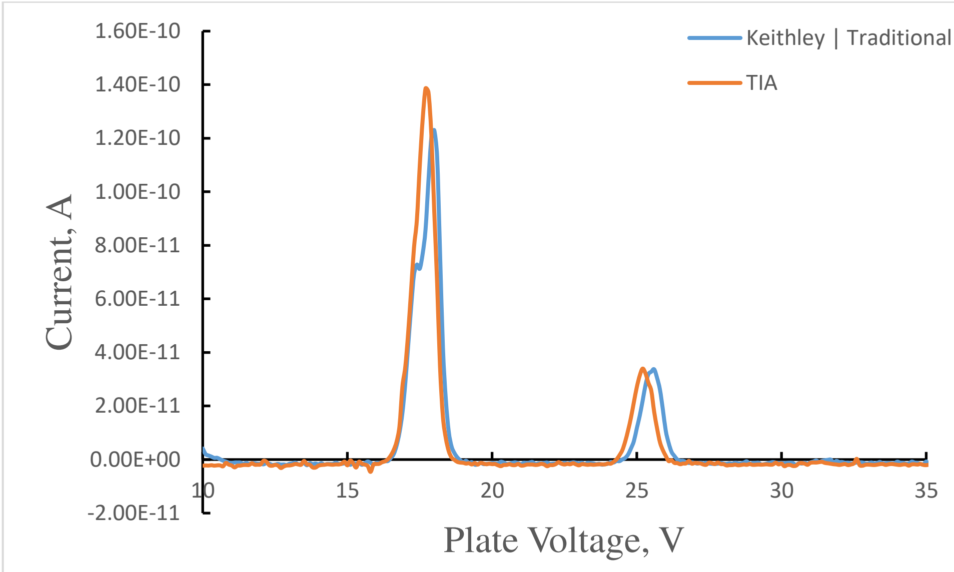

c) Trial 3

Figure 3.24: ExB traces all taken 30 cm away, compared between the traditional configuration and the TIA configuration, while immersed in the Flamethrower plume.

Chapter 4 Additional Design Concepts and Discussion

There are plans to further these efforts because, while the project was introduced by Sandia National Labs, a high-speed mass spec would be very useful to temporally resolve plasma dynamic phenomena occurring in electric propulsion devices. The following sections detail some necessary improvements in making accurate measurements of the streaming ion current density along with design concepts that may lead to improved temporal response of a mass spec based on combined electrostatic and magnetostatic techniques like those utilized in the current version of the EVADER probe.

4.1.1 Discussion of Beam Current Calculations

EVADER is a separate plasma diagnostic tool than the Faraday probe, it is important to address the non-trivial problem of accurately measuring the total number of ions produced by a plasma source that are accelerated into its exhaust plume – sometimes referred to as the beam current. A more accurate measurement and calculation will not only ensure more accurate performance studies of transient desorption events and electric propulsion devices like the Flamethrower but also of advanced diagnostic probe concepts.

There are several obstacles to measuring ion current density correctly with the method described in this thesis. First, the probe is not biased negatively enough to collect only ions—some energetic electrons from the tail of the electron energy distribution can still make it to the probe, which will cause the measured current to be less than the actual current of ions. Just biasing the probe more negative causes it to arc to the chamber walls, so it is not just a matter of changing the voltage to stop all electrons. The second issue is calculating the beam current from the measured ion beam current density profile even if only ions where measured. The Faraday probe is far enough away that charge exchange is taking place. The streaming ions are being attenuated by charge exchange reactions, and so the ion current density is lower than it would be if no charge exchange were occurring. Conversely, the low energy charge exchange ions produced within the vicinity of the Faraday probe can be collected to the probe when it is biased negative, which will cause a higher ion current density to be calculated. The two effects counteract one another in a difficult to ascertain manner. A final concern is that ions collected on a surface can lead to electrons being released from the surface—secondary electron emission due to ion collection. About ten Kr singly charged ions collected on refractory metal or graphite surfaces can result in about one secondary electron being emitted on average, which corresponds to a secondary electron coefficient of 0.1 electrons/ion [29] [30]. This is a significant source of error, and the secondary electron emission occurs at low ion energies due to Auger mechanisms so reducing the ion energy will not alleviate this problem. Furthermore, the secondary emission coefficient can approach unity when higher charge state ions are collected [29] [30], which can occur in plasma sources like the Flamethrower. The complications of charge exchange collisions, collection of low energy ions created by the charge exchange reactions, and secondary electron emission raise the uncertainty of the integrated beam current value and further complicate the determination of the actual total ion beam current leaving a plasma source. As noted in Figure 3.16b, significant charge exchange ion production was evident at the distance the Faraday probe is from the thruster. One possible method for correcting for charge exchange can be discussed by considering Equation (4.1).

$$I_{measured} = I_{original} \cdot exp\left(-1 \cdot n_{neutral\ density} \cdot \sigma CEX \cdot r\right) \tag{4.1}$$

Where $I_{measured}$ is the ion current (calculated from integration of the measured ion current density profile) expanding from the plasma source being tested assuming that no low energy ions from the Faraday probe vicinity are collected and no secondary electrons are released from its surface,

$I_{originial}$ is the total ion current leaving the plasma source that expands out into the regions downstream (the desired parameter), $n_{neutral\ density}$ is the neutral density, σCEX is the charge exchange cross section, and r is the axial distance from the thruster. One problem with Equation 4.1 is that the neutral density is not constant. This could be corrected by using a stepwise version of Equation 4.1, but the larger problem is that the neutral density is not known either. It is possible that one could model the neutral expansion problem and then use the model estimates for neutral density, but this is beyond the scope of the present work. The final problem of stopping the collection of charge exchange ions and inhibiting secondary electron emission can be addressed by using a filtered Faraday probe as described by Rovey et al [31] [32]. The filtered Faraday probe uses an applied magnetic field that is transverse to the probe surface. This transverse magnetic field allows ions to pass, but retards electrons from the plasma source plume from reaching the probe surface. One can actually operate the filtered Faraday probe at a potential above plasma potential where charge exchange ions would be repelled, and secondary electrons would be prevented from leaving the surface. Some data has been collected with a filtered Faraday probe, but the data is preliminary at this point in time and is not included in this thesis.

One other possibility of obtaining the total ion current leaving the plasma source is to bias the source quickly positive of the vacuum chamber walls and measure the current to the walls as a function of the bias voltage. Doing these measurements quickly will allow a measurement to be made before an arc occurs from the chamber walls. This technique is being evaluated, but the data is considered to be very preliminary and is not included here.

4.1.2 Microchannel Plate for Amplifying Ion Current

Even with a highly sensitive transimpedance amplifier, the signal recorded from the EVADER is quite low. Especially for pulsed power applications or temporally dynamic plasma sources, it would be beneficial to have an increased signal to analyze during a short pulse of ions. A microchannel plate (MCP) is a small, thin plate with an array of parallel channels leading through, intensifying current by the multiplication of secondary emission cascades. Figure 4.1 contains a sketch of a MCP.

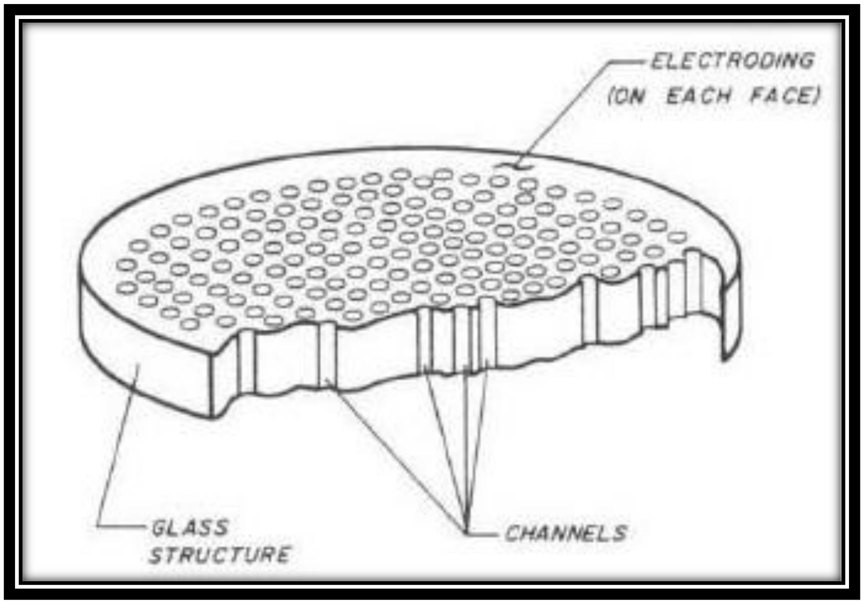

Figure 4.1: An illustration of an MCP with a section cut out for easier visibility of the channels. Taken from [33].

The channels in the MCP are set at a small angle from normal to guarantee that an incoming ion will hit the wall of the channel, knocking an electron off the wall and accelerating it with the bias that is applied between the front and back surfaces of the MCP. Then that electron hits the wall and knocks off more electrons, this creates a cascading effect that amplifies the incoming ion current as shown in the combined sketch and electrical schematic in Figure 4.2.

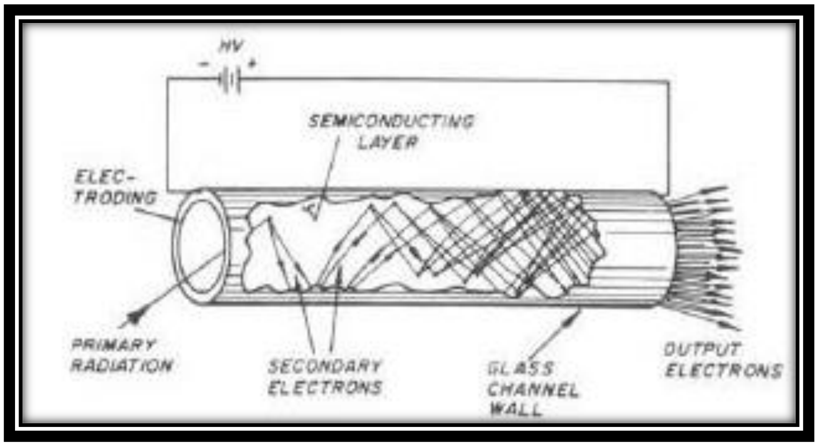

Figure 4.2: A drawing of the multiplication through cascading electrons in a single channel of an MCP. Taken from [33].

The MCP amplifier concept above suggests a design modification to the EVADER probe to replace the ESA and ExB collectors with MCPs to magnify and detect the ion signal quickly. In the EVADER, the MCP would be oriented normal to the flow of incoming ions. Each channel acts as a multiplier, where the primary single particle causes a cascade increasing its signal by $10^4 - 10^7$ [33].

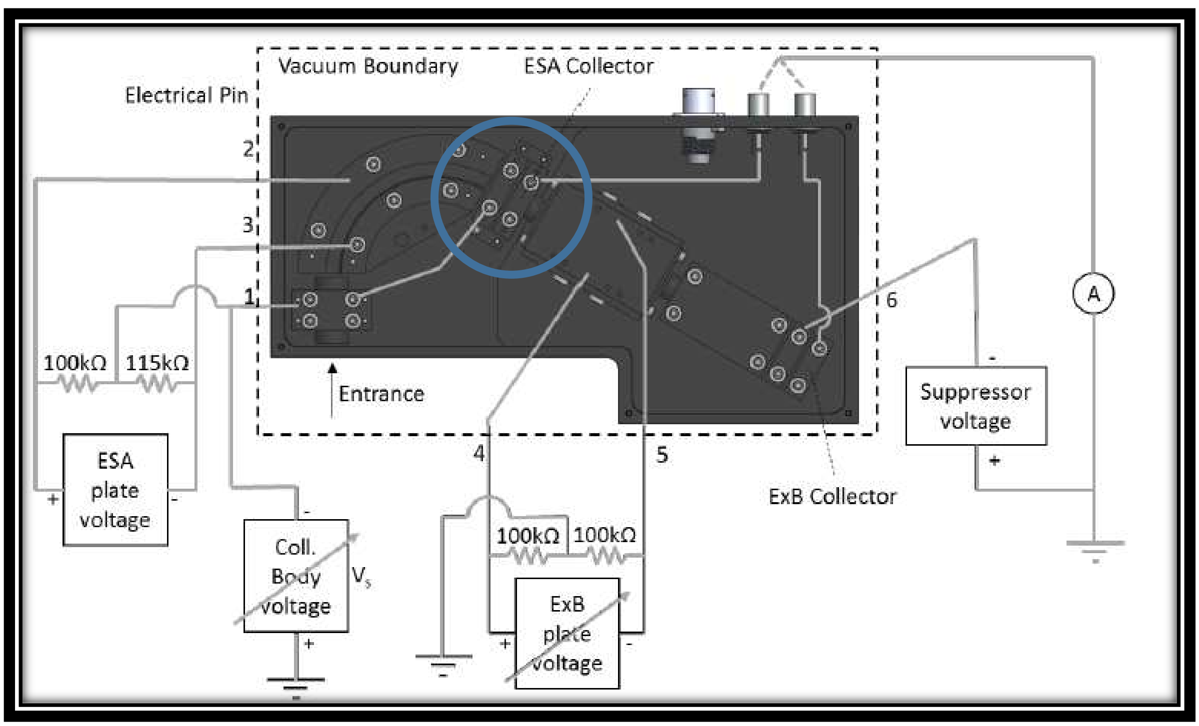

Figure 4.3: A schematic of the EVADER that indicates where the MCPs would be inserted to amplify and record the signal.

Two MCPs were purchased from Photonis Scientific where each plate has an outside diameter of 24.77mm and a thickness of 0.30mm. The MCPs are made of long-life glass with electrodes made from nichrome. They have not arrived in time to be tested, and so no data on their performance is included in this thesis.

4.1.3 Magnetic Sector

While the ExB traces can be re-scaled logarithmically and depict signatures of other species and isotopes, there needs to be a faster way to detect species rather than sweeping voltage, if one wants to characterize a plasma source very quickly. To obtain EVADER ExB data currently, the ExB plates must be swept through a range of voltages while the TIA or a combination of MCP amplification and the TIA discretely measure the incoming current at every plate voltage sampled. The speed of the sweep can be increased by using a high voltage bipolar operational amp instead of the Keithley or a Sorenson power supply, but the fastest sweeps would likely be no faster than 100 μs. An alternative method would be to detect species simultaneously as explained below.

Sandia National Labs is specifically interested in five species: hydrogen, water, carbon dioxide, carbon monoxide, and methane. Plasma sources like the Flamethrower would likely only need three species: singly, doubly, and triply charged ions created from the propellant gas fed to the device. Getting rid of the need to sweep voltages and just measure the species simultaneously can be done with a magnetic sector. A magnetic sector uses a static magnetic field to deflect ions of different masses and charges to separate collectors simultaneously. To incorporate a magnetic sector, the ExB analyzer would be removed, and the magnetic sector would take its place. An ESA would still be needed in the front because it allows one to hones in on a range of ion energies and helps distinguish particle mass between species and ions that would have the same approximate mass but not the same charge or energy.

The following figure was modeled by Dr. Shawn Farnell, a research scientist in the CEPPE lab, which illustrates that a static magnetic field of 0.1 T can cause a motely of species to disperse over a controlled area. These types of models can show where the collectors would have to be placed to detect specific species in a simultaneous manner.

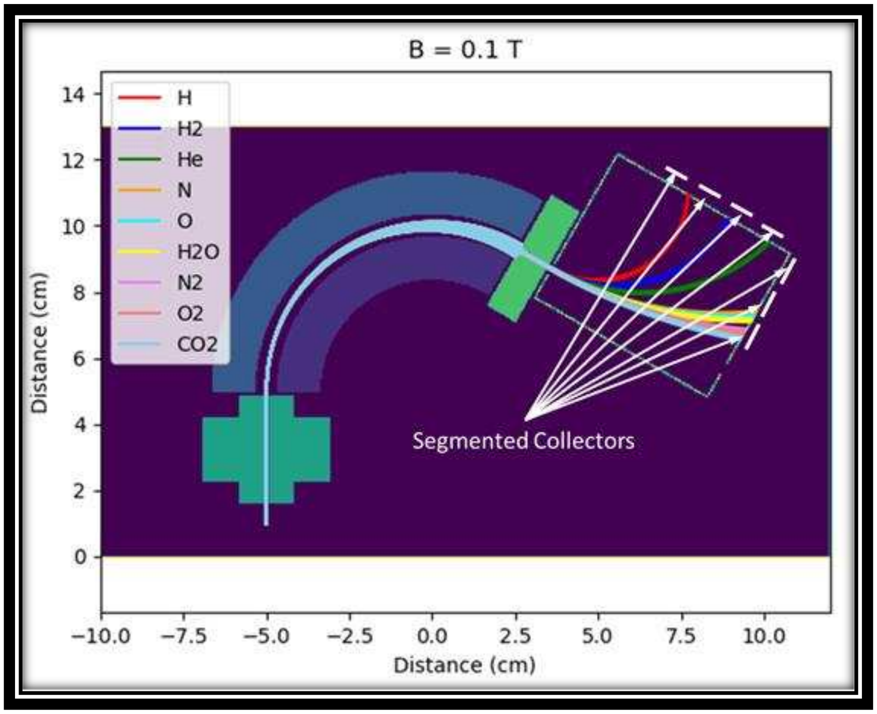

Figure 4.4: A model of a proposed magnetic sector with an applied static magnetic field of 0.1T and a list of species to potentially detect.

The model can be refined to just focus on the five species and determine where the collectors should be placed. This way, the ions would enter the magnetic sector at a set pass energy and get deflected toward the designated collector. This eliminates the need to sweep voltages on the ExB region that makes the entire probe more efficient and faster.

4.1.4 Ionizer

Laboratory testing has involved an ion source and a Flamethrower to ionize the neutral atoms that are then directed into the EVADER because the EVADER can only be used to filter and detect charged particles. However, in a pulsed power machine, it is not likely that the desorbed neutrals would be ionized quickly enough to be detected and produce enough of a signal within the EVADER. A separate ionizer would need to be mounted in front of the aperture of the probe as shown in Figure 4.5 to be sure that all the desorbed neutrals from the electrodes will be ionized.

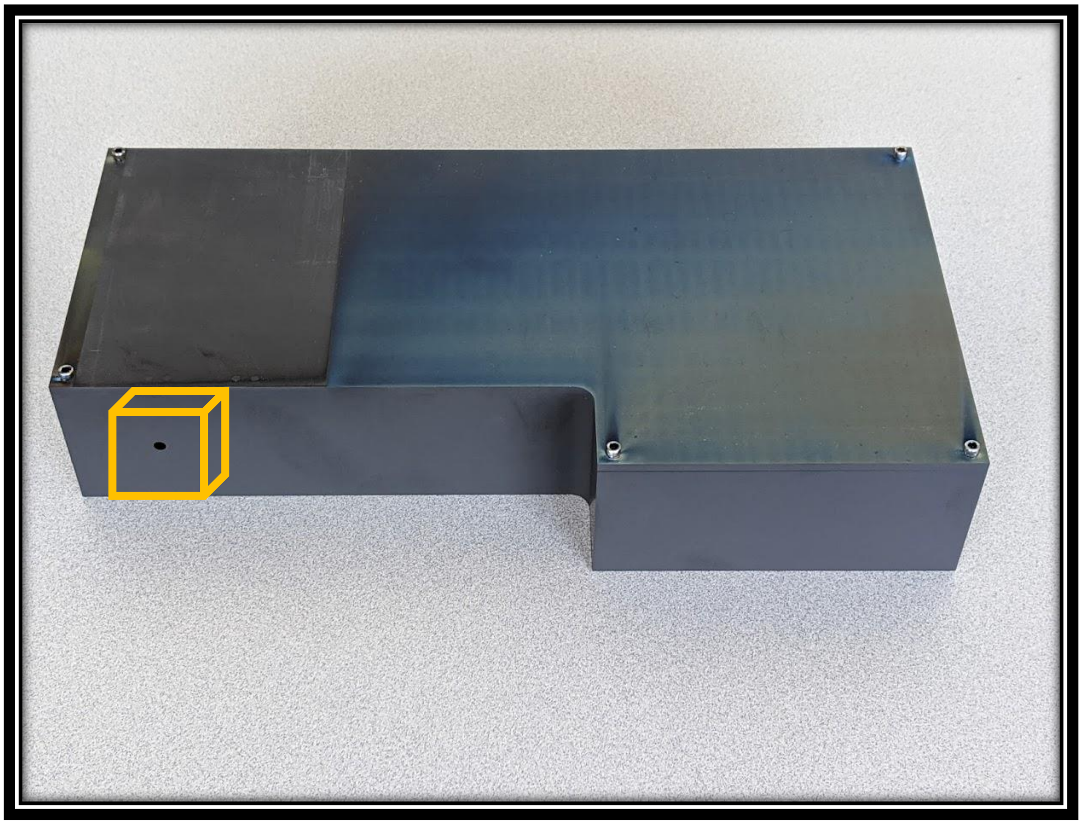

Figure 4.5: A photograph of the EVADER with a box highlighted in front of the aperture where the ionizer would be located.

An ionizer would have a hot filament to thermionically emit electrons and bombard the neutrals to ionize them. Then an ion optics system would be used to accelerate the ions into the probe.

4.1.5 Electric Shutter

Finally, an electric shutter will be implemented between the ionizer and the probe that would enable temporal control of the ions by allowing a burst of them to enter the system. This shutter would not necessarily improve the probe operation, instead its use would provide information about the measurement speed of the probe—its ability to collect data transiently so that one could judge if a transient measurement made on a plasma source is limited by the probe bandwidth.

Chapter 5 Conclusion

A study was conducted on the performance of the EVADER probe as a basis for a high-speed mass spec capable of detecting desorbed neutral species under transient conditions. The study was split into multiple steps to build a pathway to designing and testing a high-speed mass spectrometer. The steps discussed in this thesis involved replacing a commercial ammeter with a transimpedance amplifier circuit, then replacing the collectors with micro-channel plates, next replacing the sweeping power supplies with a high voltage bipolar operational amp, removing the sweeping amp entirely and replacing the ExB analyzer with a magnetic sector, and finally installing an ionizer and electric shutter to the aperture of the probe.

This thesis focused on the implementation of the transimpedance amplifier as the ammeter and beginning the process of replacing the collectors with MCPs. Looking into the results of the TIA, while there was some variability, the magnitude of the signal and the occurrence of the peaks were consistent with the original configuration that the EVADER was set up with. The transimpedance amplifier needed to be cleaned thoroughly and stored properly to operate optimally.

Chapter 6 Bibliography

[1] D. C. Lamppa, "Assessment of Electrode Contamination Mitigation at 0.5MA Scale," Sandia National Laboratories, Albuquerque, 2021.

[2] G. R. Laity, "Towards Predictive Plasma Science and Engineering through Revolutional Multi-Scale Algorithms and Models," Sandia National Laboratories, Albuquerque, 2021.

[3] J. Gansz-Torres, "2D and 3D Numerical PIC Simulations of the Low and High Current Density Mykonos V Accelerator Vacuum Region," Voss Scientific, Albuquerque, 2018.

[4] J. Halbritter, "On Contamination on Electrode Surfaces and Electric Field Limitations," *IEEE Transactions on Electrical Insulation,* Vols. EI-20, no. 4, pp. 671-681, 1985.

[5] B. T. Hutsel, "Millimeter-Gap Magnetically Insulated Transmission Line Power Flow Experiments," Sandia National Laboratories, Albuquerque.

[6] J. C. Berg, "The Role of Surfactants," *Textile Science and Technology,* vol. 13, pp. 149-195, 2002.

[7] S. C. Simpson, "Vacuum Outgassing Study of Candidate Materials for Next Generation Pulsed Power and Accelerators: Improving the Boundary Conditions for Molecular Flow Simulations," Sandia National Laboratories, Albuquerque, 2019.

[8] S. J. Cochran, "Surface Reduction of Some Transition-Metal Oxides," *Journal of the Chemical Society,* vol. 1, no. 9, pp. 2179-2190, 1985.

[9] M. V. Lee, "Potential for High-Speed Mass Spectrometry for Pulsed-Power Applications," Northern Arizona University, Flagstaff, 2018.

[10] U. Boesl, "Laser Ion Sources for Time-of-Flight Mass Spectrometry," *International Journal pf Mass Spectrometry and Ion Processes,* vol. 131, pp. 87-124, 1994.

[11] F. A. Mellon, "Principles and Instrumentation Applications," in *Mass Spectrometry*, Norwich, Elsevier Science, 2003, pp. 3739-3749.

[12] A. Velasco, "Study of the Thermal Decomposition of "Captured" Intermediates in the CVD of ZnO from DEZ and H2O by TGA-DTA and Quadrupole Mass Spectroscopy," *Journal of Crystal Growth,* vol. 311, pp. 2731-2735, 2009.

[13] L. Payne, "Evaluation of the Use of Magnetic Sector Secondary Ion Mass Spectrometry to Investigate C Distribution in Magnox Reactor Core Graphite," *Mineralogical Magazine,* vol. 79, no. 6, pp. 1327-1334, 2015.

[14] S. J. Thompson, S. C. Farnell and C. C. Farnell, "Combined Electrostatic Analyzer - Wien Filter Probe for Characterization of Species Distributions in Hall Thrusters," *Journal of Applied Physics,* vol. 130, no. 233302, pp. 1-11, 2021.

[15] C. Farnell, C. Farnell, S. Farnell and J. Williams, "Recommended Practice for Use of Electrostatic Analyzers in electric Propulsion Testing," *Journal of Propulsion and Power,* vol. 33, no. 3, pp. 638-657, 2017.

[16] R. DeSerio, "Spherical Sector Electrostatic Analyzers for Measurements of Energy and Angular Distributions," *Review of Scientific Instruments,* vol. 60, pp. 381-388, 1989.

[17] C. C. Farnell, "Electrostatic Analyzers with Application to Electric Propulsion Testing," in *33rd International Electric Propulsion Conference*, Washington D.C., 2013.

[18] K. T. a. D. Ioanoviciu, "Wien Filter Instrumentation," in *Advances in Imaging and Electron Physics* , Tokyo, ScienceDirect, 2013, pp. 105-126.

[19] S. Nguyen, "Design of an ExB Probe," NASA Glenn Research Center, Cleveland, 2004.

[20] J. M. Ekholm, "ExB Measurements of a 200 W Xenon Hall Thruster," Air Force Research Laboratory, Edwards, 2005.

[21] S. J. Zweben, "Plasma Mass Separation," *AIP Physics of Plasma,* vol. 25, pp. 1-23, 2018.

[22] H. R. Kaufman and R. S. Robinson, "Broad-Beam Ion Source Technology and Applications," *Vacuum,* vol. 39, no. 11-12, pp. 1175-1180, 1989.

[23] V. Gorokhovsky, "Low Pressure Remote Arc Assisted Magnetron Sputtering System". Longmont, CO Patent EP 2 866 246 A1, 28 10 2014.

[24] V. Gorokhovsky, "Filtered Cathodic Arc Method, Apparatus and Applications Thereof". United States Patent 9761424B1, 12 09 2017.

[25] G. Giusi, G. Cannata, G. Scandurra and C. Ciofi, "Ultra-Low-Noise Large-Bandwidth Transimpedance Amplifier," *International Journal of Circuit Theory and Applications,* vol. 43, no. 10, pp. 1455-1473, 2015.

[26] B. Razavi, "The Transimpedance Amplifier," *IEEE Solid-State Circuits ,* no. Winter, pp. 10-13, 2019.

[27] P. Grohe, "Texas Instruments," January 2010. [Online]. Available: https://www.ti.com/lit/ug/snou004/snou004.pdf. [Accessed 13 March 2022].

[28] C. Farnell, "Numerical Simulation of HiPEP Ion Optics," *American Institue of Aeronautics and Astronautics,* 2004.

[29] M. L. Hause, B. D. Prince and R. J. Bemish, "Krypton Charge Exchange Cross Sections for Hall Effect Thruster Models," *Journal of Applied Physics,* vol. 113, no. 163301, 2013.

[30] W. Huang and R. Shastry, "Analysis of Wein Filter Spectra from Hall Thruster Plumes," *Review of Scientific Instruments,* vol. 86, no. 073502, 2015.

[31] J. L. Rovey, M. L. R. Walker and A. D. Gallimore, "Magnetically Filtered Faraday Probe for Measuring the Ion Current Density Profile of a Hall Thruster," *Review of Scientific Instruments,* vol. 77, no. 013503, 2006.

[32] D. L. Brown, M. L. R. Walker, J. Szabo, W. Huang and J. E. Foster, "Recommended Practice for Use of Faraday Probes in Electric Propulsion Testing," *Journal of Propulsion and Power,* vol. 33, no. 3, pp. 582-613, 2017.

[33] J. L. Wiza, "Microchannel Plate Detectors," *Nuclear Instruments and Methods,* vol. 162, pp. 587-601, 1979.

[34] S. J. B. Reed, "Trace Element Analysis with the Ion Probe," *Scanning,* vol. 3, pp. 119-127, 1980.

[35] D. A. Armbruster and T. Pry, "Limit of Blank, Limit of Detection, and Limit of Quantitation," *The Clinical Biochemist Reviews,* vol. 29, no. 1, pp. 49-52, 2008.

[36] D. Goebel and I. Katz, Fundamentals of Electric Propulsion, NJ: John Wiley & Sons, 2008.